

Tracor Jitco, Inc. (Book/photocopy)

Date Received: 7/29/82

To:	PLASTE SYSTEM	DESTROY	TEST- BOOK
( ) Anzalone	( )	( )	( )
( ) Landrock	( )	( )	( )
( ) Latino	( )	( )	( )
( ) Olsen	( )	( )	( )
( ) Nardone	( )	( )	( )
( ) Pebly	( )	( )	( )
(X) Readdy	(✓)	( )	( )
( ) Ski	( )	( )	( )
( ) Tompkins	( )	( )	( )
( )	( )	( )	( )

**DISTRIBUTION STATEMENT A**  
 Approved for public release;  
 Distribution Unlimited

Please initial table of contents for individual papers.

Please indicate if item should enter PLASTE Computer System, PLASTE library, or BOTH.

COMMENTS: \_\_\_\_\_  
 \_\_\_\_\_  
 \_\_\_\_\_

**DTIC QUALITY INSPECTED 1**

**PLASTE 43051**

This is an authorized facsimile  
printed by microfilm/xerography on acid-free paper  
in 1982 by

**UNIVERSITY MICROFILMS INTERNATIONAL**

Ann Arbor, Michigan, U.S.A.

London, England

## INFORMATION TO USERS

This was produced from a copy of a document sent to us for microfilming. While the most advanced technological means to photograph and reproduce this document have been used, the quality is heavily dependent upon the quality of the material submitted.

The following explanation of techniques is provided to help you understand markings or notations which may appear on this reproduction.

1. The sign or "target" for pages apparently lacking from the document photographed is "Missing Page(s)". If it was possible to obtain the missing page(s) or section, they are spliced into the film along with adjacent pages. This may have necessitated cutting through an image and duplicating adjacent pages to assure you of complete continuity.
2. When an image on the film is obliterated with a round black mark it is an indication that the film inspector noticed either blurred copy because of movement during exposure, or duplicate copy. Unless we meant to delete copyrighted materials that should not have been filmed, you will find a good image of the page in the adjacent frame.
3. When a map, drawing or chart, etc., is part of the material being photographed the photographer has followed a definite method in "sectioning" the material. It is customary to begin filming at the upper left hand corner of a large sheet and to continue from left to right in equal sections with small overlaps. If necessary, sectioning is continued again—beginning below the first row and continuing on until complete.
4. For any illustrations that cannot be reproduced satisfactorily by xerography, photographic prints can be purchased at additional cost and tipped into your xerographic copy. Requests can be made to our Dissertations Customer Services Department.
5. Some pages in any document may have indistinct print. In all cases we have filmed the best available copy.

University  
Microfilms  
International

300 N. ZEEB ROAD, ANN ARBOR, MI 48106  
18 BEDFORD ROW, LONDON WC1R 4EJ, ENGLAND

19951226 011

\*\*\*DTIC DOES NOT HAVE THIS ITEM\*\*\*

-- 1 - AD NUMBER: 0405740  
-- 5 - UNCLASSIFIED TITLE: EFFECTS OF IONIZING RADIATION ON THE  
-- CHEMICAL STRUCTURE, CRYSTALLINE CONTENT AND MOLECULAR WEIGHT  
-- DISTRIBUTION OF VARIOUS TEFLON RESINS,  
--10 - PERSONAL AUTHORS: FISHER, W. K. ;  
--11 - REPORT DATE: , 1981  
--12 - PAGINATION: 156P  
--20 - REPORT CLASSIFICATION: UNCLASSIFIED  
--21 - SUPPLEMENTARY NOTE: PH.D THESIS SUBMITTED TO SENNELAER  
-- POLYTECHNIC INSTITUTE.  
--22 - LIMITATIONS (ALPHA): APPROVED FOR PUBLIC RELEASE; DISTRIBUTION  
-- UNLIMITED. AVAILABILITY: UNIVERSITY MICROFILMS INTERNATIONAL, 300 N.  
-- ZEEB RD., ANN ARBOR, MI. 48106. ORDER 8121144.  
--33 - LIMITATION CODES: 1 24

--\*\*\*\*\*

-- END OF DISPLAY LIST

-- ((ENTER NEXT COMMAND))

8121144

FISHER, WILLIAM KEITH

EFFECTS OF IONIZING RADIATION ON THE CHEMICAL STRUCTURE,  
CRYSTALLINE CONTENT AND MOLECULAR WEIGHT DISTRIBUTION  
OF VARIOUS TEFLON RESINS

Rensselaer Polytechnic Institute

PH.D. 1981

University  
Microfilms  
International 300 N. Zeeb Road, Ann Arbor, MI 48106

PLEASE NOTE:

In all cases this material has been filmed in the best possible way from the available copy.  
Problems encountered with this document have been identified here with a check mark .

1. Glossy photographs or pages
2. Colored illustrations, paper or print \_\_\_\_\_
3. Photographs with dark background
4. Illustrations are poor copy \_\_\_\_\_
5. Pages with black marks, not original copy \_\_\_\_\_
6. Print shows through as there is text on both sides of page \_\_\_\_\_
7. Indistinct, broken or small print on several pages \_\_\_\_\_
8. Print exceeds margin requirements \_\_\_\_\_
9. Tightly bound copy with print lost in spine \_\_\_\_\_
10. Computer printout pages with indistinct print \_\_\_\_\_
11. Page(s) \_\_\_\_\_ lacking when material received, and not available from school or author.
12. Page(s) \_\_\_\_\_ seem to be missing in numbering only as text follows.
13. Two pages numbered \_\_\_\_\_ . Text follows.
14. Curling and wrinkled pages \_\_\_\_\_
15. Other \_\_\_\_\_

"EFFECTS OF IONIZING RADIATION ON THE CHEMICAL STRUCTURE,  
CRYSTALLINE CONTENT AND MOLECULAR WEIGHT DISTRIBUTION OF  
VARIOUS TEFLON<sup>®</sup> RESINS"

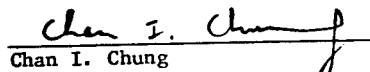
by

W. Keith Fisher

A Thesis Submitted to the Graduate  
Faculty of Rensselaer Polytechnic Institute  
in Partial Fulfillment of the  
Requirements for the Degree of  
DOCTOR OF PHILOSOPHY  
Major Subject: Nuclear Engineering

Approved by the  
Examining Committee:

  
John C. Corelli, Thesis Adviser

  
Chan I. Chung

  
James A. Moore

  
Max L. Yeater

Rensselaer Polytechnic Institute  
Troy, New York

May 1981

## Table of Contents

	<u>Page</u>
List of Figures . . . . .	iv
List of Tables . . . . .	viii
Acknowledgement . . . . .	ix
Abstract . . . . .	x
I. Introduction . . . . .	1
II. Description of PTFE Systems . . . . .	6
II.1. Molecular and Chain Structure of PTFE . . . . .	6
II.2. Crystal Structure of PTFE . . . . .	7
II.3. Molecular Weight and Molecular Weight Distribution . . . . .	10
III. Experimental Apparatus and Procedures . . . . .	13
III.1. Radiation Equipment . . . . .	13
III.2. Heat Treatment Apparatus . . . . .	15
III.3. Density Measurements . . . . .	16
III.4. Infrared Transmittance Measurements . . . . .	19
III.5. Melt Viscosity . . . . .	20
III.6. X-Ray Diffraction . . . . .	21
III.7. Differential Scanning Calorimetry . . . . .	22
IV. Results . . . . .	24
IV.1. Infrared Results . . . . .	24
IV.2. Melt Viscosity Results . . . . .	29
IV.3. Results of Density Measurements . . . . .	33
IV.4. X-Ray Diffraction Results . . . . .	35
IV.5. Differential Scanning Calorimetry Results . . . . .	36
V. Discussion . . . . .	38
V.1. Infrared Results . . . . .	38
V.2. Discussion of Melt Viscosity Results. . . . .	52
V.3. Discussion of Density Results . . . . .	68
V.4. Discussion of X-Ray Diffraction Results . . . . .	71
V.5. Discussion of DSC Results . . . . .	73
VI. Summary and Conclusions . . . . .	78
References . . . . .	83
Appendix A . . . . .	144

List of Figures

<u>Figure</u>	<u>Page</u>	
1	Point net projection of the 1*13/6 helix of PTFE in the low temperature (<19°C). Each successive step involves rotation by 166.2° and a movement along the Z axis of 1/13 of the unit cell length. Between 19°C and 30°C the helix becomes 1*15/7 where each successive step involves rotation by 168° and movement along the Z axis of 1/15 of the unit cell length. (Taken from reference 40, page 73). . . . .	87
2	Schematic diagram of a PTFE spherulite (Taken from reference 11). . . . .	88
3a	PTFE irradiation geometry	
3b	Irradiation chamber used for vacuum and wet and dry oxygen irradiations. . . . .	89
4	Radiation dose calibration curve. . . . .	90
5	Thermal quenching apparatus. Sample is heated to 380°C then the clamp is released allowing the metal rod with the sample material to be quenched in either liquid nitrogen or water. . . . .	91
6	Post-Irradiation Annealing Apparatus view of the furnace with front panel removed. . . . .	92
7	Density Gradient Column. Shown with filling apparatus in place. After column is filled the capillary is removed and the column placed in a constant temperature bath held at 23 ± 0.3°C. . . . .	93
8	Powder resin wetting apparatus . . . . .	94
9	Schematic diagram of the Instron Capillary Rheometer . . .	95
10	IR spectrum between 2200 and 1300 cm <sup>-1</sup> of quenched Teflon <sup>®</sup> resin 7A irradiated to 43 MRads in a partial vacuum (1.5x10 <sup>-4</sup> torr). . . . .	96
11	IR spectrum between 2100 and 1300 cm <sup>-1</sup> of quenched Teflon <sup>®</sup> resin 7A irradiated to 43 MRads in ambient air. . . . .	97
12	IR spectra between 2000 and 1300 cm <sup>-1</sup> of PTFE sheet irradiated to 43 MRads in wet and dry oxygen. . . . .	98
13	IR spectrum between 2000 and 1300 cm <sup>-1</sup> of quenched Teflon <sup>®</sup> resin 7A irradiated to 43 MRads in an oxygen atmosphere then stored 5 days in the oxygen atmosphere. Also shown is the IR spectrum of the same sample after storage for 35 days in ambient air. . . . .	99

List of Figures Cont'd

<u>Figure</u>		<u>Page</u>
27	Plots of log apparent melt viscosity vs. log apparent shear rate measured at 350°C for samples of Teflon <sup>®</sup> resins 7A, 6 and 6C and PTFE sheet irradiated to 5 MRads in air. . . . .	113
28	Plots of log apparent melt viscosity vs. log apparent shear rate measured at 350°C for samples of Teflon <sup>®</sup> resins 7A, 6 and 6C and PTFE sheet irradiated to 10 MRads in air. . . . .	114
29	Plots of log apparent melt viscosity vs. log apparent shear rate measured at 350°C for samples of Teflon <sup>®</sup> resins 7A, 6 and 6C and PTFE sheet irradiated to 25 MRads in air. . . . .	115
30	Plots of log apparent melt viscosity vs. log apparent shear rate measured at 350°C for Teflon <sup>®</sup> resin 6 irradiated to doses of 2.5, 5, 10 and 25 MRads in air. . . . .	116
31	Plots of log apparent melt viscosity vs. log apparent shear rate for Teflon <sup>®</sup> resin 6C irradiated to doses of 2.5, 5, 10 and 25 MRads in air. . . . .	117
32	Plots of log apparent melt viscosity vs. log apparent shear rate measured at 350°C for Teflon <sup>®</sup> resin 7A irradiated to doses of 2.5, 5, 10 and 25 MRads in air. . . . .	118
33	Plots of log apparent melt viscosity vs. log apparent shear rate measured at 350°C for PTFE sheet irradiated to doses of 5, 10 and 25 MRads in air. . . . .	119
34	Plots of apparent melt viscosity vs. dose at an apparent shear rate of 0.404 sec <sup>-1</sup> measured at 350°C for Teflon <sup>®</sup> resins 6 and 7A. . . . .	120
35	Plots of apparent melt viscosity vs. dose at an apparent shear rate of 4.04 sec <sup>-1</sup> measured at 350°C for Teflon <sup>®</sup> resins 6 and 7A. . . . .	121
36	Plot of apparent melt viscosity vs. dose measured at 350°C for PTFE sheet at an apparent shear rate of 40.37 sec <sup>-1</sup> . . . . .	122
37	Plot of apparent melt viscosity vs. dose measured at 350°C for PTFE sheet at an apparent shear rate of 0.404 sec <sup>-1</sup> . . . . .	123
38	Extrudate samples of Teflon <sup>®</sup> resin 6. . . . .	124
39	Extrudate samples of Teflon <sup>®</sup> resin 7A. . . . .	125

List of Figures Cont'd.

<u>Figure</u>		<u>Page</u>
40	Example of a twisted extrudate. . . . .	126
41	Example of an extrudate exhibiting screw dislocations. .	127
42	Plots of log apparent melt viscosity vs. log apparent shear rate for Teflon <sup>®</sup> resin 7A irradiated to 25 MRads in air taken at capillary temperatures of 335°C 350°C and 380°C. Also shown is a plot for resin 7A irradiated to 10 MRads in air determined at a capillary temperature of 380°C. . . . .	128
43	Effect of storage time in the rheometer barrel at 380°C and differences in pre-irradiation crystallinity in the post-irradiation melt viscosity for Teflon <sup>®</sup> resin 6. .	129
44	Density vs. dose for PTFE sheet irradiated in air. . . .	130
45	Density vs. post-irradiation annealing time at 300°C for PTFE sheet irradiated to 10 MRads in air. . . . .	131
46	Density vs. post-irradiation annealing time at 200°C for samples of PTFE sheet irradiated to various doses in air.	132
47	Density vs. post-irradiation annealing time at 300°C for samples of PTFE sheet irradiated to various doses in air.	133
48	Density vs. IR absorbance at 775 cm <sup>-1</sup> for samples of PTFE sheet irradiated in air. . . . .	134
49	X-ray diffraction scan of unirradiated PTFE sheet. . .	135
50	X-ray diffraction scan of PTFE sheet irradiated to 10 MRads in air. . . . .	136
51	X-ray diffraction scan of PTFE sheet irradiated to 10 MRads in air then annealed for 1 hour 10 minutes at 298°C in air. . . . .	137
52	Composite heat of transition endotherm for the transitions at 302°K and 312°K for unirradiated PTFE sheet. .	138
53	Heat of fusion endotherms for PTFE sheet irradiated to the indicated doses in ambient air. . . . .	139
54	IR spectrum between 1000 and 600 cm <sup>-1</sup> of unirradiated PTFE sheet determined at the indicated temperatures. . .	140

List of Tables

	<u>Page</u>
Table 1: Infrared Absorption Band Assignments . . . . .	141
Table 2: Flow Index Values . . . . .	142
Table 3: DSC Results . . . . .	143

#### ACKNOWLEDGEMENT

The author wishes to thank Professor John Corelli for his guidance and assistance throughout the course of this work. His support and encouragement during this research is especially appreciated.

Special thanks are extended to Professors Chan Chung, James Moore, Bernhard Wunderlich and Max Yeater for their helpful suggestions and discussions. The use of Professor Wunderlich's differential scanning calorimetry apparatus and Professor Chung's capillary rheometer is especially appreciated. Thanks are also due to Mr. Allan Fenwick of the Instron Corporation for the use of their laboratory facilities to make some of the melt viscosity measurements and to Professor Richard Harper of the Physics Department for the x-ray diffraction measurements.

The author would like to thank Mrs. Marilyn Mamone for her typing of the manuscript.

Most sincere thanks and gratitude are extended to the author's parents for their support and sacrifice throughout all stages of his higher education.

Financial support for this work was provided by Radiation Dynamics Incorporated and is gratefully acknowledged.

### ABSTRACT

Changes in the chemical composition, crystalline content and structure, flow properties and molecular weight distribution in polytetrafluoroethylene (PTFE) after exposure to ionizing radiation are described. The radiation used in this work was 0.8 MeV electrons. The effects of post-irradiation annealing on the chemical composition and crystalline content are also analyzed. Radiation-induced changes in the chemical composition and the role of oxygen and water vapor in these changes was determined by infrared spectroscopy of PTFE irradiated in ambient air, wet and dry oxygen atmosphere and under vacuum. It was found that when the irradiations are carried out in the presence of oxygen, acid fluoride endgroups are formed and that, upon exposure to water vapor, these endgroups undergo hydrolysis to form carboxylic acid endgroups. Infrared absorption bands at 1730 and 1715  $\text{cm}^{-1}$ , which appear most strongly when PTFE is irradiated in a vacuum, have been attributed to branch and crosslink formation. A set of reactions which rationalize the observed chemical changes are given. It was found that the crystalline content of PTFE increases after exposure to ionizing radiation. Changes in the crystalline content were monitored using infrared spectroscopy, density measurements, x-ray diffraction measurements on unoriented samples, and differential scanning calorimetry (DSC). A linear relation between density and the infrared absorbance at 775  $\text{cm}^{-1}$  for irradiated PTFE was found. X-ray diffraction and DSC measurements show that crystals formed after exposure to ionizing radiation are less perfect and different in nature from melt

crystallized PTFE. Changes in the melt viscosity of PTFE exposed to various radiation doses in air were measured using a capillary rheometer. It was found that the melt viscosity decreases dramatically after exposure to 2.5 MRads but between 2.5 and 5 MRads there is an increase in viscosity which is attributed to the formation of branches and crosslinks. Above 5 MRads the melt viscosity decreases with dose. Plots of log apparent melt viscosity vs. log apparent shear rate are given for PTFE exposed to various radiation doses. The data in each of these plots can be fit by a straight line (power law) and changes in the slopes of these lines are interpreted to indicate changes in the molecular weight distribution. It is postulated that the observed decrease in the slopes of these lines after irradiation is caused by a narrowing of the molecular weight distribution because of a decrease in the number of molecules at the high molecular weight end of the distribution. It was found that the melt viscosity of a PTFE sample irradiated to a given dose was less for a sample of low pre-irradiation crystallinity than for an otherwise identical sample of higher crystallinity. Also, the number of acid fluoride endgroups formed after irradiation is increased by lowering the pre-irradiation crystallinity of the sample. This crystallinity-dependence of viscosity and endgroup formation is related to differences in oxygen diffusion properties of crystalline and amorphous PTFE.

## Part I

### Introduction

The use of electron beam (EB) radiation in industrial processes is a rapidly expanding field. Electron beam radiation provides an efficient alternative to heat and/or chemical means to modify chemical and physical properties of various polymers. It is presently used to improve the properties of existing products and in some cases has provided the basis for entirely new products. A prime example of a new product which can be produced economically only through the use of EB radiation is the production of very fine, powdered polytetrafluoroethylene (PTFE) from previously sintered material. The common trade name for DuPont's PTFE polymer is Teflon.<sup>®</sup> Other important radiation processes currently in industrial use are the following:

- a) crosslinking of plastics especially for wire and cable insulation;
- b) curing of rubber for use in tires, sheets, and hoses;
- c) sterilization of medical disposable products, e.g. sutures, syringes, bandages;
- d) preparation of composites based on plastic and wood.
- e) polymer grafting to produce conducting paths of high spatial resolution ( $<0.2\mu\text{m}$ ) for use in very large scale intergrated (VLSI) circuits.

The growth in the use of EB radiation in industrial processes is largely because it is less expensive than conventional means of carrying out specific processes such as curing rubber,

modifying the properties of plastics, and sterilizing medical disposable products. The cost breakthrough has been achieved via the development of high power, dependable, electron beam accelerators. Previously, the chief source of ionizing radiation for the processing of various polymers was  $\text{Co}^{60}$  gamma rays. The gamma rays produced by a  $\text{Co}^{60}$  source are highly penetrating, so that large objects may be exposed to the gamma rays and have about the same energy deposited per unit mass at every point in the object (i.e. the dose distribution will be fairly uniform). The problem with a  $\text{Co}^{60}$  source is the low rate of energy deposition per unit mass of material being irradiated (low dose rate). In a typical  $\text{Co}^{60}$  source having total gamma ray power output of approximately 15 watts, doses on the order of 10 megarads (MRads)\* can be accumulated in the course of one day's irradiation.(1) With the electron beam accelerators presently available, dose rates on the order of 1 MRad per second are easily attainable. The problem with electrons is that their penetrating power is much less than that of gamma rays. To overcome this problem the electrons are accelerated through very high voltages (usually between 0.5 to 10 MeV) so that their range in the material being irradiated is increased. Thus the high dose rate coupled with the sufficient penetration range of the energetic electrons enables the product throughput rate to be increased dramatically over that of  $\text{Co}^{60}$  sources thereby reducing the treatment costs per unit of product. Electron beam accelerators with power outputs up to 150KW are at present commercially available. The rising cost of thermal energy favors the use of EB processing because the total energy demand for radiation treatment is less than that consumed

---

\* A dose of 1 Rad is equivalent to 100 ergs of energy deposited per gram of material being irradiated.

in thermal treatment.(2)

Examples of the efficiency of EB processing of polymers can be found in the vulcanization of rubber and butyl which, by conventional techniques, requires about 100 times the energy of the equivalent radiation process: Electron beam radiation curing of acrylic coatings on plastic or wood backings requires about 1% of the energy consumed in the equivalent thermal process. Also the radiation sterilization of medical disposable products, a process which has already achieved widespread industrial use, is much cheaper and avoids the mutagenic and industrial safety problem associated with the conventional ethylene oxide sterilization procedure.(3)

The motivation for the research reported herein came from work done here at RPI and also at Radiation Dynamics, Inc. (Mellville, New York) on a process for degrading previously sintered PTFE using EB radiation so that it can be ground into a fine powder (<10 $\mu$ m particle size). Electron beam radiation had to be used to degrade the PTFE because of the extremely high resistance of PTFE to thermal or chemical degradation. Even at elevated temperatures for long periods of time fuming sulfuric acid and nitric acids, aqua regia, hydrofluoric acid, strongly alkaline solutions, and hydrogen peroxide have no effect on the polymer. Although over several hundred solvents have been tested, none have been found to dissolve or even swell PTFE below 300 $^{\circ}$ C. Polytetrafluoroethylene also has extreme thermal stability and can be used continuously at 260 $^{\circ}$ C with no measurable degradation. Despite its chemical and thermal stability, PTFE degrades readily when exposed to ionizing radiation as manifested by a dramatic decrease in melt viscosity, losses in tensile strength, a large reduction in the zero

strength time (38), and reduction of the ultimate elongation.(45)

The sample material used in this work was unsintered DuPont PTFE resins 6, 6C and 7A. Also sintered, 0.005" thick PTFE sheet obtained from the American Durafilm Company was analyzed. This film was also made from DuPont PTFE material.

The purpose of this dissertation is to investigate the changes in chemical structure, crystalline structure, and in the flow properties of PTFE induced by ionizing radiation. The goal was to construct a model, utilizing a wide range of measurement techniques, that explains the observed property changes in PTFE after exposure to various doses of ionizing radiation and under different ambient conditions of O<sub>2</sub>, water vapor et cetera.

The ionizing radiations used throughout this work consisted of 0.8 MeV electrons. To investigate the effect of oxygen and water vapor on the property changes of PTFE induced by radiation, irradiations are carried out in ambient air, in a dry oxygen atmosphere, in a wet oxygen atmosphere, and under a partial vacuum. Also, the pre-irradiation crystalline content is varied to see the effect of this parameter on the final post-irradiation properties. The techniques employed to monitor the radiation effects are infrared spectroscopy, density measurements, x-ray diffraction measurement, melt viscosity determinations, and differential scanning calorimetry.

The infrared spectroscopy measurement will yield information on the radiation induced chemical changes in PTFE and also information on the crystalline content. Density measurements provide an easy way to get quantitative estimates on radiation induced changes in the crystalline content of a polymer sample since, for a given polymer, the density in the crystalline form is greater than in the amorphous

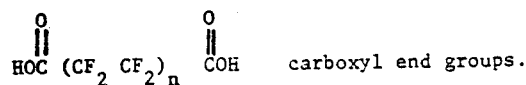
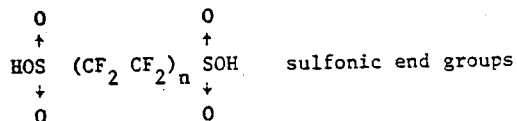
form. Also x-ray diffraction measurements and heat of fusion determinations using differential scanning calorimetry will yield information on relative changes in crystalline content brought about by exposure to ionizing radiation. The well ordered crystalline phase of PTFE gives a sharp x-ray diffraction peak. Changes in the full width at half maximum of this peak is indicative of changes in crystalline perfection. Because radiation created defects in crystalline material yielding less perfect crystals, one would expect the full width at half maximum of the crystalline diffraction peak to increase. Coupled with the increase in full width at half maximum the appearance of low temperature melting peaks in the differential scanning calorimetry scan of the irradiated sample due to the melting of the less perfect crystals is to be expected. Melt viscosity gives a relative indication of radiation induced changes in molecular weight. Since radiation causes chain scission in PTFE, resulting in a lower average molecular weight, the melt viscosity should decrease upon irradiation.

## Part II

### Description of PTFE Systems

#### II.1 Molecular and Chain Structure of PTFE

Polytetrafluoroethylene is a linear polymer consisting of the repeat group - (CF<sub>2</sub>-CF<sub>2</sub>-). A single polymer molecule may have on the order of tens to several hundreds of thousands of these repeat units connected together in a linear fashion. The polymerization of the tetrafluoroethylene monomer (CF<sub>2</sub>=CF<sub>2</sub>) proceeds via free radical addition polymerization with respect to the initiation and propagation steps. Termination by the combination of free radicals on the ends of two growing polymer chains seems to be the most favorable mechanism for the termination step.(5) The end groups on each PTFE molecule probably consist of two sulfonic or two carboxyl groups depending on the type of initiator used.(6)



Polytetrafluoroethylene is a linear, unbranched, non-crosslinked polymer because of its sharp melting point, its high degree of crystallinity as polymerized, and its ability to be oriented. As polymerized, unmelted PTFE has a crystallinity in the range between 93% and 98%. To achieve such a high degree of crystallinity the molecules must be able to pack very tightly together. This strongly

suggested the absence of any branching which would tend to inhibit tight packing. Chain branching is considered unlikely because this would involve the rupture of the strong carbon-fluorine bond, which is reported to have a bond strength of about 110 kcal/mol.(5)

## II.2. Crystal Structure of PTFE

As with many solid polymers, PTFE exhibits macroscopic properties which are intermediate between those expected of the perfectly crystalline and completely amorphous polymer. Traditionally, these intermediate properties are explained on the basis that polymers are a mixture of crystalline and amorphous regions, the fraction of material in the crystalline phase being called the "degree of crystallinity" or merely the crystallinity. It is possible to define either a weight fraction or volume fraction crystallinity. This crystal-amorphous or two-phase model is only a useful approximation to describe the actual polymer crystal structure. In reality there is no sharp division between the crystalline and amorphous phase but rather there exists a continuous spectrum of "degrees of order" between the perfectly crystalline and completely amorphous phases. No single, experimentally-determined parameter is sufficient to completely describe the crystallinity of a polymer. In the case of PTFE however, the amount of material in the transition region between the crystalline and amorphous phases is small (not more than 2 or 3 percent of the mass of the sample) so that the assumption of a two-phase model is quite good and crystallinity values obtained by various experimental techniques (x-ray diffraction, density heat of fusion, etc.) should be similar.(44)

Polytetrafluoroethylene exhibits two first order crystalline transitions below its melting temperature, one at 19°C and the other at 30°C. Below 19°C the chain conformation is that of a zig-zag arrangement that has been given a twist of 180° per 13 carbon atoms (a 1\*13/6 helix). The repeat unit contains 13 CF<sub>2</sub> groups with a repeat distance of 16.9 Å. The unit cell is triclinic. The molecules pack in the lateral direction like cylindrical rods in a nearly hexagonal arrangement with a nearest neighbor repeat distance of 5.62 Å. At the 19°C transition the chain helix relaxes somewhat so that between 19°C and 30°C transition the chain helix relaxes somewhat so that between 19°C and 30°C there are 15 CF<sub>2</sub> groups per 180° (a 1\*15/7 helix) twist in a zig-zag conformation. The unit cell is trigonal with a lateral chain axis separation of 5.66 Å. Both types of unit cells contain only one chain.(40) Between 19°C and 30°C the molecular segments undergo small angular displacement about their long axis with respect to a preferred direction perpendicular to the chain axis. Above the 30°C transition the amplitude of motion of the individual chain segments increases to the point where all order along the chain axis is lost. The separation between neighboring molecular chains increases and the packing in the lateral direction exhibits trigonal symmetry. Above the 30°C transition there is crystalline regularity of molecular chains only in two dimensions (in the plan oriented at right angles to the chain axis). This trigonal packing in the lateral direction is retained up to the melting point. (6,40,43,44)

Polytetrafluoroethylene is remarkable in that it is very highly crystalline as polymerized (93-98% crystallinity). The origin of this high crystallinity in samples that have not been previously melted is that the polymer chains are almost fully extended (although

some chain folding does exist) so that most of the molecular segments can pack very tightly side by side like rigid rods. This form of PTFE, i.e. unmelted, has such poor mechanical properties that it is usual to sinter pre-formed objects at about 380°C to make commercial products. (8) If specimens of PTFE are cooled slowly from the sintering temperature the polymer will recrystallize, the ultimate crystallinity being greater the more slowly the object is cooled, although it will rarely reach that of the unsintered resin. The ultimate crystallinity of sintered PTFE is rarely as high as that of the unsintered material because the amount of chain folding increases upon recrystallization from the melt. The originally nearly fully extended helical molecules are, after sintering, packed into chain-folded crystals in which, after a succession of repeat units (up to a few hundred) in a regular helical conformation the molecular chain folds back in the opposite direction and once again packs regularly. The folds, where the molecule bends back, lie on a regular surface and a sintered specimen consists of an assembly of these folded chain lamellae, together with interlamellar material which is assumed to be conformationally irregular (amorphous). Because of the interlamellar amorphous material and the chain folds, which contain a substantial number of repeat units not packed regularly parallel to other portions of the molecular chain, the crystallinity of sintered material is usually less than of unsintered material.

The lamellar structure is revealed by studying fracture surfaces of PTFE using scanning electron microscopy. The structure revealed on the fracture surfaces consists of long, but rather thin, narrow bands containing fine parallel striations perpendicular to the band length. These bands are the lamellae mentioned above with the

polymer chains parallel to the striations. Typical dimensions of this lamellar structure are 100  $\mu\text{m}$  in length by 0.2-1  $\mu\text{m}$  in width with about 300 $\text{\AA}$  separation between striations.(10) The width of the lamellae corresponds to the distance between chain folds. Even though the molecular chains of sintered PTFE are folded they are still considered to be extended chain molecules if the spacing between fold surfaces is 2000 $\text{\AA}$  or greater.(11)

From microstructure studies on fracture surfaces it has been found that the extended chain lamellae of PTFE grow radially outward from a central point. These spherulitic structures are commonly 10-25 $\mu\text{m}$  in diameter (Figure 2). The lamellae are observed to get thicker with increasing radial distance from the central growth point. The spherulitic order is initially maintained by lamellar thickening, but at larger radial distances it is disrupted by an increase in the number of lamellae with different orientations. These lamellae grow from the fold surface of the radially oriented parent lamellae and are oriented almost perpendicularly to the larger parent lamellae.

### II.3. Molecular Weight and Molecular Weight Distribution

In general, a polymeric sample consists of molecules having many different chain lengths so that it cannot be characterized by a single molecular weight value. Instead, there is a distribution of molecular weights and various averages or moments can be defined to describe this distribution.

The first moment of a molecular weight distribution is the number-average molecular weight  $\bar{M}_n$  and is given by:

$$\bar{M}_n = \frac{\sum_{i=1}^{\infty} N_i M_i}{\sum_{i=1}^{\infty} N_i} \quad \text{II.3.1.}$$

where  $N_i$  is the number of molecules of molecular weight  $M_i$  in a sample of known mass. The number-average usually lies near the peak or most probable molecular weight in the distribution.

The second moment is known as the weight-average molecular weight  $\bar{M}_w$  and is given by:

$$\bar{M}_w = \frac{\sum_{i=1}^{\infty} N_i M_i^2}{\sum_{i=1}^{\infty} N_i M_i} \quad \text{II.3.2.}$$

Except for a monodisperse system (one which can be characterized by a single molecular weight value) the weight-average molecular weight is greater than the number-average.

The ratio  $\bar{M}_w/\bar{M}_n$  is often used as a measure of the breadth of the molecular weight distribution and is called the polydispersity of the system. A sample which cannot be described by a single value of molecular weight is known as a polydisperse system.

The determination of molecular weight averages for PTFE poses problems which are not encountered in most other polymers. Both these polymers are insoluble at moderate temperatures, and the usual methods for determining molecular weight, which employ dilute solutions, are not applicable. Quantitative estimates of the number-average molecular weight of PTFE have been obtained by measuring the number of endgroups derived from a polymerization initiation system containing radioactive sulfur,  $S^{35}$ . For the PTFE resins used in this work estimates of the number-average molecular weight are given

below:(29)

Resin 6 : 2 to 5 x 10<sup>6</sup> Daltons

Resin 7A 50 to 500 x 10<sup>6</sup> Daltons

As can be seen, both are high molecular weight resins and that only a range of molecular weight values can be determined.

### Part III

#### Experimental Apparatus and Procedures

##### III.1. Radiation Equipment

The radiation source was a 0.5 to 0.8 MeV cathode ray accelerator built by the General Electric Company in 1939. The accelerating principal is based on the resonant transformer concept. (12) The dose rate used in this work was about 1 MRad/min.

The dosimetry was carried out using thin film cellophane dosimeters provided by the Westinghouse Electric Corporation. Upon exposure to ionizing radiation the optical density of the dosimeter decreases, the decrease being proportional to the dose received. A calibration curve provided with the dosimeters relates the change in optical density to the dose in megarads. The change in optical density (optical density before minus optical density after irradiation) was measured at 655nm using a Bausch and Lomb Spectronic 20 spectrophotometer.

The dosimetry measurements were carried out using exactly the same arrangement as was used for the PTFE irradiations except that a thin film dosimeter was irradiated instead of sample material. Figure 3 shows the irradiation geometry.

A series of irradiations to various doses were carried out and the resulting collected charge measured on the charge integrator, which was located at the accelerator control panel. A plot of dose vs. collected charge was then made and this plot served as the dose calibration for all irradiations. Figure 4 shows this plot.

The sample irradiation geometry used in these experiments was either a thin film of PTFE (0.005 to 0.010 inches) or a thin layer of

unsintered PTFE powder. It is desirable to have a sample thickness small compared to the range of the electron beam in the material being irradiated ( $\sim 2$ mm) so that the dose distribution throughout the thickness of the sample is essentially uniform. In this case, the dose as measured by the thin film cellophane dosimeters can be directly related to the dose received by the sample material.

The ambient air irradiations were carried out by placing the sample material in a 6 cm diameter Petri dish located 13 cm below the beam exit window. For the irradiations in wet and dry oxygen and in vacuum the irradiation chamber shown in Figure 3 was constructed. The Petri dish used in the ambient air irradiations was replaced by the irradiation chamber when an irradiation in oxygen or vacuum was required, otherwise the irradiation geometry was the same as for the ambient air irradiations.

The dry oxygen used for these experiments was ultra-high purity, with less than 3ppm of water vapor. Other contaminants which may be present in trace amounts are Kr, Ar,  $N_2$ , He, methane and other hydrocarbons. The wet oxygen irradiations were accomplished by slowly bubbling oxygen through a wash bottle filled with distilled water. One day prior to the oxygen irradiation the chamber, with the sample in place, was evacuated to less than 1 torr and this vacuum was maintained until shortly before the irradiation. The chamber was then filled with wet or dry oxygen so that the pressure inside the chamber was about 3 psi greater than atmospheric pressure. After irradiation the sample was maintained in the wet or dry oxygen atmosphere for 3 days before analysis.

For the vacuum irradiations the chamber was evacuated to about  $10^{-4}$  torr and the sample was stored under this vacuum for two days prior to the irradiation. After the irradiation at  $10^{-4}$  torr the sample was stored for 3 days under this vacuum before being removed for analysis.

### III.2. Heat Treatment Apparatus

A schematic diagram of the pre-irradiation thermal quenching apparatus is shown in Figure 5. The purpose of the pre-irradiation thermal quench was to lower the crystallinity of the sample material so that the effect of initial crystalline content on the resultant radiation response of the material could be investigated. The sample was heated to about  $380^{\circ}\text{C}$  and maintained at this temperature for 15 minutes. The metal rod from which the sample was suspended was then released by loosening the clamp causing the sample to fall into either a liquid nitrogen or cold water bath. When unsintered PTFE resin is quenched from  $380^{\circ}\text{C}$  in either cold water or liquid nitrogen the crystallinity is about 1/3 its initial value (as measured by differential scanning calorimetry).

The post-irradiation annealing apparatus is shown schematically in Figure 6. The purpose of this heat treatment was to investigate the effects of thermal annealing for different amounts of time on the ultimate density of PTFE irradiated to various doses. The on-off temperature controller was able to control the oven temperature to  $\pm 1^{\circ}\text{C}$ . The temperature was measured using a copper-constantan thermocouple suspended in the center of the furnace and referenced to room temperature. A Leeds and Northrup millivolt potentiometer was used to monitor the junction potential.

### III.3. Density Measurements

In PTFE the density of the crystalline phase ( $\rho_c$ ) is greater than that of the amorphous phase ( $\rho_a$ ). This is because the molecular chains in the crystalline region pack more tightly than do the randomly oriented chains (or portions of chains) in the amorphous phase. As the degree of crystallinity increases so does the density of the sample as a whole ( $\rho_a + \rho_c$ ). Thus the density of a sample is an indication of the crystalline content.

A degree of crystallinity by mass ( $\alpha_m$ ) can be determined from the observed density, assuming a two-phase model. Let  $v_c$  and  $v_a$  be the specific volumes of the crystalline and amorphous regions respectively and let  $v$  be the total specific volume of the sample. Then

$$v = \alpha_m v_c + (1 - \alpha_m) v_a \quad \text{III.3.1.}$$

solving for  $\alpha_m$  yields

$$\alpha_m = \frac{v - v_a}{v_c - v_a} = \frac{\frac{1}{\rho} - \frac{1}{\rho_a}}{\frac{1}{\rho_c} - \frac{1}{\rho_a}} \quad \text{III.3.2.}$$

where  $\rho$  is the measured density.

Similarly one can calculate a degree of crystallinity by volume  $\alpha_v$

$$\alpha_v = \frac{\rho - \rho_a}{\rho_c - \rho_a} \quad \text{III.3.3.}$$

For PTFE  $\rho_c = 2.301 \text{ g/cm}^3$  and  $\rho_a = 2.004 \text{ g/cm}^3$  (30).

To make precise density measurement a density gradient column was used (Figure 7). The column contains a liquid the density

of which increases linearly from top to bottom. The liquid consists of the following organic solvents the densities of which are suitable to make a column covering the entire range of densities of PTFE:

<u>Solvent</u>	<u>Density (g/cm<sup>3</sup>)</u>
1,3 dibromopropane	1.979
Ethylene Bromide	2.170
Bromoform	2.876

The solvents used to make up the column must not dissolve or swell the samples but must completely wet them. By mixing appropriate amounts of these solvents one can obtain a density gradient ranging from 1.979 g/cm<sup>3</sup> to 2.876 g/cm<sup>3</sup>.

To fill the column about 500 ml of the less dense liquid is placed in the flask closest to the graduated cylinder which will contain the density gradient. The same amount of the more dense liquid is placed in the flask furthest from the density gradient column. The magnetic stirrer is started and both stopcocks are opened. The less dense liquid flows through the capillary tube and into the bottom of the column. As time goes on the liquid being fed into the bottom of the column gradually gets more dense, thus a density gradient is formed with the lowest density on top and the highest density at the base. If the liquid levels in each flask are kept approximately the same then a linear density gradient results. A typical filling time is about 30 minutes. A single column should retain its linearity in density for a period of a month or more.

After filling the column, small glass calibration beads of known density are dropped into the column along with the sample the

density of which is to be determined. A plot of density vs. bead position is constructed using a cathetometer so that by measuring the position of the sample in the column its density can be obtained. The density gradient column is immersed in a constant temperature bath maintained at  $23 \pm 0.03^{\circ}\text{C}$ .

To measure the density of sintered, pre-formed, void-free material all that need be done is to drop the sample into the column, let it settle, then determine its position. The measurement of virgin unsintered PTFE resin is somewhat more involved because this material is very porous and will not be completely wetted by the liquid in the column because of trapped air. The apparatus used to wet the unsintered PTFE powder is shown in Figure 8. The powder is inserted into a thick walled flask. The flask is then evacuated to about 0.5 torr. The valve on the pump line is closed and then the stopcock between the solvent reservoir and the thick walled flask is opened allowing solvent to enter the flask and wet the powder. The solvent used is the same as the least dense solvent in the density gradient column. After enough powder to make a density determination has settled to the bottom of the flask it is opened and some powder removed using a small cupfull of solvent and powder in such a way that the powder never comes in contact with air. This material is then carefully inserted into the top of the density gradient column. About one day should be allowed for the powder to settle in the column. If the powder has been properly wetted it should settle to a fairly narrow distribution of densities.

#### III.4. Infrared Transmittance Measurements

The chemical changes in PTFE induced by ionizing radiation were monitored using infrared spectroscopy. Radiation-induced chemical changes are characterized by the appearance of new absorption bands in the infrared spectrum of these resins. Changes in the crystalline content of both these polymers can be obtained using absorption bands which are characteristic of conformations found only in the amorphous phase. (9,13,14)

The infrared spectra were measured using a Perkin-Elmer Model 621 double-beam, grating spectrophotometer. The Model 621 is capable of covering the wavelength region from 2.5 to 50  $\mu\text{m}$  (4000 to 20  $\text{cm}^{-1}$ ), and employs the optical null method to obtain the transmittance of the sample.

In the optical null method, two infrared radiation beams are taken from the same source and, by means of a rotating mirror (chopper), each beam traverses the monochromator-detector system on alternating half cycles. If the two beams have the same intensity, a d.c. signal will be produced at the detector. If they are unbalanced, an a.c. signal results. The sample is placed in one beam and an optical attenuator (wedge), graduated from 0 to 100% transmission, is placed in the other (reference beam). The a.c. signal resulting from unbalance is used to drive the optical attenuator to achieve balance. At balance, the position of the attenuator is directly related to the transmittance of the sample and the position of the attenuator is recorded on a chart recorder as a percent transmittance. (15,16,17)

The samples used for infrared analysis consisted of 0.005" sheets of sintered PTFE. Samples of unsintered PTFE powder were pre-

pared for infrared analysis by cold pressing at 2000 psi for 3 minutes.

To investigate the infrared spectrum of PTFE sheet above its melting point ( $327^{\circ}\text{C}$ ) a cylindrical furnace with open ends was situated in the spectrophotometer such that the infrared beam could pass through it. A sample of PTFE sheet was mounted at the middle of the furnace. The temperature was measured using a copper-constantan thermocouple which was referenced to room temperature and connected to a Leeds and Northrup millivolt potentiometer.

### III.5. Melt Viscosity

The changes in melt viscosity induced in PTFE by ionizing radiation were measured using an Instron Model 3211 constant shear capillary rheometer system. Upon exposure to ionizing radiation the melt viscosity of PTFE decreases dramatically because of chain scission. The resulting decrease in melt viscosity is a measure of the amount of degradation taking place.

The Model 3211 consists of a heated barrel with a capillary at one end (Figure 9). The capillary used in this work was 0.1532 cm in diameter by 2.516 cm in length. The sample was packed into the cylinder and left to melt for 20 minutes prior to measurement. The material was then forced through the capillary at a constant shear rate using a plunger connected to a force transducer. The force necessary to push the material through the capillary at the constant shear rate was measured and from this measurement the shear stress at the capillary wall can be easily calculated. Knowing the shear stress and the shear rate the viscosity can be calculated (shear stress/shear rate). Viscosity measurements were made at 335, 350, and  $380^{\circ}\text{C}$ .

### III.6. X-Ray Diffraction

If a beam of x-ray impinges upon a crystalline, or partially crystalline solid, and the intensity of the diffracted beam is measured as a function of the angle of incidence, it is found that there are discrete peaks in the diffracted x-ray intensity distribution. These peaks are caused by constructive interference of x-ray beams scattered by various atoms in the solid. The condition that must be satisfied for this constructive interference to occur is that the path lengths along the incident beam from any given wavefront to any two atoms in the solid, and then in the direction of the diffracted beam to any other wavefront must be an integral number of wavelengths of the x-ray beam. This condition is stated mathematically by the Bragg Equation stated below:

$$n\lambda = 2d \sin\theta$$

where  $n$  is an integer,  $\lambda$  is the wavelength of the incident x-ray beam,  $d$  is the separation of the atoms and  $\theta$  is the angle between the incident x-ray beam and the surface of the sample. To obtain a strong diffraction peak many atoms must be regularly spaced and their spacing must satisfy the above condition. Regularly spaced atoms are found only in the crystalline phase of a semi-crystalline polymer. Thus comparisons of the intensity of the peaks caused by scattering by atoms in the crystalline phase (or the area under the peak) to the total area under the diffracted x-ray intensity vs. angle of incidence distribution is a measure of the crystalline content. Also the full width at half maximum of crystalline diffraction peaks gives an indication of crystallite size and degree of disorder in the

crystals. (41)

The x-ray diffraction measurements, were made with a General Electric GE 11 GN1 diffractometer using copper  $K_{\alpha}$  x-rays which have a wavelength of 1.54178 Å and a NaI(Tl) scintillation crystal detector. The sample material used for these measurements was sintered Teflon<sup>®</sup> PTFE sheet of 0.005" thickness. The sintered sheet was chosen for these experiments because of the ease of mounting the sample in the x-ray beam and because the sheet presents a flat uniform surface to the x-ray beam so that the diffraction peaks will not be displaced by surface curvature of the sample. All measurements were made at room temperature (above the 19°C transition of PTFE).

### III.7. Differential Scanning Calorimetry

The heat of fusion of a sample is the heat absorbed when the crystalline portion of the material melts. The heat of fusion is proportional to the amount of crystalline material present in the sample and can be used as a measure of the degree of crystallinity. The shape of the melting endotherm gives information on the type of crystals formed as a result of irradiation. To measure the heat of fusion a differential scanning calorimeter (DSC) was used.

In the type of DSC measurement used in this work a temperature monitoring circuit measures and controls the temperatures of the sample and reference holders (pans) to conform to a predetermined time-temperature program. This temperature is plotted on the x-axis of an x-y recorder. Simultaneously, a temperature-difference circuit compares the temperatures of the sample and reference holders, and proportions power to the heater in each holder to keep their temperatures equal. When the sample undergoes a thermal transition, the

power to the heaters is adjusted to maintain their temperatures, and a signal proportional to the power difference between the sample and reference pans is plotted on the y axis of the recorder. The area under the resulting curve is a direct measure of the heat of transition. (37)

In addition to the heat of fusion the low temperature transitions of PTFE at nominal temperatures of 19 and 30°C appears as a composite peak corresponding to absorption of heat (endotherm). Because these are crystalline transitions they can be used to yield information on the nature of radiation-crystallized material.

A Perkin-Elmer Model DSC-2 differential scanning calorimeter, operating at a heating rate of 20° K/min was used for the thermal analysis. The continuous transformation differential scanning calorimeter (DSC) analog output was transformed to digital form, suitable for further analysis, was accomplished through the use of an analog/digital converter (Perkin-Elmer). The interval between digital recording of DSC amplitude readings was 1.2 seconds. The temperature range over which the scans were made was 220°K to 650°K. At the conclusion of a measurement on the DSC, the data, stored on paper tape, were read by a tape reader (Hewlett Packard Model 2748B) into a computer (Hewlett Packard Model 9821A). A program using proportional base line evaluation was developed and is described together with detailed calibration on over 80 runs.(35). Heats of fusion could be reproduced to  $\pm 0.5\%$ . (36)

## Part IV

### Results

#### IV.1. Infrared Results

Figures 10 through 17 show the changes in the infrared (IR) spectrum of PTFE exposed to 43 MRads in a partial vacuum, in ambient air, and in wet and dry oxygen atmospheres. If one compares Figures 10 through 12 it is apparent that the peak at  $1880\text{ cm}^{-1}$  appears strongly when irradiations are carried out in ambient air and in wet and dry oxygen. Also this peak is more intense in dry oxygen than in wet oxygen. The absorption at  $1790\text{ cm}^{-1}$  increases slightly under all four irradiation conditions. In Figure 12, for the dry oxygen irradiations, it can be seen that the absorption band at  $1790\text{ cm}^{-1}$  becomes slightly broader on the long wavelength side. For the wet oxygen irradiation this same band broadens considerably on both the short and long wavelength sides. Figure 13 is a spectrum of PTFE irradiated to 43 MRads in dry oxygen and then stored for 35 days in ambient air. It can be seen that the absorption band at  $1880\text{ cm}^{-1}$  and  $1775\text{ cm}^{-1}$  increase in intensity so that this spectrum strongly resembles the wet oxygen spectrum shown in Figure 12. The IR spectrum of PTFE irradiated under a partial vacuum (Figure 10) shows two absorption bands appearing at  $1735$  and  $1715\text{ cm}^{-1}$ . These bands are much more intense in the vacuum irradiation than in either the air or oxygen irradiations. The absorptions at  $1548$ ,  $1450$ , and  $1425\text{ cm}^{-1}$  do not change significantly in any of the irradiations. The absorption shoulder at  $1345\text{ cm}^{-1}$  is reduced upon irradiation under all conditions except under vacuum where it changes very little.

Figures 14 and 15 show the portion of the IR region between

1000 and 200  $\text{cm}^{-1}$  for irradiations of virgin PTFE resin (Dupont resin 7A), which was cold pressed then quenched from the melt, then irradiated in vacuum (Figure 14) and in ambient air (Figure 15). Figures 16 and 17 show the IR region between 1000 and 200  $\text{cm}^{-1}$  for irradiations of PTFE sheet (0.005") carried out in dry and wet oxygen respectively. The absorption band at 375  $\text{cm}^{-1}$  is seen to decrease under all irradiation conditions, the decrease in intensity being more pronounced when the irradiation is carried out in air or in wet or dry oxygen than under vacuum. The absorption band at 270  $\text{cm}^{-1}$  decreases in intensity upon exposure to ionizing radiation, the most dramatic decrease occurring in the dry and wet oxygen irradiations (Figures 16 and 17 respectively) and the smallest decrease occurring in the vacuum irradiation (Figure 14). Concurrent with the decrease in absorption at 270  $\text{cm}^{-1}$  is an increase in absorption at about 286  $\text{cm}^{-1}$  in all irradiations. This increase in absorption at 286  $\text{cm}^{-1}$  is largest for the dry and wet oxygen irradiations and smallest in the vacuum irradiation. Examining Figures 16 and 17 one finds that there is a general decrease in absorption between 1000 and 700  $\text{cm}^{-1}$ . Especially important is the decrease in intensity of the band at 775  $\text{cm}^{-1}$  because the decrease in absorbance of this band has been linearly related to the increase in density of PTFE after exposure to ionizing radiation (see Figure 53).

Some other changes in the IR spectrum of irradiated PTFE which are not shown in Figures 10 through 17 are given below. In the ambient air irradiation and wet oxygen irradiations a sharp band appears at 2920  $\text{cm}^{-1}$ , a small band appears in the region between 2340

and  $2850\text{ cm}^{-1}$ , and a small absorption shoulder appears at  $980\text{ cm}^{-1}$ . In the spectra of the PTFE samples irradiated in air and especially wet oxygen, a sharp absorption band appears at about  $3550\text{ cm}^{-1}$ . The IR spectra of the samples irradiated in dry oxygen and in vacuum show no change in absorption at  $3550\text{ cm}^{-1}$  upon comparison to the spectra for the unirradiated control sample.

Figures 18 and 19 show the IR spectrum of unquenched, highly crystalline, PTFE before and after exposure to 43 MRads in ambient air. As in the quenched sample a strong absorption peak appears at  $1880\text{ cm}^{-1}$  (Figure 18). Again, as in the quenched sample irradiated in vacuum an absorption appears at  $1730\text{ cm}^{-1}$  and also a small increase in absorption occurs at about  $1715\text{ cm}^{-1}$ . The absorption peaks at  $1548$ ,  $1450$  and  $1425\text{ cm}^{-1}$  decrease in intensity with irradiation. It should be mentioned that upon irradiation of the unquenched sample the entire background transmittance level drops considerably, i.e., the sample as a whole is less transparent. In Figures 18 and 19 the spectrum of the irradiated sample was displaced upward on the figure to match as closely as possible the unirradiated spectrum. Thus it is not possible to say anything quantitatively about the radiation-induced change in the number of chemical species responsible for the absorptions at  $1790$ ,  $1548$ ,  $1450$  and  $1425\text{ cm}^{-1}$  on the basis of changes in intensities of these bands. One can say definitely that the absorption bands at  $1880$ ,  $1730$ , and  $1715\text{ cm}^{-1}$  are caused by radiation-induced chemical changes in the PTFE sample because prior to irradiation these peaks are not present in the spectrum and appear only after exposure to radiation.

Figure 19 shows the IR spectrum of unquenched PTFE in the range between 1000 and 200  $\text{cm}^{-1}$ . A small absorption at 960  $\text{cm}^{-1}$  is seen to appear upon irradiation. It is of interest to compare the region between 350 and 250  $\text{cm}^{-1}$  in Figure 19 to the corresponding region in Figure 15 (IR spectrum of quenched PTFE). The absorption bands between 350 and 310  $\text{cm}^{-1}$  in the spectrum for unirradiated material of Figure 15 are not apparent in the unirradiated sample spectrum in Figure 19 and there is no change in absorption in this region after irradiation. In the spectrum of the unquenched sample there occurs a strong absorption at 286  $\text{cm}^{-1}$  with shoulders at about 293 and 270  $\text{cm}^{-1}$ . This band shows little or no change upon irradiation which is in sharp contrast to the radiation-induced changes in the corresponding region of the quenched sample. Additionally, the band at 375  $\text{cm}^{-1}$  in the spectrum of the quenched sample which is observed to decrease in strength with irradiation (see Figure 15) appears only as an absorption shoulder in the unquenched sample and undergoes very little if any change upon irradiation.

Figures 20 and 21 show the effect of post-irradiation annealing in air on the IR spectrum of 0.005" PTFE sheet irradiated in air to 10 MRads. It can be seen in Figure 20 that the absorption band at 1880  $\text{cm}^{-1}$ , which is formed upon exposure to radiation in air, decreases in intensity with subsequent annealing and the absorption at 1790  $\text{cm}^{-1}$ , which increases in intensity with irradiation, increases still further with post-irradiation annealing. After annealing an absorption feature appears about 1715  $\text{cm}^{-1}$  and also at 1700  $\text{cm}^{-1}$ . The shoulder at 1345  $\text{cm}^{-1}$  partly disappears with just radiation and vanishes altogether after annealing. Figure 21 shows that the absorp-

tion throughout the entire region between 1000 and 200  $\text{cm}^{-1}$  decreases. It is interesting to note that the absorption band at 285  $\text{cm}^{-1}$  becomes more intense with respect to the band at 270  $\text{cm}^{-1}$  after annealing. Also the intensity of the band at 775  $\text{cm}^{-1}$  decreases considerably with post-irradiation annealing.

The effect of differences in the initial, pre-irradiation, crystalline content on the extent of the radiation-induced chemical changes in PTFE sheet as indicated by IR spectroscopy is indicated in Figure 22. Both spectra shown in Figure 22 were taken from samples of sintered, pre-formed, 0.005" thick PTFE sheet. The sample labeled "fast water quench" was heated to 380°C for 10 minutes then immediately immersed in cold water resulting in a much reduced degree of crystallinity as compared to the unquenched sample. The density of the quenched sample was 2.133 gm/cc as compared to 2.177 gm/cc for the unquenched sample. Figure 22 shows that the absorption band at 1880  $\text{cm}^{-1}$  is more intense in the fast-quenched, less crystalline sample, than in the unquenched sample. Both these spectra were taken immediately after irradiation.

The effect of storing irradiated 0.005" PTFE sheet in ambient air after irradiation to 125 MRads is shown in Figures 23 and 24. It can be seen from Figure 27 that the band at 1880  $\text{cm}^{-1}$  appears upon irradiation then decreases with time after irradiation. The absorption band at 1790  $\text{cm}^{-1}$  is seen to broaden considerably as a function of time after irradiation. No time-dependent effects were exhibited in the region between 1000 and 200  $\text{cm}^{-1}$ . The time dependent effects shown in Figure 23 are the same as those of Figure 13 where PTFE was irradiated in dry oxygen then stored for 35 days in ambient air.

Figure 24 is a plot of absorbance vs. time after irradiation for absorption bands at 3560, 1880, and 1775  $\text{cm}^{-1}$  for PTFE. This plot shows that the bands at 3560 and 1775  $\text{cm}^{-1}$  increase in intensity at the expense of the absorption band at 1880  $\text{cm}^{-1}$ .

Figure 25 is the IR spectrum of a sample of PTFE resin 7A which was annealed after having been stored in ambient air for 55 days after irradiation. Upon annealing the absorption bands at 1810 and 1780  $\text{cm}^{-1}$  disappear while there is little change in intensity at 1790  $\text{cm}^{-1}$ . This is in contrast to the spectra of the sample annealed immediately after irradiation, where the absorption at 1790  $\text{cm}^{-1}$  increased considerably.

The changes in the infrared spectrum produced by irradiating PTFE are indicative of chemical changes. These results show that the nature of the radiation induced chemical changes depends on the presence of oxygen and water vapor. Also, as will be discussed in Section V.1., the intensity of the absorption bands at 775, 375, 286 and 270  $\text{cm}^{-1}$  can be used as a measure of the relative crystalline content of various samples. These bands were seen to vary in intensity upon irradiation and post-irradiation annealing. It is interesting to note that the magnitude of the radiation induced change in the number of chemical groups responsible for the absorption at 1880  $\text{cm}^{-1}$  depends upon the initial, pre-irradiation crystallinity of the sample.

#### IV.2. Melt Viscosity Results

Figures 26 through 29 show plots of log apparent melt viscosity ( $\log \eta_a$ ) vs. log apparent shear rate ( $\log \dot{\gamma}_a$ ) for virgin Teflon<sup>®</sup> resins 7A, 6C, 6 and sintered PTFE sheet at 2.5, 5, 10, and 25 MRads respectively. The capillary temperature ( $T_c$ ) was 350°C.

It is interesting to note the slopes of the lines in these figures because this is an indication of the molecular weight distribution. These slopes are tabulated in Table 2 under the column headed  $n-1$ . It is seen from Table 2 that the slopes for PTFE resins, 6, 6C, and 7A decrease dramatically between 5 and 10 MRads while the slopes of the PTFE sheet decrease monotonically with dose. The slopes in Table 2 were obtained by fitting a straight line to the data in Figures 30 and 31 using a linear least squares procedure. The  $r$  values given in Table 2 are the correlation coefficients indicating how well the data are fit by a straight line ( $r=1.0$  is a perfect fit).

Figures 30 through 33 show the same data as that in Figures 26 through 29 except that the log apparent viscosity vs. log apparent shear rate data are plotted for a particular resin at various doses. It can be seen from Figures 30 through 32 (PTFE resins 6, 6C, and 7A respectively) that, in the low shear rate range, the viscosity drops considerably between 5 and 10 MRads and decreases further after exposure to 25 MRads. Figure 33 shows the results for the PTFE sheet. It can be seen from this figure that there is a large decrease in viscosity between 10 and 25 MRads at all shear rates measured.

Figures 34 through 37 are plots of apparent viscosity vs. dose at a particular shear rate. All this data was taken at a capillary temperature of  $350^{\circ}\text{C}$ . Figures 34 and 35 (PTFE resins 6 and 7A) show an increase in viscosity between 2.5 and 5 MRads followed by a sharp drop between 5 and 10 MRads at shear rates of 0.404 and  $4.04 \text{ sec}^{-1}$ . The data for the PTFE sheet is plotted in Figures 36 and

37. It can be seen from Figure 36 that at a shear rate of  $40.37 \text{ sec}^{-1}$  there is an increase in viscosity between 5 and 10 MRads followed by a sharp drop between 10 and 25 MRads. At a shear rate of  $0.404 \text{ sec}^{-1}$  the viscosity of the PTFE sheet seems to decrease monotonically with dose (Figure 37).

Figures 38 through 41 shows photographs of pieces of extrudate from the capillary rheometer for various resins under the conditions listed. The most interesting extrudate is the PTFE resin 7A irradiated to 5 MRads (Figure 41). The shear rate was  $2.02 \text{ sec}^{-1}$  and the capillary temperature was  $380^{\circ}\text{C}$ . This sample shows a very pronounced screw dislocation. At  $T_c = 350^{\circ}\text{C}$ , resin 7A irradiated to 5 MRads shows slight screw dislocation at a shear rate of  $13.46 \text{ sec}^{-1}$  and no screw dislocation at a shear rate of  $4.04 \text{ sec}^{-1}$  (Figure 39). Also PTFE resin 6 exhibits a slight screw dislocation at 5 MRads,  $T_c = 350^{\circ}\text{C}$ , and a shear rate of  $13.46 \text{ sec}^{-1}$  (Figure 38).

It is interesting to note that the extrudate of resin 7A irradiated to 5 MRads and extruded at a shear rate of  $4.04 \text{ sec}^{-1}$  is very smooth but twisted while the surface of the extrudate of the 2.5 MRad irradiation is slightly rough but not twisted as in the 5 MRad irradiation (Figure 34). The extrudate of the 5 MRad irradiation is much more flexible than that of the 2.5 MRad irradiation and shows a tendency to orient just before breaking. The same is true for PTFE resin 6 (Figure 33). Another example of a smooth twisted extrudate is shown in Figure 40.

Figure 42 is a plot of log apparent viscosity vs. log apparent shear rate for PTFE resin 7A irradiated to 25 MRad at three

different capillary temperatures, 335, 350, and 380°C. Also included in this plot is the data for resin 7A irradiated to 10 MRads and measured at a capillary temperature of 380°C. As expected, the viscosity decreases at all shear rates as the capillary temperature increases. Again, as in Figure 36, there is a large decrease in viscosity between 10 and 25 MRads at all shear rates measured.

Figure 43 shows the effect of initial, pre-irradiation crystallinity on the final viscosity of the irradiated PTFE resin 6. It is a plot of apparent viscosity vs. the time after the initial viscosity measurement for shear rates 2.018, 6.728, and 20.18 sec<sup>-1</sup>. The sample material was maintained in the capillary barrel for 15 minutes prior to the first viscosity measurement. The viscosities at the three shear rates indicated above were then measured at various intervals to see the effect on the melt viscosity of storing the material at 380°C. Figure 48 shows that the low crystallinity sample (cold water quenched) gave a lower melt viscosity after exposure to 10.8 MRads than the higher crystallinity (slow-cooled) sample at all shear rates measured. Also the data in this figure indicates that the viscosity measured at lower shear rates varies more with storage time at 380°C than at higher shear rates.

To summarize, irradiation of PTFE produces a dramatic decrease in viscosity when compared to that of the unirradiated material. The increase in viscosity for the PTFE resins between 2.5 and 5 MRads (Figures 34 and 35) and between 5 and 10 MRads (Figure 36) may, as will be discussed in Section V.2., be caused by some degree of branching and crosslinking. The increase in  $n$  values (Table 2) indicates that the molecular weight distribution of PTFE is changed after exposure to ionizing radiation. As with the chemical

changes indicated in the infrared spectrum of Figure 22, Figure 43 shows that the melt viscosity of an irradiated sample depends on the initial, pre-irradiation crystalline content.

#### IV.3. Results of Density Measurements

Figure 44 shows plots of density vs. dose for PTFE sheet. The density increases with dose up to about 50 MRads then begins to decrease.

Figure 45 shows the effect of post-irradiation annealing at 300°C in ambient air on the density of PTFE sheet. It can be seen that the density increases rapidly with annealing time and then levels off. Also shown in this Figure is the effect of annealing unirradiated PTFE sheet. The increase in density after 18 hours at 300°C is much smaller than after just 10 minutes at 300°C for the sample irradiated to 10 MRads. For the irradiated sample there is very little change in density after 30 minutes of post-irradiation annealing.

Figures 46 and 47 are plots of density vs. post-irradiation annealing time at 200 and 300°C respectively for PTFE sheet irradiated to the various doses indicated. Both Figures 46 and 47 indicate that the density after 3 hours annealing increases with dose up to about 10 MRads. There is little difference between the density of PTFE sheet irradiated to 10 MRads or 50 MRads after 3 hours post-irradiation annealing at 200 or 300°C. Figure 47 shows that the density of the 100 MRad material after 3 hours at 300°C is less than that of both the 10 and 50 MRad points. Comparing Figures 46 and 47 one sees that the density after any given annealing time at each of the doses indicated is greater when the annealing is done at 300°C

rather than at 200°C.

For the melt viscosity measurements of PTFE of different pre-irradiation crystallinities (Figure 43) PTFE resin 6, which is in the form of a fine powder, was used. The densities of the high and low crystallinity samples were measured using the method for determining powder densities discussed in Section III.3. The density results for the low crystallinity sample were 2.135 g/cc which yields a mass fraction crystallinity of 43% using Equation III.3.2. For the high crystallinity material the density was found to be 2.26 g/cc yielding a mass fraction degree of crystallinity of 88%.

Figure 48 is a plot of density vs. absorbance at  $775\text{ cm}^{-1}$  in the infrared spectrum of PTFE for various samples of irradiated PTFE sheet. The intensity of the absorption band at  $775\text{ cm}^{-1}$  is indicative of the amorphous content in the polymer sample. Table 3 is a listing of the data plotted in Figure 53. The data point at an absorbance value of 0.143 corresponding to a dose of 50 MRads deviates from the straight line shown in the figure. The data point corresponding to a density of 2.280 g/cc was taken using a sample irradiated to 10 MRads and then annealed for 26 hours at 295°C lies on the line formed by the data points at absorbance values of 0.177, 0.190, 0.210, 0.253 and 0.466 which were obtained from unannealed samples.

In summary exposure to ionizing radiation results in an increase in density of PTFE up to a certain dose (approximately 50 MRads) beyond which the density begins to decrease with dose. Post-irradiation annealing produces a rapid increase in density above that obtained by just irradiation and this increase is greater when the samples are annealed at 300°C than at 200°C (Figures 50 through 52).

As shall be mentioned in Section V.3., this increase in density is caused by an increase in the crystalline content of the sample.

#### IV.4. X-Ray Diffraction Results

Figures 49, 50 and 51 show the effect of irradiation and post-irradiation heat treatment on the x-ray diffraction pattern of unoriented PTFE sheet. These measurements were made at room temperature ( $\sim 22^{\circ}\text{C}$ ). A sharp peak because of diffraction from the well ordered crystalline phase appears at  $2\theta = 18.3^{\circ}$  corresponding to a Bragg spacing between crystalline planes of  $4.84 \text{ \AA}$ . Another, weaker, crystalline peak appears at  $2\theta = 16.5^{\circ}$  corresponding to a crystalline plane spacing of  $5.34 \text{ \AA}$ . By comparing Figures 49 and 50 one can see that the strong peak because of diffraction from the crystalline phase gets larger upon irradiation. This trend was also found by Nishioka et. al. (38) The peak height in Figure 51 cannot be directly compared to those in Figures 54 and 55 because, as a result of the extremely brittle nature of the sample after annealing, a portion of the sample broke off. The loss of a portion of the sample is not a problem when making quantitative comparison of crystallinity because, to calculate crystallinity, only ratios of the crystalline and amorphous scattering areas are used. The areas, in arbitrary units, in the x-ray diffraction patterns of Figures 49, 50 and 51 from the amorphous phase ( $I_a$ ) and the crystalline phase ( $I_c$ ) measured using a planimeter are tabulated below.

Sample	$I_a$	$I_c^{18.3^\circ}$	$I_c^{16.5^\circ}$
0 MRads	0.065	0.067	0.005
10 MRads	0.050	0.080	0.006
10 MRads 1h 10 m anneal at 298°C	0.014	0.071	0.004

The baselines used to define these areas are shown in Figures 49, 50 and 51. It can be seen that the crystalline scattering area gets larger relative to the total scattering area upon irradiation and post-irradiation annealing.

#### IV.5. Differential Scanning Calorimetry Results

Figure 52 shows a plot of relative heat input vs. temperature in the range between 270 and 330°K (-3°C to 57°C) for unirradiated PTFE sheet. There is an inflection in the peak at about 312°K suggesting that the peak is a composite of two crystalline transitions.

Plotted in Figure 53 are the melting endotherms of PTFE sheet at doses of 0, 25 and 150 MRads. The interesting thing to observe from this figure is that upon irradiation a shoulder develops in the low temperature side of the melting endotherm. The low temperature shoulder is especially pronounced in the 150 MRad sample.

Finally, Table 3 is a tabulation of data taken from all the DSC measurements. The heat of transition ( $\Delta H_f$ ) is the area under each of the endotherms shown in Figure 53. The symbols  $T_f$  and  $T_f'$  are the temperatures at which the maximum amplitude occurs for the endotherms

in Figures 52 and 53 respectively. The last column in the table is the ratio of the heat of fusion to the heat of transition ( $\Delta H_f/\Delta H_T$ ). The runs marked "2nd H" were taken after the initial DSC run after the sample had been quenched from 650°K down to 220°K.

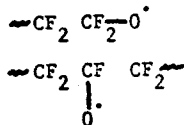
## Part V

### Discussion

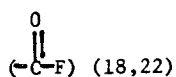
#### V.1. Infrared Results

The chemical processes which take place when PTFE is exposed to ionizing radiation was followed using infrared spectroscopy. The absorption bands characteristic of endgroup formation are those at 3550, 1880, 1810, 1790 and 1785  $\text{cm}^{-1}$ . Table 1 gives a listing of chemical species which may be present in irradiated PTFE and their corresponding IR absorption bands.

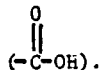
Previous work using electron spin resonance spectroscopy has shown that, upon exposure to ionizing radiation,  $\text{CF}_2\text{CFCF}_2$  and  $\text{CF}_2\text{CF}_2$  groups are formed. (18-21) These free radicals react readily with oxygen to yield perfluoroalkylperoxy radicals which through thermal activation or interaction with each other, can yield perfluoroalkoxy radicals, e.g.(20)



Comparing Figures 10, 11 and 12 (vacuum, ambient air, dry oxygen and wet oxygen irradiations respectively) one sees that the absorption band at 1880  $\text{cm}^{-1}$  appears strongly under all irradiation conditions except under vacuum and appears more intense in the dry oxygen irradiation than in the wet oxygen irradiation. This indicates that this absorption band is caused by an oxygen-related chemical species which has been formed in the PTFE sample after exposure to ionizing radiation. The absorption peak at 1880  $\text{cm}^{-1}$  has been identified with the acid fluoride endgroup

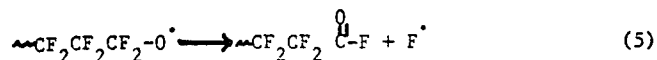
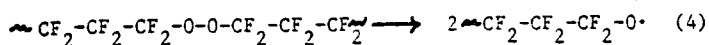
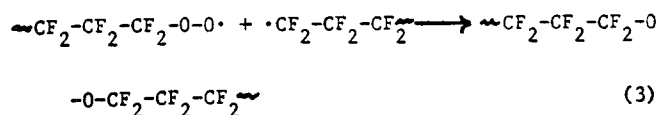
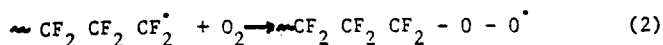
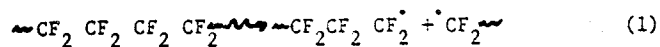


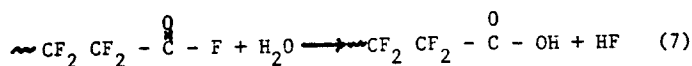
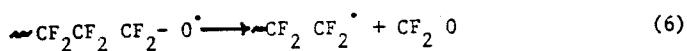
and from Figure 12 one observes that there is a much larger radiation-induced increase in absorption at 1810 and 1780  $\text{cm}^{-1}$  in the wet oxygen irradiation than in the dry oxygen irradiation. Bro and Sperati (23) have identified the absorptions at 1810 and 1780  $\text{cm}^{-1}$  as being caused by the free and bonded carbonyl stretch of carboxylic acid endgroups



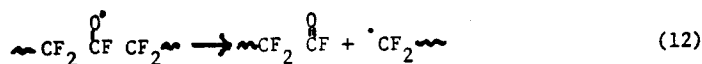
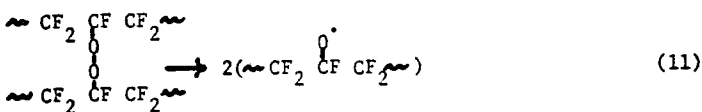
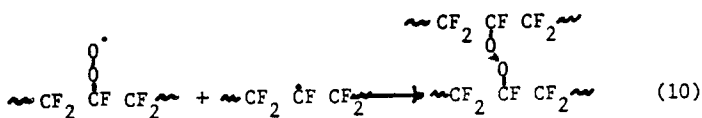
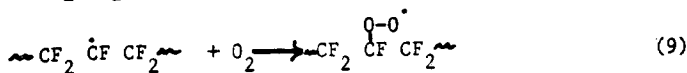
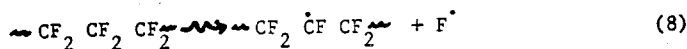
As would be expected, the oxygen-associated absorption bands at 1880, 1810, and 1780  $\text{cm}^{-1}$  are absent in the spectra of samples irradiated in vacuum.

A combination of chemical reactions which rationalize the observed data are listed below. The symbol  $\rightsquigarrow$  indicates the reaction is initiated by ionizing radiation; all other symbols have their usual meaning. Equations 1 through 7 show the reactions initiated by radiation produced primary free radicals.





secondary radical reactions are



Most of the primary free radicals formed via reaction 1 are eliminated by recombination of radical pairs. The recombination of radical pairs formed in this way is rapid because of the limited mobility of the polymer chains because of the "cage" effect. (24) The lifetime of primary radical pairs formed from chain scission is less than 20 seconds. (19) Most of the primary free radicals which would remain available to participate in reaction 2 arise from chain scissions close to one end of a polymer chain. The chance that the radical would be eliminated by recombination are less in this case because the resulting small radical fragment has enough mobility to diffuse away from the point of scission, leaving the primary free

radical on the main polymer chain intact. Reaction 3 shows the formation of peroxide groups by the interaction of a primary free radical and a perfluoroalkoxyperoxy radical. The decomposition of this peroxide group into a perfluoroalkoxy radical is given by reaction 4. Evidence for the existence of peroxide radicals formed via reaction 2 and also those peroxide radicals formed via reaction 9 comes from the electron spin resonance studies of Lerner (19) and also Siegel and Hedgpeth.(21) Reaction 5 shows the formation of the acid fluoride endgroup and also a fluorine radical. Finally, reaction 7 shows the formation of the carboxylic acid endgroup along with hydrogen fluoride. Evidence for reaction 7 comes from examining Figure 12. It is clear that the absorptions at 1810 and 1780  $\text{cm}^{-1}$  from the  $\overset{\text{O}}{\text{-C-OH}}$  group are much stronger in the wet oxygen irradiation than in the dry oxygen irradiation. Reaction 6 is a possible source of carbonyl fluoride which has been observed by infrared analysis in the gasses evolved during irradiation of PTFE. (18)

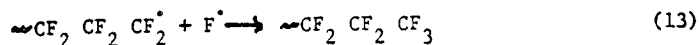
Reactions 8 through 12 show the possible fate of secondary free radicals formed upon exposure to ionizing radiation. Because of the large percentage of primary free radical pairs produced by chain scission which recombine, secondary free radicals are about 10 times more numerous as primary free radicals. (21) Reaction 12 shows the formation of the acid fluoride endgroup along with a primary free radical. This acid fluoride endgroup is free to react with water forming a carboxyl endgroup as shown in reaction 7.

Figures 13 and 23 show the effect of storing irradiated PTFE in ambient air. Examining Figure 23 one observes the 1880  $\text{cm}^{-1}$  peak.

which is associated with the acid fluoride endgroup, to appear strongly immediately after irradiation and subsequently decrease in intensity as a function of storage time in ambient air. As the  $1880\text{ cm}^{-1}$  peak decreases the absorptions at  $1810$  and  $1780\text{ cm}^{-1}$  come in (free and bonded carbonyl absorptions respectively). This can be explained on the basis of water vapor in air reacting with the acid fluoride endgroups to produce carboxyl endgroups as shown in reaction 7.

Figure 24 shows the absorbance as a function of storage time in ambient air for the absorption bands at  $1810$ ,  $1780$  and  $3560\text{ cm}^{-1}$ . As mentioned in connection with Figure 23 and shown again in Figure 24 the absorption band at  $1780\text{ cm}^{-1}$  decreases in intensity. This is a result of the hydrolysis of the acid fluoride endgroup to form a carboxylic acid endgroup as given in reaction 7.

Another possible reaction of irradiated PTFE which results in the formation of a perfluoromethyl endgroup is:

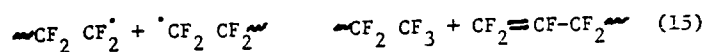
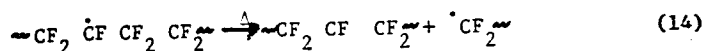


This reaction does not occur to any great extent in PTFE because there is no appreciable increase in absorption at  $980\text{ cm}^{-1}$  which would indicate an increase of  $\text{CF}_3\text{CF}_2\text{CF}_3$  after exposure to ionizing radiation (see figures 14-17).

The absorption band at  $1790\text{ cm}^{-1}$  has been identified as being caused by the olefin endgroup



This peak gets slightly stronger for irradiations carried out in air, under vacuum, and in wet and dry oxygen (see Figures 10-12). Also the number of olefin endgroups increases as a function of time after irradiation, as can be seen by examining Figure 13. Possible reactions leading to olefin endgroups are:



Reaction 14 is endothermic with an enthalpy of reaction

$$\Delta H_{298.15}^{\circ} = 38.10 \text{ kcal}^5.$$

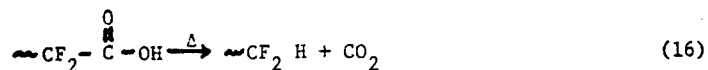
The fact that the number of  $\text{CF}_2 - \underset{\text{F}}{\overset{\text{F}}{\text{C}}} \text{C}$  endgroups increases immediately after irradiation (as evidenced by the increase in absorption at  $1790 \text{ cm}^{-1}$ ) indicates that the secondary free radicals formed upon irradiation are highly excited and able to cause reaction 14 to occur spontaneously, without any additional heat being added. The disproportionation reaction, reaction 15, may occur as two low molecular weight molecules diffuse through the polymer matrix and encounter one another. The lack of any evidence for an increase in the number of perfluoromethyl endgroups, however, indicates that this reaction is not important. Most probably, when two primary free radicals encounter one another they undergo mutual termination, which is a more favorable reaction thermodynamically than the disproportionation reaction. (5)

Figures 20, 21 and 25 show the effect of post-irradiation annealing on PTFE. In Figure 20 the PTFE was annealed immediately after irradiation at  $295^{\circ}\text{C}$  for 26 hours in air while in Figure 25 the PTFE was stored in ambient air for 55 days after irradiation then

annealed for 18 hours at about 300°C. The interesting effect shown in these two figures is the growth of the absorption band at 1790 cm<sup>-1</sup> (corresponding to the -CF=CF<sub>2</sub> group) when PTFE is annealed immediately after irradiation. If the material is stored for 55 days in ambient air then annealed (Figure 25) there is no increase in absorption at 1790 cm<sup>-1</sup> but the absorption features at 1810 and 1780 cm<sup>-1</sup> (characteristic of the



group) disappear indicating decarboxylation. A possible cause for the difference in behavior of these two samples is that immediately after irradiation many of the radiation-induced secondary free radicals have not yet reacted with oxygen dissolved in the polymer matrix. When the sample is annealed immediately after irradiation the secondary free radicals can either react with oxygen and water vapor to form carboxyl endgroups as evidenced by the increase in absorption at 1810 cm<sup>-1</sup> (reaction 7) in Figure 20 or they may react to form olefin endgroups (reaction 14). Upon annealing, decarboxylation occurs as evidenced by the disappearance of the absorption bands at 1810 and 1780 cm<sup>-1</sup> in Figure 29. Decarboxylation occurs via the reaction:



Reaction 16 explains the observed presence of CO<sub>2</sub> in the offgases of post-irradiation heat treated PTFE. (18)

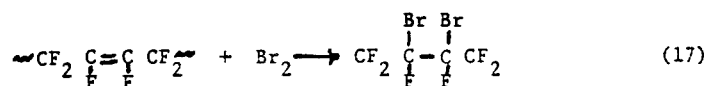
Figure 21, which is the IR spectrum between 1000 and 200 cm<sup>-1</sup> of the same sample used in Figure 20, shows the appearance of a small

absorption band at  $980\text{ cm}^{-1}$  after heat treatment. This band also appears in the spectrum of the sample stored in ambient air for 55 days and then annealed and corresponds to the formation of trifluoromethyl endgroups ( $\text{CF}_2\text{-CF}_3$ ) was shown by reaction 13. The appearance of this band after heat treatment may be attributable to the increase in the number of isolated primary free radicals because of reactions 6, 12 and 14. These isolated primary free radicals (i.e. not a part of a free radical pair) are then able to react with mobile fluorine radicals.

Examination of Figure 10 (vacuum irradiation) shows that an absorption feature appears between  $1735$  and  $1715\text{ cm}^{-1}$  and that this absorption occurs much more strongly in the vacuum irradiation than in the ambient air, wet oxygen or dry oxygen irradiations. This band may be characteristic of internal olefin formation or to bond configurations characteristic of branching or crosslinking (i.e.  $\text{-C-}$ ).

C

These reactions are likely to occur when the irradiation is done in a vacuum because there is no oxygen present to scavenge the radiation-produced free radicals. To test for the presence of double bonds, the PTFE sample used to obtain Figure 10 was exposed to bromine vapors for 10 days. Exposure to bromine vapor should result in the removal of any unsaturation via the following reaction:



provided the bromine is able to diffuse into the solid PTFE material to reach double bond sites. The infrared spectrum of the sample used in Figure 10 showed no change in the region between  $1735$  and  $1715\text{ cm}^{-1}$  after exposure to bromine vapor for 10 days

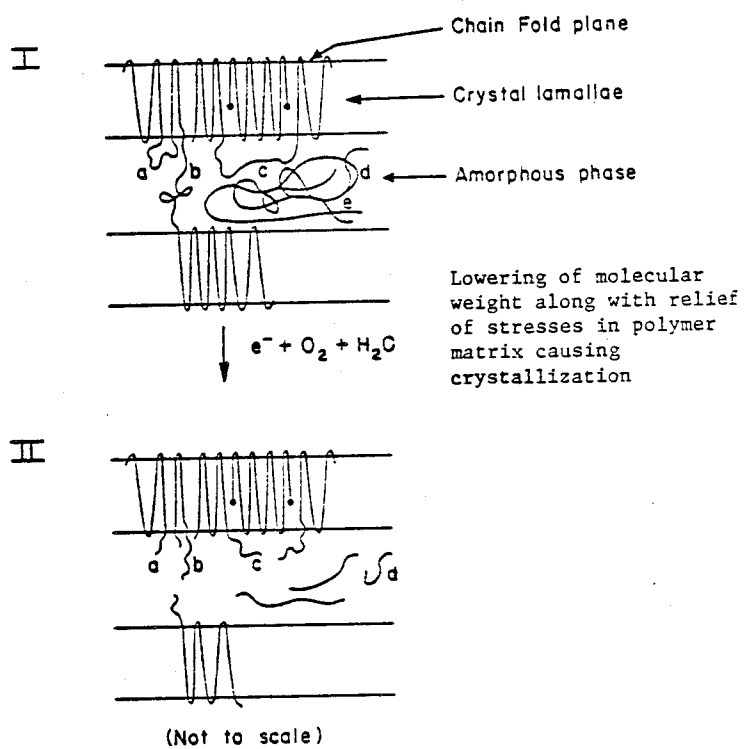
indicating either that there is no internal unsaturation or that if there are some double bonds present, they are not reactive with the bromine vapor under the conditions of this experiment. However, because of the favorable thermodynamics of the branching reaction(5) (to be discussed in Section V.2) it is postulated that the absorptions between 1735 and 1715  $\text{cm}^{-1}$  are caused by branch formation.

Figures 14 through 17 show the IR spectrum of PTFE in the range between 1000 and 200  $\text{cm}^{-1}$  for irradiations carried out under vacuum, in ambient air, in dry oxygen and in wet oxygen respectively. The absorption bands in the region between 800 and 700  $\text{cm}^{-1}$  at 375  $\text{cm}^{-1}$  and at 270  $\text{cm}^{-1}$ (9) are attributed to conformations in the amorphous phase of the polymer. In Figure 14 it can be seen that the absorption band at 270  $\text{cm}^{-1}$  of the amorphous phase decreases and another band at about 286  $\text{cm}^{-1}$  gets stronger. This effect is more pronounced in Figure 15 where there is a greater decrease in the 270  $\text{cm}^{-1}$  band and a larger increase in the band at 286  $\text{cm}^{-1}$ . In the oxygen irradiations of Figures 16 and 17 the absorption band at 270  $\text{cm}^{-1}$  is greatly decreased in intensity while the absorption for the band at 286  $\text{cm}^{-1}$  is strongly increased. The absorption at 286  $\text{cm}^{-1}$  has been attributed to chain folds in the crystalline phase of PTFE. (9)

What the results described above suggest, is that irradiation of PTFE under all conditions examined in this work causes an increase in the crystallinity to some degree as shown by the decrease in intensity of the amorphous absorption (270  $\text{cm}^{-1}$  band) and the increased absorption of the crystalline chain fold band at 286  $\text{cm}^{-1}$ .

The magnitude of the increase depends upon the conditions under which the PTFE is irradiated, which can be understood by realizing that irradiation of PTFE, under all conditions, lowers the molecular weight of the polymer through chain scissions. The above mentioned increase in the number of chain endgroups and the melt viscosity data to be discussed below clearly indicate a reduction in molecular weight. Also, as will be discussed below, most of the endgroup formation occurs in the amorphous region of the polymer. The lower molecular weight molecules (most of which are formed in the amorphous region), being more mobile, are able to move about so as to assume the lower free energy conformation of the regularly packed crystalline phase. In addition, the breaking of molecular chains in the amorphous region relieves stresses built up in the polymer matrix because of the original non-equilibrium crystallization of the PTFE resin. This reduction in stress permits further crystallization. The diagram on the following page shows schematically some of the important processes in radiation-induced recrystallization. The reason for the greater decrease in amorphous content when the irradiation is carried out in ambient air or in oxygen than in vacuum is that oxygen is present to scavenge the radiation-induced free radicals. Oxygen can react with a primary free radical to produce an acid fluoride endgroup (reaction 5) thus eliminating the possibility of that radical recombining. This reaction of a primary free radical with oxygen to produce a stable endgroup results in a lowering of the molecular weight. Secondary free radicals can react with oxygen to cause chain scission, with one stable acid fluoride endgroup and one primary free radical being formed

Schematic of important processes in radiation-induced crystallization



I. Unirradiated

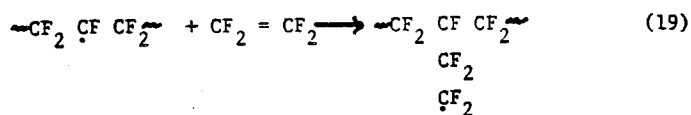
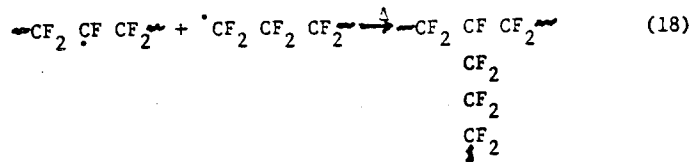
- a) Loose fold
- b) Tie molecule
- c) Non-adjacent re-entry
- d) Entirely amorphous molecule
- e) Entanglement point

II. Radiation-induced

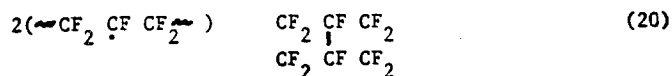
- a) Ruptured loose fold
- b) Ruptured tie molecule
- c) Ruptured non-adjacent re-entry
- d) Scissioned molecule
- e) Shorter molecules, fewer entanglements.

(reaction 12) which again results in a lowering of the molecular weight. When the irradiation is performed in vacuum, stable olefin endgroups may be formed (reaction 14) along with some stable trifluoromethyl endgroups (reaction 13) but there is also a strong possibility for recombination reactions and even chain branching or crosslinking to occur (reactions 18 through 20).

The chain branching reactions are



The crosslinking reaction is



These reactions are discussed in more detail in Section V.2.

Another possibility is that when PTFE is irradiated in a vacuum the secondary free radicals and those primary free radicals that do not undergo recombination, do not react at all. The extreme stability of these radicals, especially the secondary free radicals, has been determined using electron spin resonance spectroscopy. (19,21,25) Thus it is argued that the decrease in molecular weight will be greater when PTFE is irradiated to a given dose in the presence of oxygen than when irradiated in vacuum. The lower molecular weight material will then crystallize to a greater degree at any given temperature than

will the higher molecular weight vacuum-irradiated material.

The amorphous absorptions at 375 and 775  $\text{cm}^{-1}$  are also seen to decrease with irradiation (Figures 14 through 17). Because of the high amorphous content of the sample used to obtain the spectrum of Figure 14 and its thickness, it is not possible to detect the amorphous absorption at 775  $\text{cm}^{-1}$  in Figure 14. The absorption band at 775  $\text{cm}^{-1}$  has been used as a means of obtaining one measure of the crystallinity of PTFE. (26)

The effect of post-irradiation annealing on the IR spectrum in the region between 1000 and 200  $\text{cm}^{-1}$  is shown in Figure 21. As can be seen by the decrease in intensity of the amorphous absorption bands at 775, 375 and 270  $\text{cm}^{-1}$  the amorphous content decreases considerably with post-irradiation annealing. The band at 286  $\text{cm}^{-1}$  attributed to chain folds in the crystalline phase increases in intensity upon annealing after irradiation. This behavior is to be expected on the basis of a two-phase model where a decrease in amorphous content must result in a corresponding increase in crystalline content.

The IR spectra in Figure 22 show the effect of differences in initial, pre-irradiation crystalline content on the radiation-induced chemical changes on the PTFE sheet. The unquenched PTFE material had a density of 2.177 g/cc while the density of the fast-quenched sample was 2.134 g/cc indicating that the fast-quenched material had a lower crystallinity than the unquenched PTFE. Other than this difference in pre-irradiation amorphous content, both samples were the same. The interesting part of Figure 22 is the band at 1330  $\text{cm}^{-1}$  for the acid fluoroide endgroup structure. It is seen that this band is stronger in the spectrum of

the sample with the higher amorphous content. The reason why the acid fluoride band is stronger in the sample with the higher amorphous content lies in the fact that the crystalline material packs much more closely (higher density) than does the material in the amorphous phase. The packing in the crystalline phase is so close that little if any oxygen or water vapor can diffuse in. Thus, essentially all of the oxygen related reactions are limited to free radicals formed in the amorphous region. From this argument one would expect that, for a given radiation dose, material with a higher amorphous content would suffer a larger degree of molecular weight degradation than a sample with a low amorphous content because, with a high amorphous content, more chains are available to undergo chain scission via oxygen related reactions. This hypothesis is borne out by melt viscosity measurements to be discussed below on two PTFE samples which are identical except for their pre-irradiation amorphous content.

In summary, exposure of PTFE to ionizing radiation results in the formation of primary and secondary free radicals, the secondary free radicals being about 10 times more numerous than the primary radicals as reported in ESR studies. (21) If a sample is irradiated and stored in a vacuum the primary free radicals may recombine or form trifluoromethyl endgroups. The secondary free radicals may react to form olefin endgroups, double bonds within the polymer molecule, branches or crosslinks. Also the radicals may not react at all. When the irradiations are carried out in the presence of oxygen and water vapor the radicals react to form acid fluoride endgroups resulting in degradation of the molecular weight. These acid fluoride endgroups

subsequently react with water vapor to form carboxyl endgroups. Because of the reduction in molecular weight after exposure to ionizing radiation the crystallinity of PTFE increases. Post-irradiation annealing increases the crystallinity still further. The large increase in crystallinity upon irradiation in the presence of oxygen and water vapor and after post-irradiation annealing indicates that branching and crosslinking reactions are not important. The larger molecules formed from branching and crosslinking reactions would tend to inhibit crystallization.

#### V.2. Discussion of Melt Viscosity Results

An Instron capillary rheometer was used to measure the melt viscosity of irradiated PTFE. This instrument is described in Section III.7. on experimental methods. The observed decrease in melt viscosity upon irradiation gives an indication of the degree of molecular weight degradation. The slope of the viscosity vs. shear rate curve yields qualitative information on the radiation-induced changes in the molecular weight distribution. Also the amount of swelling and the general appearance of the polymer extrudate as it leaves the capillary gives information on the deviation from purely viscous Newtonian flow behavior.

In general, non-Newtonian and viscoelastic behavior are characteristic of polymer melt flow. The purely viscous flow of an ideal Newtonian fluid involves no recoverable deformation, just the relative motion of successive layers of fluid past each other at fixed velocities as long as a shearing force is applied. For an ideal Newtonian fluid the shear stress,  $\tau$ , is directly proportional to the

time rate of change of shear strain (shear rate,  $\dot{\gamma}$ ).

$$\tau = \eta \dot{\gamma} \quad (\text{V.2.1})$$

The proportionality constant  $\eta$  is the Newtonian viscosity. Low molecular weight gases and liquids exhibit ideal Newtonian flow behavior.

At the other extreme a material may exhibit completely reversible deformation in response to an applied shearing stress. This is called elastic deformation. Upon application of a shearing stress to an elastic body, that body will deform instantly and, if the stress is removed, it will return essentially instantaneously to its initial shape and size. For an ideal elastic body the shear stress,  $\tau$ , is directly proportional to the magnitude of the shear strain ( $\gamma$ ).

$$\tau = G\gamma \quad (\text{V.2.2})$$

the constant  $G$  is the shear modulus.

In general, flow properties of polymer melts are between those of an ideally elastic and an ideally viscous material and they exhibit what is known as viscoelastic flow characteristics. For polymer melts the following equation relates to shear stress,  $\tau$ , to the shear rate  $\dot{\gamma}$ :

$$\tau = \eta(\dot{\gamma})\dot{\gamma} \quad (\text{V.2.3})$$

Unlike the case of a Newtonian fluid where the viscosity is constant, here the viscosity is a function of the shear rate  $\eta(\dot{\gamma})$ . Thus it is necessary to measure the viscosity over a wide range of shear rates to characterize the flow properties of a viscoelastic fluid.

In many cases the dependence of viscosity on shear rate over a wide range of shear rates may be expressed in a simple mathematical form called the power law, which is given by the equation

$$\eta = \eta_0 \left| \frac{\dot{\gamma}}{\dot{\gamma}_0} \right|^{n-1} \quad (\text{V.2.4})$$

where the subscripted quantities refer to a reference state. For most polymer melts  $n < 1$  so that the viscosity decreases with increasing shear rate. This sort of behavior is called "shear-thinning" and is characteristic of the melt flow of irradiated PTFE. Newtonian flow is characterized by  $n=1$ . As  $n$  becomes smaller the shear-thinning deviation from ideal Newtonian flow becomes greater. Thus  $n$  may be considered as a measure of the non-Newtonian character of a polymer melt and is often known as the "flow index" of a material. Some flow index values are calculated in Table 2 for various samples of irradiated PTFE.

Qualitatively, the cause of the decrease in viscosity with increasing shear rate has to do with the length and flexibility of macromolecules. Because of the length of polymer chains, the molecules tend to become entangled. These entanglements are not permanent chemical bonds (i.e. not crosslinks), but merely are molecules which are looped about one another so that they still have some freedom to move relative to each other. At low shear rates the molecular entanglements remain intact because of the low velocity gradient in the polymer stream. Thus, with the application of a shearing stress the molecules are unable to move independently of one another, but the movement of one molecule causes an adjacent molecule to be dragged along with it.

This coordinated motion causes the viscosity to be higher at low shear rates. At higher shear rates (higher shear stresses) the molecules begin to become untangled and are able to orient themselves in the direction of flow. Because of the reduction in the number of entanglements the molecules are able to slide by each other more easily so that the viscosity of the polymer melt is lowered. Bueche (27) has developed a theory to calculate melt viscosities considering chain entanglement.

The  $n$  values listed in Table 2 were obtained from linear least squares fits to the data plotted in Figures 26 through 29. These figures show plots of the log of the apparent viscosity ( $\log \eta_a$ ) vs. the log of the apparent shear rate ( $\log \dot{\gamma}_a$ ). The apparent shear rate is the shear rate of a Newtonian fluid extruded under the same conditions as the actual polymer melt and is given by

$$\dot{\gamma}_a = \frac{4Q}{\pi R^3} \quad (\text{V.2.5})$$

where  $Q$  is the volumetric flow rate of the melt and  $R$  is the capillary radius. The apparent viscosity is given by

$$\eta_a = \frac{\tau}{\dot{\gamma}_a} \quad (\text{V.2.6})$$

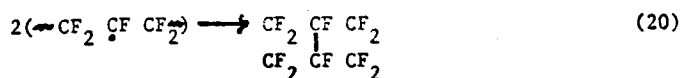
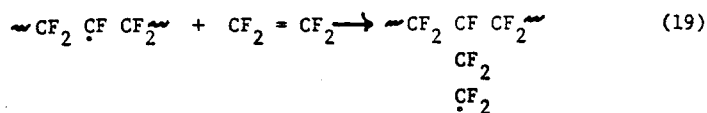
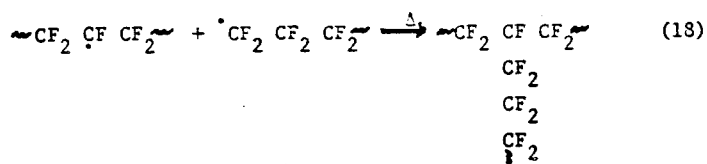
The apparent shear rate is only an approximation to the actual shear rate but it is common practice for melt viscosity data to be presented in the form of a plot of apparent viscosity vs. apparent shear rate. It can be seen by examining Table 2 that for the PTFE resins (resin 7A, 6, and 6C) the value of  $n$  decreases between 2.5 and 5 MRads then increases dramatically between 5 and 10 MRads. This large increase in the  $n$  value indicates that the polymer melt is behaving more like an

ideal Newtonian liquid. The tendency toward Newtonian flow as the radiation dose is increased is also exhibited by the PTFE sheet. Also, Figures 30 through 33 show a large drop in apparent melt viscosity between 5 and 10 MRads for PTFE resins 6, 6C and 7A and between 10 and 25 MRads for the PTFE sheet (Figure 33). There is also a large drop in melt viscosity between 0 and 2.5 MRads because the viscosity of unirradiated PTFE is approximately  $10^{11}$  poise at  $380^{\circ}\text{C}$ . (13)

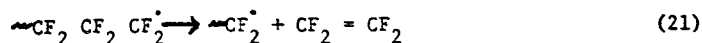
The tendency towards Newtonian flow and the drop in viscosity can be explained in terms of radiation-induced chain scission which results in a lowering of the molecular weight. Shorter molecules will have fewer entanglements per molecule so that they will be able to flow past one another more easily, thus resulting in a lowering of the viscosity after irradiation of the polymer material. The increase in the  $n$  value is also caused by the reduction in entanglement density upon exposure to radiation. The fewer entanglements present, the more the polymer molecules will be independent of each other and will therefore exhibit flow properties closer to those of a Newtonian fluid (where there is no physical connection between molecules).

The net decrease in viscosity with radiation dose for PTFE indicates that chain scission is dominant when the irradiation is carried out in air. The increases in the  $n$  value and also the increase in viscosity between 2.5 and 5 MRads for the PTFE resins at low shear rates (Figures 30 through 32) indicate that there may be some other reactions which occur upon exposure to radiation which result in an increase in the number of molecules at the high end of the molecular weight distribution.

Reactions which would accomplish this are the crosslinking reaction (Reaction 18) and branching or grafting reactions (Reactions 18 and 20) mentioned in Section V.1. and repeated here:



The crosslinking reaction (Reaction 20) is highly unlikely for reasons of steric hindrance. (20) Reaction 18, which involves the combination of 2 long polymer chain fragments, is possible but probably only occurs at elevated temperatures where there is greater chain mobility. The grafting experiments of Bro et. al. (18) and also the thermodynamic analysis of Bryant (5) have shown the validity of Reaction 19. Tetrafluoroethylene monomer may be produced upon exposure to ionizing radiation via the following reaction:



The double arrows on Reaction 21 indicate that much of the monomer almost immediately repolymerizes but some may remain to be consumed via Reaction 19. The chain branches produced in Reaction 19 may lead to some degree of crosslinking if the propagating branch chain is terminated via recombination with a secondary free radical on a

neighboring polymer chain.

The radiation-induced decrease in melt viscosity is some 10 to 100 fold less when the irradiation is carried out in an inert atmosphere or vacuum. (15) Under these conditions there is no oxygen available to react with the radiation-induced free radicals so that recombination, branching, and crosslinking reactions become more important relative to the number of chain scissions. That there are fewer endgroups formed can be seen from the infrared results obtained from PTFE irradiated under vacuum (see Figure 10). The band corresponding to the acid fluoride endgroup does not appear but the branching or crosslinking absorptions come in more strongly than if the irradiation was done in the presence of oxygen.

Generally, an increase in the  $n$  value for a polymer melt indicates not only that the flow properties are closer to those of a Newtonian fluid but also a narrowing of the molecular weight distribution. It is postulated that the increase in  $n$  values with increasing dose for PTFE is caused by a narrowing of the molecular weight distribution because of a reduction in the number of polymer molecules at the high end of the molecular weight distribution. The higher molecular weight molecules, because of their large physical size, will suffer more chain scissions per molecule than low molecular weight molecules so that the number of molecules at the high end of the molecular weight distribution will be reduced. It is these long, high molecular weight molecules that would have the most entanglements and would be largely responsible for deviations from Newtonian flow behavior.

As mentioned above, for a polydisperse system, the number average molecular weight is given by:

$$\bar{M}_n = \frac{\sum_{i=1}^{\infty} N_i M_i}{\sum_{i=1}^{\infty} N_i} \quad (\text{V.2.7})$$

and the weight average molecular weight is given by:

$$\bar{M}_w = \frac{\sum_{i=1}^{\infty} N_i M_i^2}{\sum_{i=1}^{\infty} N_i M_i} \quad (\text{V.2.8})$$

there  $N_i$  is the number of molecules of molecular weight  $M_i$  in a sample of known mass. The polydispersity is the ratio of the weight average to the number average molecular weight and is a measure of the width of the molecular weight distribution.

$$\frac{\bar{M}_w}{\bar{M}_n} = \frac{\sum_{i=1}^{\infty} N_i M_i^2}{\sum_{i=1}^{\infty} N_i M_i} \frac{\sum_{i=1}^{\infty} N_i}{\sum_{i=1}^{\infty} N_i M_i} \quad (\text{V.2.9})$$

The polydispersity is always greater than one except for a monodisperse system where it equals one. To show that the preferential scissioning of the high molecular weight chains results in a narrowing of the molecular weight distribution (reduction in the polydispersity) two cases are considered: 1) chain scissioning is independent of molecular weight, and 2) chain scissioning depends on the molecular weight to the first order. (42)

For case 1 the total number of chain scissions occurring in all polymer molecules of molecular weight  $M_i$  is:

$$n_i = K_1 N_i \quad (\text{V.2.10})$$

where  $n_i$  is the total number of chain scission,  $N_i$  is the number of molecules of molecular weight  $M_i$  in a sample of known mass and  $K_1$  is a constant. The molecular weight after radiation-induced chain scissioning of all molecules with initial molecular weight  $M_i$  is;

$$m_i = \frac{M_i}{K_1} \quad (\text{V.2.11})$$

Substituting Equations V.2.10 and V.2.11 into Equations V.2.7 and V.2.8 yields:

$$\bar{M}_n = \frac{\sum_{i=1}^{\infty} \frac{n_i}{K_1} K_1 m_i}{\sum_{i=1}^{\infty} \frac{n_i}{K_1}} = \frac{K_1 \sum_{i=1}^{\infty} n_i m_i}{\sum_{i=1}^{\infty} n_i} \quad (\text{V.2.12})$$

$$\bar{M}_w = \frac{\sum_{i=1}^{\infty} \frac{n_i}{K_1} (K_1 m_i)^2}{\sum_{i=1}^{\infty} \frac{n_i}{K_1} K_1 m_i} = \frac{K_1 \sum_{i=1}^{\infty} n_i m_i^2}{\sum_{i=1}^{\infty} n_i m_i} \quad (\text{V.2.13})$$

The final, post-irradiation, polydispersity becomes:

$$\left. \frac{\bar{M}_w}{\bar{M}_n} \right|_{\text{Final}} = \frac{\sum_{i=1}^{\infty} n_i m_i^2}{\sum_{i=1}^{\infty} n_i m_i} \bigg/ \frac{\sum_{i=1}^{\infty} n_i}{\sum_{i=1}^{\infty} n_i m_i} = \frac{\bar{M}_w}{\bar{M}_n} \bigg|_{\text{Initial}} \quad (\text{V.2.14})$$

Because one sums overall molecular weight fractions, Equation V.2.14 indicates that the polydispersity does not change when chain scission is independent of molecular weight.

For case 2 the following relations are true:

$$n_i = (K_2 M_i) N_i \quad (\text{V.2.15})$$

and

$$m_i = \frac{M_i}{K_2 M_i} = \frac{1}{K_2} \quad (\text{V.2.16})$$

where  $K_2$  is a constant.

Equation V.2.15 says that the number of chain scissions ( $n_i$ ) occurring in all polymer molecules of molecular weight  $M_i$  depends upon  $M_i$  to the first order. Substituting Equations V.2.15 and V.2.16 into Equations V.2.7 and V.2.8 yields:

$$\bar{M}_n = \frac{\sum_{i=1}^{\infty} \frac{n_i}{K_2 M_i} \frac{1}{K_2}}{\sum_{i=1}^{\infty} \frac{n_i}{K_2 M_i}} = \frac{1}{K_2} \quad (\text{V.2.17})$$

and

$$\bar{M}_w = \frac{\sum_{i=1}^{\infty} \frac{n_i}{K_2 M_i} \left(\frac{1}{K_2}\right)^2}{\sum_{i=1}^{\infty} \frac{n_i}{K_2 M_i} \frac{1}{K_2}} = \frac{1}{K_2} \quad (\text{V.2.18})$$

The polydispersity now becomes:

$$\left. \frac{\bar{M}_w}{\bar{M}_n} \right|_{\text{Final}} = 1 \quad (\text{V.2.19})$$

This shows that when the number of chain scissions per molecule in a polymer fraction of molecular weight  $M_i$  depends on  $M_i$  then the polydispersity narrows dramatically from its initial value down to that corresponding to a monodisperse distribution.

The data in Table 2 indicates qualitatively that there is narrowing of the molecular weight distribution because  $n$  increases with dose. Thus there would seem to be some dependence of the number of chain scissions per molecule on the molecular weight of that molecule. The dependence of the number of chain scissions per molecule on the molecular weight lies somewhere between cases 1 and 2.

Physically, the dependence of the number of chain scissions per polymer molecule ( $\frac{n_i}{N_i}$ ) of molecular weight fraction  $M_i$  on  $M_i$  may be explained in terms of the size of the molecule. The higher molecular weight molecules are larger than the molecules of lower molecular weight and therefore, assuming the radiation-induced free radicals are created uniformly throughout the polymer matrix, would undergo more chain scissions.

Data for apparent viscosity vs. dose at shear rates of 40.4 and 0.404  $\text{sec}^{-1}$  for the PTFE sheet are plotted in Figures 36 and 37 respectively. In Figure 36 as in Figures 34 and 35, there is a small increase in viscosity then a large drop. The increase in viscosity in Figure 23, 35 and 36 is caused by the branching and crosslinking reactions mentioned above. The decrease in viscosity of PTFE sheet with dose up to 50 MRads at the low shear rate of 0.404  $\text{sec}^{-1}$  is shown in Figure 37. This plot can be fitted to an equation of the form,

$$\eta_a = 2.52 \times 10^6 \exp [-0.0564 (\text{Dose})] \quad (\text{V.2.20})$$

where  $\eta_a$  is the apparent viscosity in poise and the dose is in megarads.

Figures 34 and 35 show apparent melt viscosity vs. dose for PTFE resins 6 and 7A at shear rates of 0.404 and 4.04  $\text{sec}^{-1}$  respectively. These figures show clearly the increase in viscosity between 2.5 and 5 MRads, and as mentioned above this increase in viscosity could be caused by the chain branching reaction (Reaction 19). It is interesting to note in Figure 34 that the viscosity of resin 6 at 5 MRads is double valued. This double valued viscosity was caused by severe stick-slip of the polymer melt at the capillary wall as it was being extruded.

In Figure 38 are shown photographic enlargements of the extrudate of PTFE resin 6 irradiated to 2.5 and 5 MRads as it emerged from the capillary at apparent shear rates of 0.404 and 13.46  $\text{sec}^{-1}$ . Also indicated are the die swell measurements. The 2.5 MRad extrudate at  $\dot{\gamma}_a = 0.404 \text{ sec}^{-1}$  shows slight surface irregularity in the form of ripples. The 5 MRad extrudate at  $\dot{\gamma}_a = 0.404 \text{ sec}^{-1}$  corresponds to the double valued viscosity indicated in Figure 34 and is characteristic of the type of extrudate produced by severe stick-slip behavior. The portion of extrudate to the left of the arrow exhibits a very fine surface roughness and corresponds to the condition in which the polymer melt was slipping through the capillary at a higher shear rate than the low shear rate portion of the extrudate to the right of the arrow. The smooth portion of the extrudate, instead of emerging from the capillary in a straight thread tended to become twisted as it cooled.

This effect is shown in Figure 40. Again, during the extrusion of the sample shown in Figure 40 stick-slip behavior was observed. Referring again to Figure 38, the higher shear rate extrudate shows a more severe melt fracture than the lower shear rate extrudate. The 2.5 MRad sample exhibits surface ripples and the 5 MRad sample shows some screw dislocation behavior.

Figure 39 shows extrudate samples of PTFE resin 7A irradiated to 2.5 and 5 MRads and extruded at shear rates of 4.04 and 13.46  $\text{cm}^{-1}$ . At  $\dot{\gamma}_a = 4.04 \text{ sec}^{-1}$  the 2.5 MRad samples indicate some surface ripples. The 5 MRad extrudate is very smooth but is somewhat twisted. At  $\dot{\gamma}_a = 13.46 \text{ sec}^{-1}$  the 2.5 MRad extrudate again shows surface ripples and the 5 MRad sample exhibits screw dislocations. Figure 41 shows a sample of the extrudate of PTFE resin 7A irradiated to 5 MRads and extruded at a shear rate of 2.02  $\text{sec}^{-1}$ . A high degree of screw dislocation behavior is apparent. In all the samples of Figures 38 and 41 the die swell increases in going from 2.5 to 5.0 MRads.

Samples of PTFE measured at shear rates of 40.37 and 134.6  $\text{sec}^{-1}$  showed severe melt fracture at all dose levels investigated in this work.

In general, the deviating shapes of polymer extrudates have been attributed to non-Newtonian elastic response of the polymer melts after being forced through a capillary. (30) The deviation in the shape of the extrudate thread begins after a certain critical shear stress is exceeded, usually about  $2 \times 10^6 \text{ dynes/cm}^2$ . (31) Birefringence studies have shown that the first departure from smooth laminar flow occurs within the capillary. Presumably, this first departure from

smooth laminar flow results in the ripple type of surface roughness observed in the PTFE extrudates mentioned above. At a somewhat higher shear stress stick-slip behavior occurs at the capillary wall. (32) Examples of this type of extrudate behavior are shown in Figure 38 and 39. It has been shown by photographic techniques that, at a still higher shear stress, fracturing, or breaking, of the elastically deformed flowing polymer stream occurs at the capillary entrance. This is the cause of the large scale melt fracture observed in PTFE extruded at shear rates of 40.37 and 134.6  $\text{sec}^{-1}$ . (33,34)

The observed twisting of the extrudate thread (see Figure 42) may be explained on the basis of elastic response of the melt as it leaves the capillary. The thin layer of polymer melt just adjacent to the capillary wall experiences a higher velocity gradient as it flows through the capillary than do the layers of polymer melt further from the wall. A relatively large amount of elastic energy is stored in this outer layer because of this high velocity gradient. This system is unstable and, upon emerging from the capillary, the outer layer contracts more than the inner layers causing the polymer thread to become twisted. (35) This may also explain why some of the observed swell values are less than unity.

Figure 42 shows the effect of capillary temperature on the apparent melt viscosity of PTFE resin 7A irradiated to 25 MRads. Also shown in this figure are plots of log apparent viscosity ( $\eta_a$ ), vs. log apparent shear rate ( $\dot{\gamma}_a$ ), for PTFE resin 7A irradiated to doses of 10 and 25 MRads and measured at a capillary temperature of 380°C. The log apparent viscosity of PTFE resin 6 irradiated to a dose of 25 MRads and measured at a capillary temperature of 380°C is

also plotted on Figure 46 at an apparent shear rate of  $20.2 \text{ sec}^{-1}$ . As expected, the viscosity decreases as the capillary temperature increases at all shear rates measured. There is a large decrease in viscosity between 10 and 25 MRads when the viscosity is measured at  $380^\circ\text{C}$  and as stated earlier can be attributed to radiation-induced chain scissions resulting in a lowering of the molecular weight.

Only one data point for resin 6 was obtained (see Figure 47) because of a large number of bubbles in the polymer melt which made the acquisition of reliable data very difficult. This problem of bubble formation in the polymer melt stream was particularly severe at doses greater than 10 MRads. Viscosity measurements were attempted for PTFE irradiated to 50 MRads but, because of the formation of a large number of bubbles in the polymer melt, consistent data could not be obtained. These bubbles are caused by pyrolysis within the viscometer barrel of the irradiated polymer. The number of bubbles formed increases with increasing radiation dose. The bubbles consist of  $\text{CO}_2$ ,  $\text{CF}_2\text{O}$ , and  $\text{C}_2\text{F}_6$  gases as determined by infrared analysis. (20)

Finally, Figure 43 shows the effect of differing pre-irradiation crystallinity on the apparent viscosity of PTFE resin 6 irradiated to 10.8 MRads. Before irradiation, the sample material was melted and held at  $380^\circ\text{C}$  for 15 minutes. Some of the material was cooled from the melt very slowly (yielding a more crystalline sample) while the rest of the material was quenched from  $380^\circ\text{C}$  in cold water (yielding a sample of lower crystallinity). The slow-cooled sample had a density of 2.26 g/cc while the density of the quenched sample was 2.13 g/cc. As can be seen from Figure 43, the sample of higher crystallinity had a higher viscosity at each of the

three shear rates measured. Also, the effect of storage time in the rheometer barrel at 380°C on viscosity is shown.

The lower viscosity for the sample of lower crystallinity can be explained by realizing that most of the chain scission reactions mentioned in Section V.1. involved oxygen. In the sample of low crystallinity a greater amount of polymer material is able to react with oxygen. Oxygen molecules are unable to diffuse into the tightly packed crystalline phase so that oxygen-related scission reactions will not occur in the crystalline phase. Thus, because more material is available to react with oxygen in the sample of low crystallinity, more chain scission reactions will occur in this sample resulting in a lower molecular weight than in the highly crystalline material. A lower molecular weight means a lower viscosity and this is what is observed (Figure 43). That more oxygen related endgroups are formed in a sample of low crystallinity than in a highly crystalline sample is shown by the infrared results given in Figure 22. The acid fluoride endgroup absorption band appears much more strongly in the low crystalline material.

Plotted in Figure 43 is the apparent viscosity vs. storage time at 380°C in the rheometer capillary. The decrease in viscosity with storage time can be explained by two mechanisms. First, storage at high temperature may cause residual unreacted free radicals to react causing further chain scissions. Second, after storage at 380°C for extended periods of time some thermal degradation occurs. Some of the sample material which had been stored the longest began to show discoloration (turning from white to a yellow-brown hue) indicative of thermal degradation.

In summary, exposure of PTFE to ionizing radiation causes a decrease in viscosity due to chain scission. There is a slight increase in viscosity between 2.5 and 5 MRads for PTFE resins 6, 6C, and 7A probably caused by branching and crosslinking reactions in the crystalline region of the polymer. The flow index values increase at doses greater than 5 MRads indicating that the flow properties are closer to those of a Newtonian fluid. It is concluded that the approach to Newtonian flow properties is caused chiefly by a reduction in the number of molecules at the high end of the molecular weight distribution. Departure from purely viscose flow is shown by the deviating shapes of the PTFE extrudate and is caused by radiation-induced chain branching and crosslinking reactions and also chain entanglements. The viscosity of a sample of PTFE irradiated to a given dose depends on its pre-irradiation crystalline content, a sample of low crystallinity will yield a lower viscosity than a high crystallinity sample irradiated to the same dose.

### V.3. Discussion of Density Results

Referring to Figure 44 the decrease in density at high radiation doses may be caused by the formation of a high concentration of defects within the crystalline region. The rate of formation of the crystalline defects with dose will initially be much less than the chain scission and crystallization of initially amorphous material because of the lack of oxygen in the crystalline region. As mentioned earlier, oxygen acts to scavenge radiation-produced free radicals yielding stable endgroups and a lowering of the molecular weight. In the absence of oxygen the recombination reactions are important,

especially in the crystalline region, where the mobility of the primary free radicals is limited by the cage effect. The secondary free radicals may remain unreacted or react to form branches or crosslinks. The branching and crosslinking reactions would not be very common at room temperature because of the lack of chain mobility. Also the formation of olefin endgroups from primary free radicals occurs to some degree. As the amorphous content is depleted by further crystallization brought about by radiation-induced chain scission, defect formation in the crystalline region becomes more important relative to the crystallization reaction. Finally, at a high enough dose, the rate of crystalline defect formation exceeds that of the crystallization reaction and, because the defects appear amorphous in character to a density measurement, the density decreases with dose.

Figure 45 shows the effect post-irradiation annealing at 300°C has on a sample of PTFE irradiated to 10 MRads. These data show that radiation plus post-irradiation annealing is necessary to achieve a large increase in density or crystallinity. Annealing alone for 18 hours at 300°C resulted in only a small density increase as is evident in Figure 45. The radiation acts to lower the average molecular weight and the post-irradiation heat treatment provides the activation energy necessary for crystallization to occur. The lower molecular weight post-irradiation molecules present after irradiation are able to crystallize more readily because the smaller molecules are more mobile and have fewer chain entanglements per molecule. Also, the increase in density is essentially complete after only about 30 minutes post-irradiation annealing time.

Figures 46 and 47 are plots of density vs. post-irradiation

annealing time at 200 and 300°C, respectively, for samples of PTFE sheet irradiated to the various doses indicated. The degree of increase in density is greater for an annealing temperature of 300°C than at 200°C for all doses indicated (compare Figures 46 and 47). The higher temperature imparts a greater mobility to the molecules and hence more crystallization occurs. It is interesting to note that the density, after 3 hours post-irradiation annealing at 200 and 300°C, for both the 10 and 50 MRad samples yielded very close to the same density even though the density of the 10 MRad sample was considerably below that of the 50 MRad sample at zero post-irradiation annealing time. At both these temperatures the 10 MRad sample, the molecules of which have, on the average, a higher molecular weight because of lower dose, possess enough thermal energy to crystallize to approximately the same degree as those of the 50 MRad sample. Figure 47 shows that after 3 hours at 300°C the 100 MRad sample has a smaller density than both the 10 and 50 MRad samples indicating that the defects formed (for 100 MRad dose) in the crystalline region are not removed by this annealing process.

Figure 48 combines density data with the infrared measurement of the absorbance at 775 cm<sup>-1</sup> which is indicative of the amorphous content. The line drawn in the figure is a linear least squares fit to the data points indicated by  $\theta$ . This line is represented by the equation

$$\rho(\text{g/cc}) = - 0.2594 A + 2.297 \quad (\text{V.3.1})$$

where  $\rho$  is the density and A the absorbance at 775 cm<sup>-1</sup>. This equation, at zero absorbance (100% crystallinity) yields a density value of

2.297 g/cc which is in very good agreement with the 100% crystalline density 2.301 g/cc obtained by Ruland (30) from x-ray measurements. The single datum corresponding to the 50 MRad irradiation indicated by  $\square$  deviates from the straight line derived above. This deviation may be because the density responds to defects in the crystalline phase introduced upon irradiation as if they were amorphous in character but the conformations characteristic of these defects may not be the same as those in the amorphous region which cause the absorption band at  $775 \text{ cm}^{-1}$ . At a dose of 50 MRads, where the number of these defects becomes appreciable, one would expect the data to deviate to the small absorbance side of the straight line because the infrared measurement would not respond to these defects. The data point at an absorbance of 0.0665 is from a sample which was irradiated to 10 MRads and then annealed for 26 hours at  $295^\circ\text{C}$ . This point is seen to lie on the line formed from data points taken using samples which had no post-irradiation heat treatment. As far as these measurements indicate, post-irradiation heat treatment does not introduce any new crystallization process different from just radiation-induced crystallization, but merely acts as a means of giving the polymer molecules enough mobility so that they are able to crystallize.

#### V.4. Discussion of X-Ray Diffraction Results

Tabulated below are quantitative results of mass fraction crystallinity ( $\alpha_m$ ) calculations using the calibration equations of Ruland (30) and of Hilian and Henckel (39,40) given by equations V.4.1 and V.4.2 respectively.

$$\text{Ruland: } \frac{M_a}{M_c} = 0.56 \frac{I_a}{I_c}$$

$$\alpha_m = \frac{100}{1 + \frac{M_a}{M_c}} \quad (\text{V.4.1})$$

Kilian and Jenckel:

$$\alpha_m = \frac{I_c}{I_c + KI_a}$$

$$K = 1.00 \quad (\text{V.4.2})$$

The symbols  $I_c$  and  $I_a$  are the crystalline and amorphous scattering areas of the x-ray diffraction patterns given in Section IV.4. Also given in the table below are crystallinities calculated on the basis of density measurements using equation 2 (Section III.3.).

Sample	$\alpha_m$ (Ruland)	$\alpha_m$ (Kilian and Jenckel)	$\alpha_m$ (density)
0 MRads	66	54	61
10 MRads	75	63	75
10 MRads Annealed 1h 10m at 298°C	91	84	94

In conclusion, even though there is a disparity in the crystallinity values they all show the trend of increasing crystallinity upon irradiation and a further increase after post-irradiation annealing. This agrees with the density, infrared and, as shown in Section V.5. the differential scanning calorimetry results. The differences in crystallinity values between the calibration of Ruland and Kilian

and Jenckel are, most likely, from uncertainty in the separation of the crystalline and amorphous scattering areas. One would not necessarily expect x-ray and density crystallinity values to agree because they each measure a different moment of the crystalline order distribution.

#### V.5. Discussion of DSC Results

From Table 3 it can be seen that the heat of fusion increases rapidly after exposure to low doses of radiation for all samples. The heat of fusion follows the same trend as the radiation-induced increase in crystallinity indicated by density measurements (Figure 44). An increase in  $\Delta H_f$  is to be expected because a more highly crystalline sample will have a greater  $\Delta H_f$ . The lower  $\Delta H_f$  (lower crystallinity) for all the 2nd heating samples is caused by the rapid cooling from the melt after the initial measurement.

The melting temperature of the PTFE sheet is seen to decrease with irradiation after exposure to at least 1 MRad. This decrease in melting temperature is attributed to the presence of a large number of defects formed within the crystalline region after irradiation. These defects raise the free energy of the crystal thereby lowering the melting temperature ( $T_m$ ). Also the decrease in  $T_m$  may be partially caused by a decrease in superheating at higher doses because radiation-induced chain scissions result in a lowering of the molecular weight. For the quenched PTFE samples there is an increase in  $T_m$  after a dose of 1 MRad. The unirradiated quenched samples consist of a very high amorphous content and very badly formed non-equilibrium crystals. Exposure to radiation will cause chain scissions thereby relieving residual stress

present in the badly formed crystals. Relief of these residual internal stresses will cause increased molecular mobility allowing the molecules to better order themselves forming a crystal closer to equilibrium with a higher  $T_m$ . The previous DSC work of Kusy and Turner (32) also shows an increase in  $T_m$  with increasing dose up to about 8 MRads for samples of PTFE resin 6 quenched from the melt. These same workers have shown that  $T_m$  decreases monotonically with dose for well crystallized samples for PTFE resin 6. This result supports the assertion that upon irradiation better crystals, with a higher  $T_m$ , are formed from the initially poor crystals in the quenched samples because of increased molecular mobility, while for an initially well crystallized sample the decrease in  $T_m$  is caused by radiation-induced defects in the crystalline material.

As mentioned in Section II.2., PTFE exhibits two low temperature transitions at about 19 and 30°C. Both of these transitions are caused by changes in the chain conformation and unit cell structure in the crystalline phase. Both of these transitions are indicated by vertical arrows in Figure 52. In this figure the two transitions are seen to occur at about 302°K (29°C) and 312°K (39°C). The higher temperature measured for these transitions are caused by superheating effect. The heat of transition ( $\Delta H_T$ ) values listed in Table 3 are the composite changes in enthalpy of both these transitions.

Because these transitions involve only molecules in the crystalline phase one would expect that the value of  $\Delta H_T$  would depend on the crystalline content, as indicated by the heat of fusion ( $\Delta H_f$ ). The dependence of  $\Delta H_T$  on  $\Delta H_f$  can be seen by comparing the  $\Delta H_T$  values (see Table 3) of samples 6 and 6Q and also 6C and 6CQ. An examina-

tion of the 1st heat values of  $\Delta H_T$  vs. dose reveals that there is no systematic change in this quantity with dose up to 25 MRads. At 150 MRads  $\Delta H_T$  has decreased from 1.70 cal/g to 1.18 cal/g. This decrease is somewhat surprising because according to the  $\Delta H_f$  values, the crystalline content increases with irradiation. Also the ratio of heat of fusion to heat of transition (last column in Table 3) increases with crystallinity for the first heating measurements showing that the crystal structure responsible for the composite transition at 302°K and 312°K is not present in the material which has been crystallized from initially amorphous material after exposure to radiation. The values of the ratio of heat of fusion to heat of transition for the second heating measurements show a much smaller change with increasing crystallinity (increasing  $\Delta H_f$ ) than the values of this ratio for the first heating measurements. This indicates that the crystal structures which give rise to the heat of transition are present to a much greater extent in the irradiated material which has been melted and then recrystallized from the melt. The decrease in the ratio  $\Delta H_f/\Delta H_T$  between first and second heatings for the 1 MRad and 25 MRad samples also shows that there is a change in the nature of the crystal structure when the irradiated material is heated above  $T_m$  and then recrystallized from the melt.

An increase in the ratio of heat of fusion to heat of transition for first heating measurements is also shown by PTFE resin 6 which had been rapidly quenched from the melt prior to irradiation (see Table 3).

Upon quenching from the melt the heat of fusion drops from 16.75 cal/g to 6.11 cal/g while the heat of transition decreases from

2.43 cal/g to 1.24 cal/g. After irradiation of the quenched sample to 1 MRad the  $\Delta H_f$  value increases to 13.06 cal/g, an increase by about a factor of 2 over its pre-irradiation value and 78% of the  $\Delta H_f$  of the virgin resin. The corresponding change in  $\Delta H_T$  after a 1 MRad irradiation is from 1.24 cal/g to 1.39 cal/g, an increase of only 12% over the pre-irradiation value and only 57% of the  $\Delta H_T$  value of the virgin resin. Thus, the irradiation-induced increase in crystallinity as measured by  $\Delta H_f$  is not accompanied by a corresponding increase in  $\Delta H_T$ . Also the work of Pinkerton and Thompson (33) using scanning electron microscopy to study fracture surfaces of irradiated PTFE show that fracture surfaces of samples the crystallinity of which has been increased by irradiation exhibit a different appearance from fracture surfaces crystallized from the melt.

It is interesting to compare the melting endotherms in Figure 53 with the x-ray diffraction pattern of PTFE irradiated to 10 MRads then annealed at 296°C for 1 hour and 10 minutes (Figure 51). As mentioned in Section V.4. the crystallinity of this sample increased from 75% to 94% as determined by density measurements and the full width at half maximum (FWHM) of the crystalline peak at a value of 2θ of 18.3° increased from 0.50° to 0.65° after irradiation and annealing. The increase in FWHM indicates disorder in the crystal structure. (34) The disorder is caused by the crystallization of initially amorphous material as a result of the radiation plus annealing process. If radiation-induced crystallization results in less perfect crystals, different in nature from crystals formed from the melt one would expect to see a low temperature shoulder on the heat of fusion endotherm caused by the melting of these less perfect crystals. The

appearance of a low temperature shoulder on the melting endotherms of irradiated PTFE sheet is shown in Figure 53. A low temperature inflection on the melting endotherm is present in the 25 MRad irradiation and becomes quite pronounced for the sample irradiated to 150 MRads.

In summary, the DSC results correlate very well with the infrared, density, and x-ray diffraction results which all indicate an increase in crystallinity occurs upon irradiation and that a further increase in crystallinity results after post-irradiation annealing. The DSC and x-ray results show that the crystals formed after exposure to radiation are of a different and less perfect nature than crystals formed from the melt.

## Part VI

## Summary and Conclusions

The dominant effect of ionizing radiation on PTFE is molecular weight degradation caused by polymer chain scission. Radiation-induced primary and secondary free radicals are produced which can react with oxygen and water vapor to form stable endgroups (acid fluoride and carboxyl groups) resulting in a lowering of the molecular weight. Formation of olefin endgroups occurs to some degree, probably in the crystalline phase where there is no oxygen available to form acid fluoride endgroups. Evidence of molecular weight degradation comes from the dramatic decrease in melt viscosity of the irradiated material. Also the observed increase in the flow index numbers (Table 2) indicates that irradiated PTFE behaves like a low molecular weight Newtonian fluid. The data indicate that the number of molecules at the high molecular weight end of the molecular weight distribution is reduced resulting in a narrowing of the distribution.

Radiation-induced chain scission, by creating shorter polymer chains, reduces the number of entanglements per molecule which in turn increases molecular mobility. Also, chain scission can act to relieve intramolecular stresses of molecules or portions of molecules in the amorphous phase of the polymer matrix, thus increasing chain mobility. The increase in mobility causes the polymer molecules in the amorphous phase to crystallize upon irradiation. An increase in crystalline content upon irradiation of PTFE is indicated by increases in density and heat of fusion, the reduction in intensity of absorption

bands in the infrared spectrum caused by conformations in the amorphous phase (bands at 775, 375 and  $270\text{ cm}^{-1}$ ) and an increase in intensity of the absorption band at  $286\text{ cm}^{-1}$  caused by crystalline chain folding and also an increase in area relative to the total area, of the crystalline peak in the x-ray diffraction intensity distribution.

Post-irradiation annealing below  $T_m$  causes a further increase in crystallinity by increasing chain mobility, a process that is thermally activated as can be seen from the density results in Figures 46 and 47 which show that the degree of increase in crystallinity depends upon the annealing temperature. The crystallinity also increases as a function of radiation dose up to approximately 50 MRads and then decreases with dose (Figure 44). This conclusion is based on the fact that there are two competing processes occurring when PTFE is irradiated. One is the above mentioned crystallization of molecules (or portions of molecules) initially in the amorphous phase. The other process is the introduction of defects in the crystalline phase (branches, crosslinks, chain ends, etc.) which responds to a density measurement as amorphous material. The retardation of the rate of crystallization of initially amorphous material due to depletion of the amorphous material coupled with the steady increase in the crystalline defect concentration causes the density to decrease as a function of dose after a certain critical dose.

The heat of transition results presented in Table 3, the DSC plots shown in Figure 53 and the increase in the full width at half maximum of the crystalline peak in the x-ray diffraction intensity distribution shown in Figure 51 all lead to the conclusion that the crystals formed via irradiation are less perfect, further from

equilibrium, than melt crystallized material. The decrease in the ratio  $\Delta H_f/\Delta H_T$  between first and second heats in Table 3 show that there is a change in the nature of the crystal structure when the irradiated material is heated above  $T_m$ , recrystallized and then heated again. Also, comparison of the first heat values for  $\Delta H_T$  of the irradiated material to that of the unirradiated material shows that there is little change in  $\Delta H_T$  although the increase in  $\Delta H_f$  values indicates that the crystalline content increases significantly. Thus the crystal structure responsible for the low temperature transitions is not present in the crystals formed after irradiation. The heat of fusion endotherms plotted in Figure 53 show that, upon irradiation, a low temperature shoulder appears with the melting peak, and it is concluded that this shoulder is caused by the melting of the less perfect crystals produced upon irradiation. The melting peak of the 150 MRad irradiation (Figure 53) occurs at a lower temperature than the 0 MRad or the 25 MRad peaks and may be in part because of an accumulation of radiation-produced defects in the initially crystalline region, raising the free energy of the crystals thereby lowering  $T_m$ . A reduction in the superheating effect because of the relatively low molecular weight of the 150 MRad sample would also cause the apparent melting temperature to decrease.

It is concluded that most of the molecular weight degradation and endgroup formation reactions occur in the amorphous phase, as evidenced by examining the relative amount of endgroup formation of samples of widely differing crystallinities via infrared analysis (Figure 22). The absorption peak corresponding to the acid fluoride endgroup ( $1880\text{ cm}^{-1}$ ) comes in much more strongly in the fast quench,

low crystallinity sample. A larger number of endgroups means a lower molecular weight. Figure 43 shows the apparent melt viscosity of two samples of PTFE of widely differing crystallinities irradiated to the same dose. For each of the three shear rates shown, the fast quenched low crystallinity sample had a lower viscosity, indicative of a lower molecular weight relative to the high crystallinity sample.

The radiation-induced chemical reactions in PTFE do not take place immediately upon irradiation but continue to occur for some days after irradiation, a conclusion drawn from the infrared results shown in Figures 23 and 24. Initially after irradiation, the absorption band caused by the acid fluoride endgroup appears and upon storing the irradiated sample in ambient air, the acid fluoride band decreases in intensity while absorption bands corresponding to free and bonded carbonyl structures of carboxylic acid endgroups come in. It is concluded that this is caused by hydrolysis of the acid fluoride endgroups. The infrared absorption bands sensitive to the amorphous content show no time dependence when the sample is stored at room temperature. The time dependence of the increase in crystallinity caused by post-irradiation annealing is shown by the density measurements in Figure 45 through 47. The crystallinity reaches very close to its ultimate value after only about a half hour post-irradiation annealing at 200 and 300°C.

The melt viscosity measurements were complicated because of deviations from laminar flow resulting in melt fracture in some cases (chiefly stick-slip behavior) and bubble formation in the polymer melt. The melt fracture is probably caused by chain entanglements which give the polymer melt non-Newtonian elastic properties.

It is concluded that the formation of branches and crosslinks in the crystalline phase of irradiated PTFE contribute to the observed non-Newtonian elastic response of the melt during the viscosity measurement. Bubble formation in the polymer melt of an irradiated sample is the result of pyrolysis which yields low molecular weight compounds such as  $\text{CF}_4$ ,  $\text{C}_2\text{F}_6$ ,  $\text{CF}_2\text{O}$  and  $\text{CO}_2$ . This phenomenon which is minor at low doses becomes more pronounced as the radiation dose is increase.

### References

1. Charlesby, A., Atomic Radiation and Polymers, Pergamon Press, Inc., New York, NY, 1960, p. 68.
2. Cleland, M. R., "The Prospects for Very High-Power Electron Accelerators for Processing Bulk Materials", presented at the International Meeting on Radiation Processing held in Puerto Rico, May 9-13, 1976.
3. "Report on Survey and Workshop on Industrial Radiation Processing," Industrial Research Institute Research Corporation for the Office of Cooperative Technology, National Bureau of Standards, U. S. Department of Commerce, October 1979.
4. Wall, L. A., Fluoropolymers, Wiley-Interscience, New York, 1972, pp. 354-356.
5. Bryant, W. M. D., *J. Polym. Sci.*, 56, pp. 277-296 (1962).
6. Sperati, C. A. and Starkweather, H. W., *Fortschr. Hochpolym.-Forsch* 2, pp. 465-495 (1961).
7. Miller, R. L., "Crystallinity" Vol. 4., pp. 449-528, *Encyclopedia of Polymer Sci. and Tech.*, Wiley-Interscience (1966).
8. McCane, D. I., "Tetrafluoroethylene Polymers", Encyclopedia of Polymer Science and Technology, Vol. 13, pp. 623-670, Wiley-Interscience (1970).
9. Willis, H. A., Cudby, M. E. A., Chantry, G. W., Nicol, Elizabeth H., and Fleming, J. W., *Polymer*, 16 (1975).
10. Speerschneider, C. J. and Li, C. H., *J. Appl. Phys.*, 33, No. 5, (1962).
11. Melillo, L. and Wunderlich, B., *Kolloid, Z. Z., Polym.*, 250 pp. 417- (1972).

12. Westendorp, W. F., Radiation Sources, A. Charlesby Editor, McMillan Company, New York, 1964, p. 171.
13. Blair, J. A., "Fluorocarbons, Polymers," Encyclopedia of Industrial Chemical Analysis, 13, p. 80 (1971).
14. Lian, C. Y. and Krimm, S., J. Chem. Phys., 25, No. 3, pp.563-571 (1956).
15. Alpert, N. L. Keiser, W. E. and Szymanski, H. A., I.R.-Theory Practice of Infrared Spectroscopy, Plenum Press, New York, 2nd, 1970, pp. 24-30.
16. Instruction Manual, Perkin-Elmer Infrared Equipment, Vol. I, Introduction to Infrared Spectroscopy, The Perkin-Elmer Co., Norwalk, Conn. (1952).
17. Conley, R. T., Infrared Spectroscopy, Allyn and Baco, Inc. Boston, 1972, Cp. 3.
18. Bro, M. I., Lovejoy, E. R. and McKay, G. R., J. Appl. Polym. Sci., 7, pp. 2121-2133(1963).
19. Lerner, N. R., J. Chem. Phys., 50, No. 7, pp. 2902-2910 (1969).
20. Golden, J. H., J. Polym. Sci., XLV, Issure 146, pp. 534-536 (1960).
21. Siegel, S. and Hedgpeth, H., J. Chem. Phys. 46, No. 10, pp. 3904-3912 (1967).
22. Weiblen, D. C., Fluorine Chemistry, J. H. Simons, Ed., Vol. III, Academic Press, New York, 1954, Cp. 7.
23. Bro, M. I. and Sperati, C. H., J. Polym. Sci., Vol. XXXVIII, pp. 284-295 (1959).
24. Ibid 1, p. 185.

25. Saika, A., Nishiguchi-Ohya, Hiroaki, Satokawa, Takaomi and Ohmori, Akira, *J. Polym. Sci.*, 15, pp. 1073-1079 (1977).
26. Miller, R. G. J. and Willis, H. A., *J. Polym. Sci.*, XIX, pp. 485-495 (1956).
27. Bueche, F., *J. Chem. Phys.*, 20, 1959 (1952).
28. Florin, R. E., Wall, L. A. and Brown, D. W., *J. Res. Natl. Bur. Std.*, 644, 269 (1960).
29. Dr. Carlton Sperati, Ohio University, Department of Chemical Engineering (private communication).
30. Ruland, A. L., *J. Chem. Ed.*, 35, No. 2, pp. 80-83 (1958).
31. Lovejoy, E. R., Bro, M. I. and Bowers, G. H., *J. Appl. Polym. Sci.*, 9, pp. 401-410 (1965).
32. Kusy, R. P. and Turner, D. T., *J. Polym. Sci.*, A-1, 10, pp. 1745-1762 (1972).
33. Pinkerton, D. M. and Thompson, K. R. L., *J. Polym. Sci.*, A-2, 10, pp. 473-488 (1972).
34. Billmeyer, F., Textbook of Polymer Science, 2nd ed., Wiley-Interscience, New York, p. 113., (1971).
35. Mehta, A., Wunderlich, B., *Coatings Plast. Prepr., Am. Chem. Soc.* 35 (2), 393 (1975).
36. Mehta, A., Gaur, U., and Wunderlich, B., *J. Polym. Sci., Polym. Phys. ed.*, 16, pp. 289-296 (1978).
37. *Ibid*, 34, page 121.
38. Nishioka, A., Matsumae, K., Watanabe, M., Tajima, M., Owaki, M., *J. Appl. Sci.*, 2, No. 4, pp. 114-119 (1959).
39. Kilian, H. G. and Jenckel, E., *Z. Electrochem.* 63, pp. 308-321 (1959).

40. Wunderlich, B., Macromolecular Physics, Vol. 1, Academic Press, New York (1973).
41. Leighton, R. B., Principles of Modern Physics, McGraw-Hill, New York (1959).
42. Dr. Chan Chung, Rensselaer Polytechnic Institute, Private Communication.
43. Clark, E. S. and Muus, L. T., Z. Krist., 117, 119 (1962).
44. Dr. Bernard Wunderlich, Rensselaer Polytechnic Institute, Private Communication.
45. Chapiro, A. C., Radiation Chemistry of Polymeric Systems, pp. 526-532, Wiley-Interscience, New York, (1962).

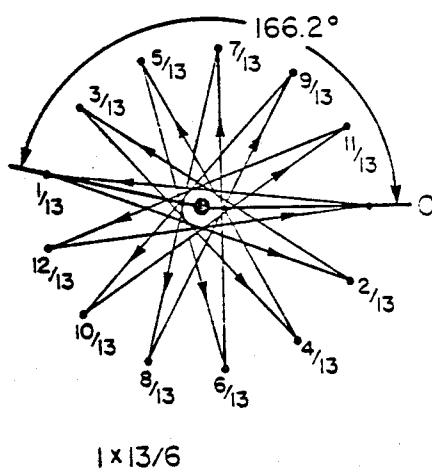


Figure 1: Point net projection of the  $1 \times 13/6$  helix of PTFE in the low temperature ( $< 19^\circ\text{C}$ ). Each successive step involves rotation by  $166.2^\circ$  and a movement along the Z axis of  $1/13$  of the unit cell length. Between  $19^\circ\text{C}$  and  $30^\circ\text{C}$  the helix becomes  $1 \times 15/7$  where each successive step involves rotation by  $168^\circ$  and movement along the Z axis of  $1/15$  of the unit cell length. (Taken from reference 40, page 73).

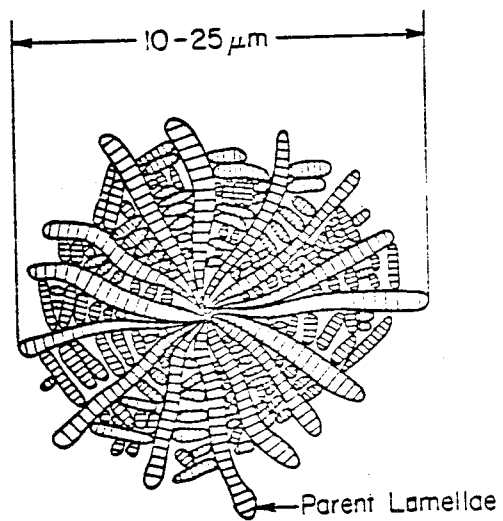


Figure 2: Schematic diagram of a PTFE spherulite (taken from reference 11).

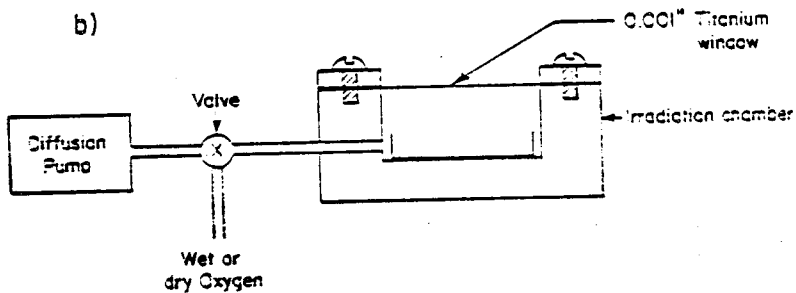
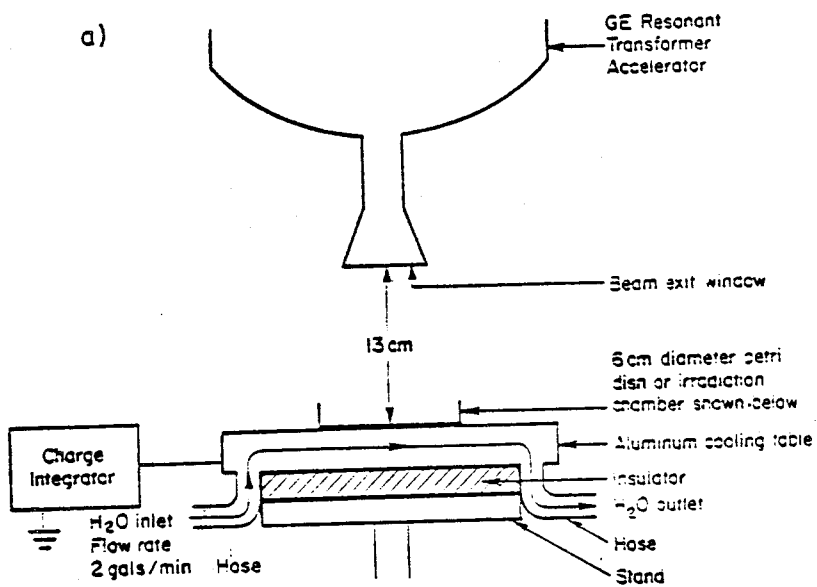


Figure 3a: PTFE irradiation geometry.

Figure 3b: Irradiation chamber used for vacuum and wet and dry oxygen irradiations.

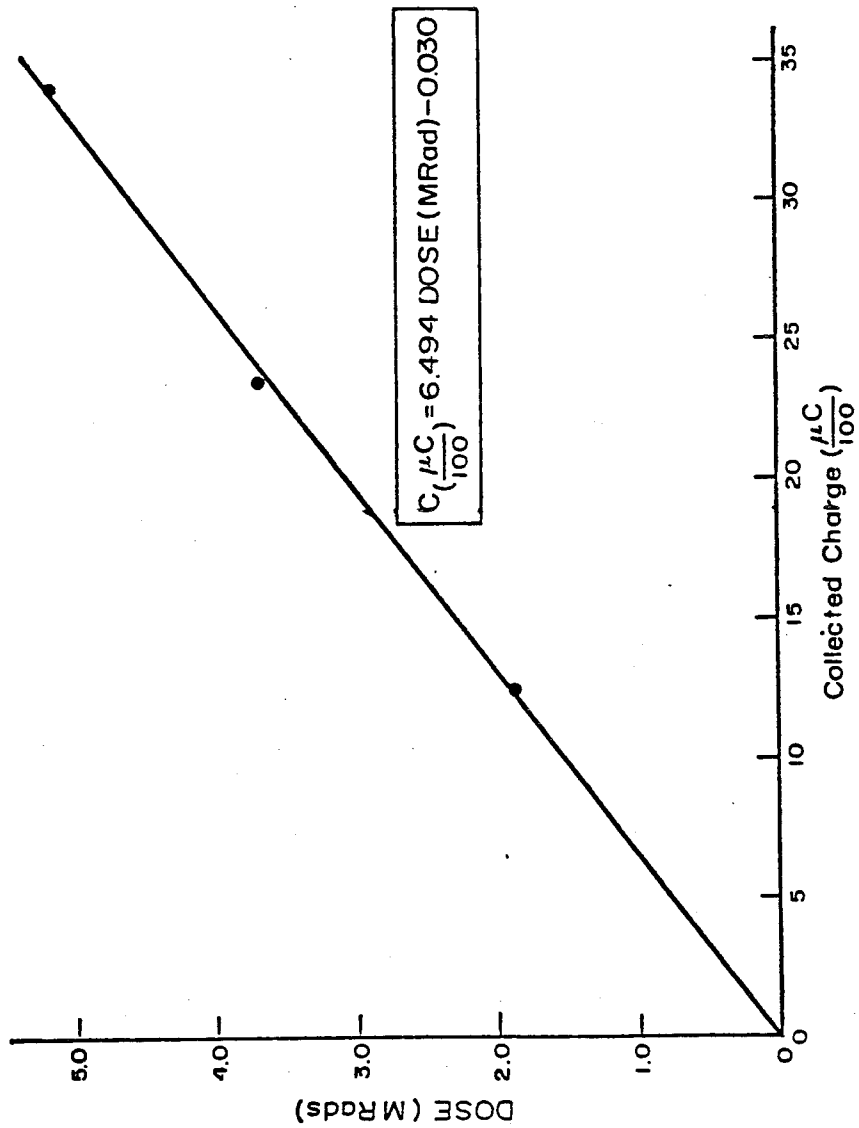


Figure 4: Radiation dose calibration curve.

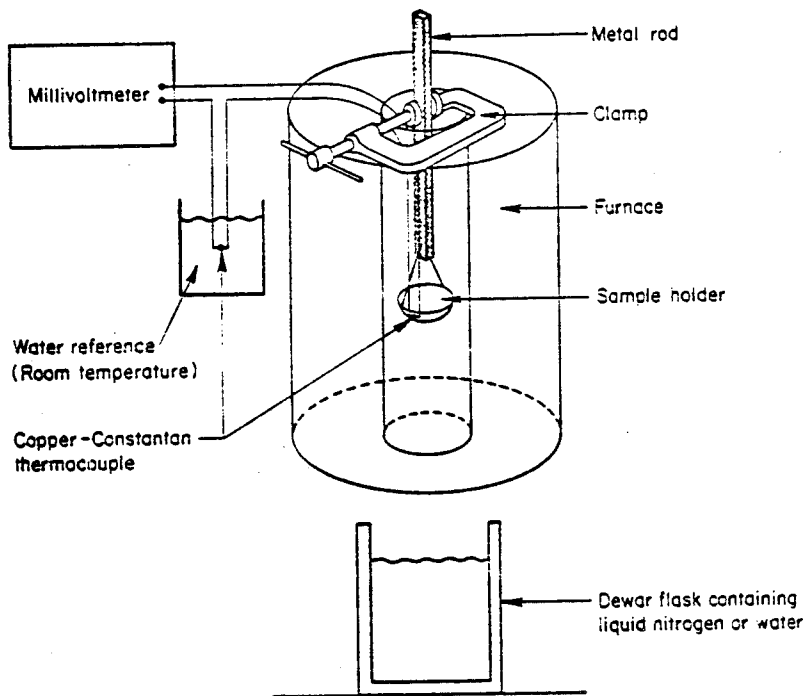


Figure 5: Thermal quenching apparatus. Sample is heated to  $380^{\circ}\text{C}$  then the clamp is released allowing the metal rod with the sample material to be quenched in either liquid nitrogen or water.

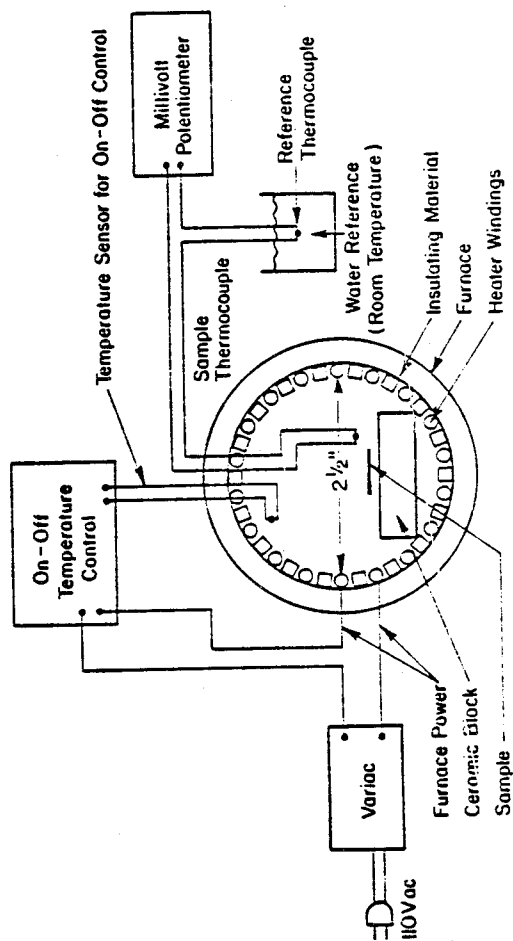


Figure 6: Post-Irradiation Annealing Apparatus view of the furnace with front panel removed.

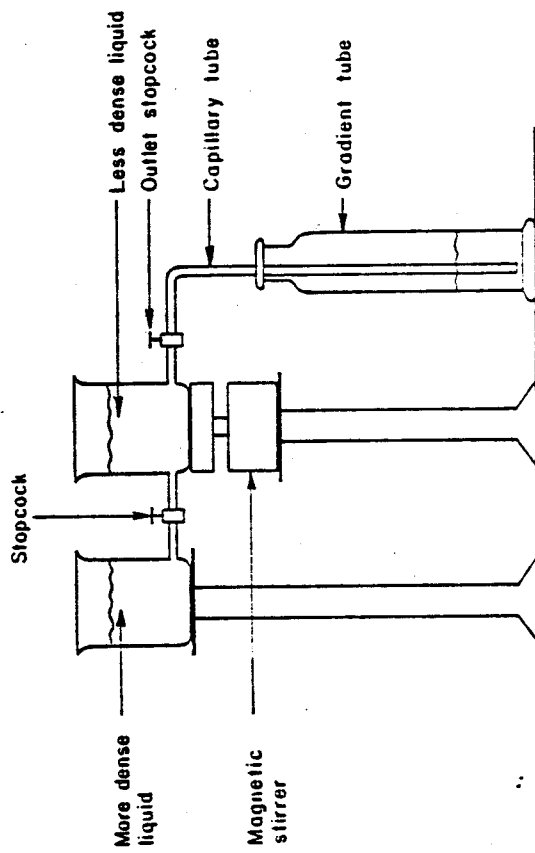


Figure 7: Density Gradient Column. Shown with filling apparatus in place. After column is filled the capillary is removed and the column placed in a constant temperature bath held at  $23 \pm 0.3^\circ\text{C}$ .

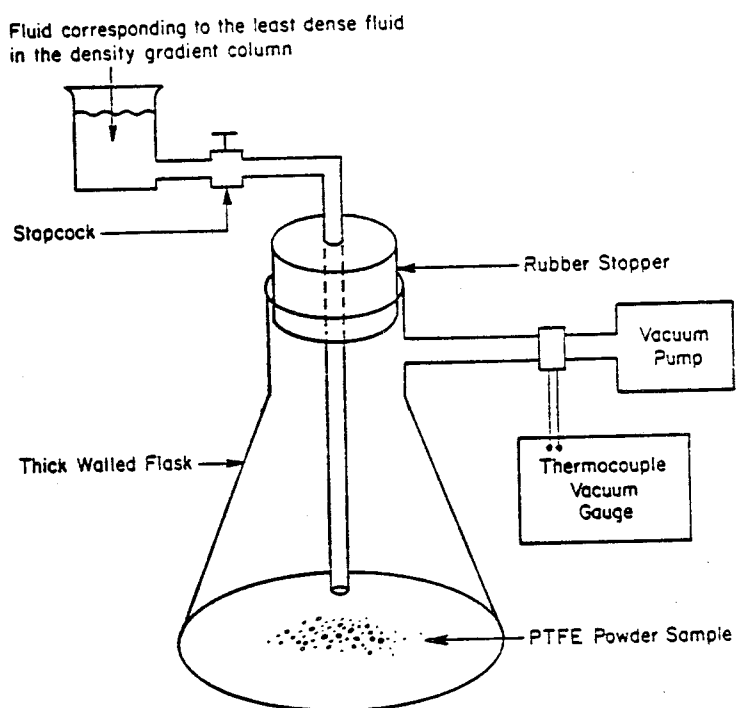
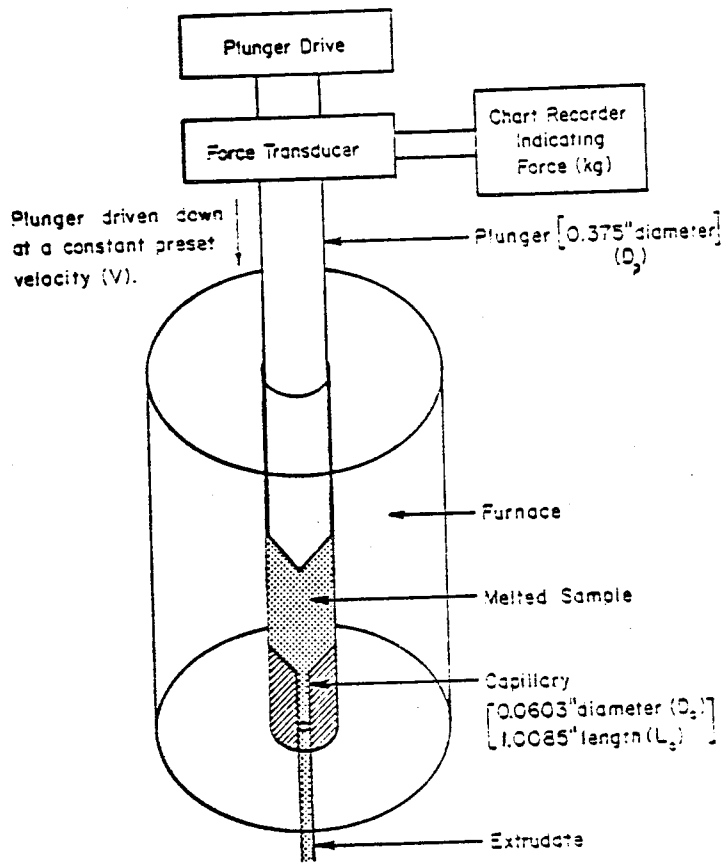


Figure 8: Powder resin wetting apparatus



$$\dot{\gamma}_3 (\text{sec}^{-1}) = \frac{2}{15} \frac{D_2^2}{D_1^2} V = 33.64 V (\text{cm/min})$$

$$\text{Shear Stress} = \frac{980655}{\pi D_1^2} \frac{D_2}{L_2} (\text{Force}) = 20,577 \cdot \text{Force (kg)}$$

Figure 9: Schematic diagram of the Instron Capillary Rheometer.

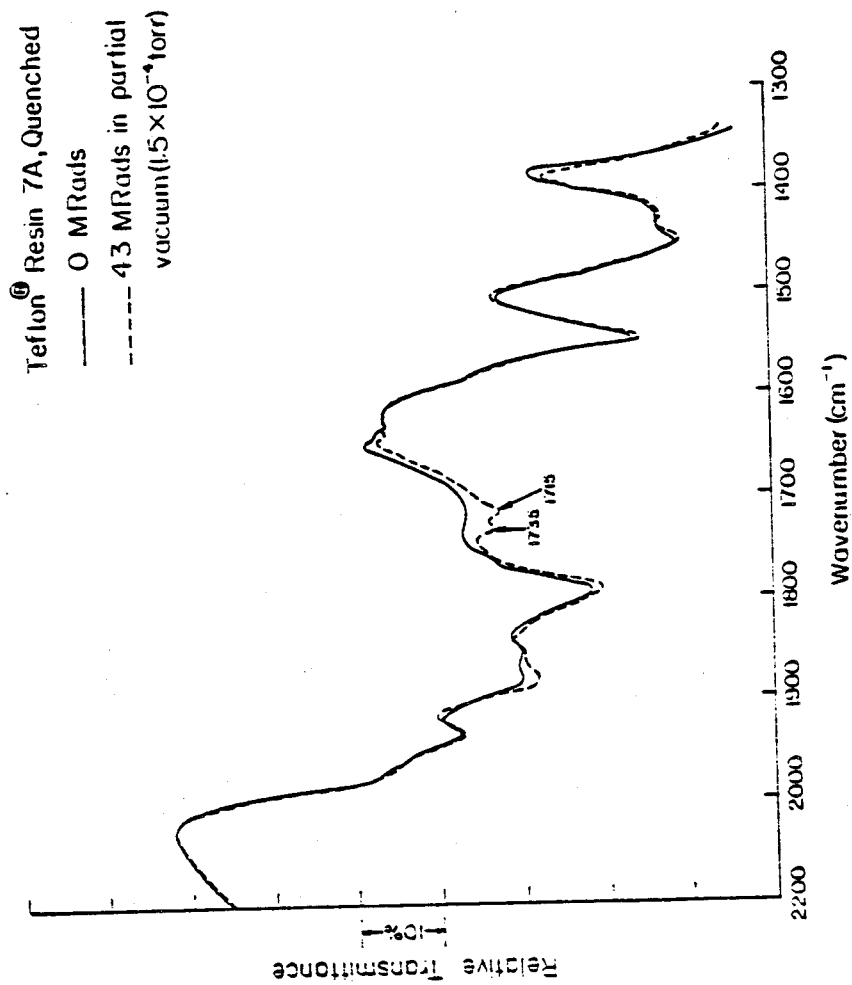


Figure 10: IR spectrum between  $2200$  and  $1300 \text{ cm}^{-1}$  of quenched Teflon<sup>®</sup> resin 7A irradiated to 43 MRads in a partial vacuum ( $1.5 \times 10^{-4}$  torr).

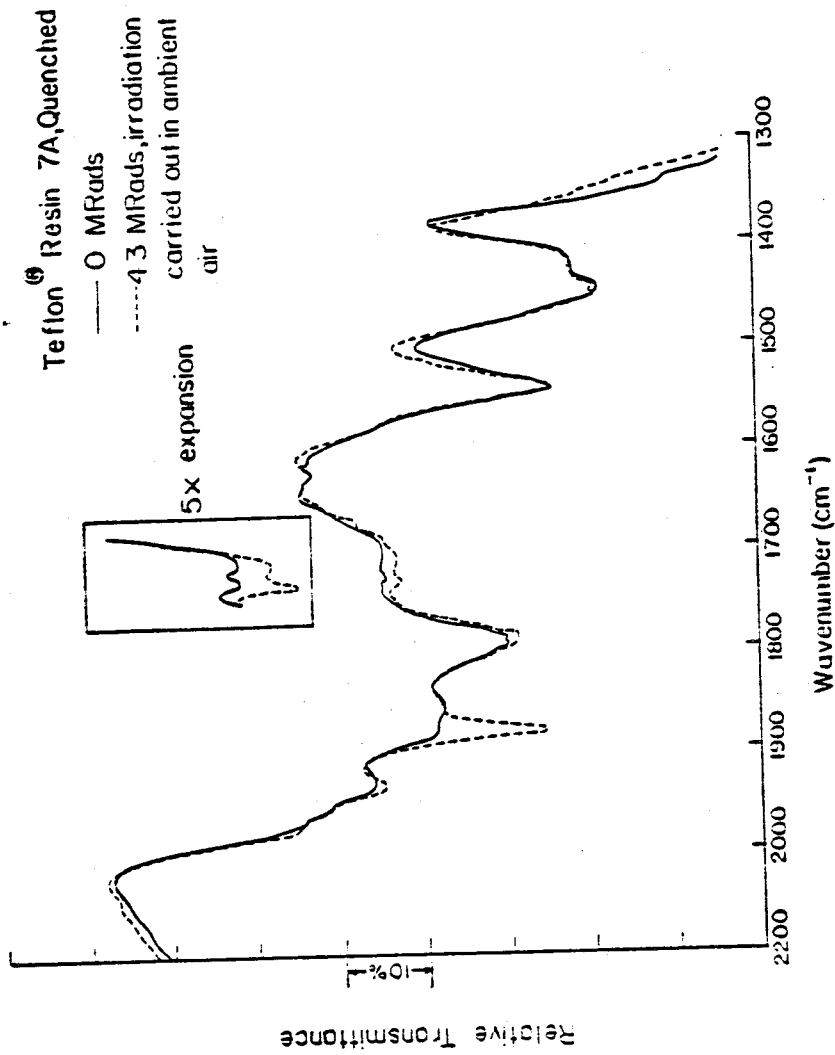


Figure 11: IR spectrum between 2100 and 1300 cm<sup>-1</sup> of quenched Teflon<sup>®</sup> resin 7A irradiated to 43 MRads in ambient air.

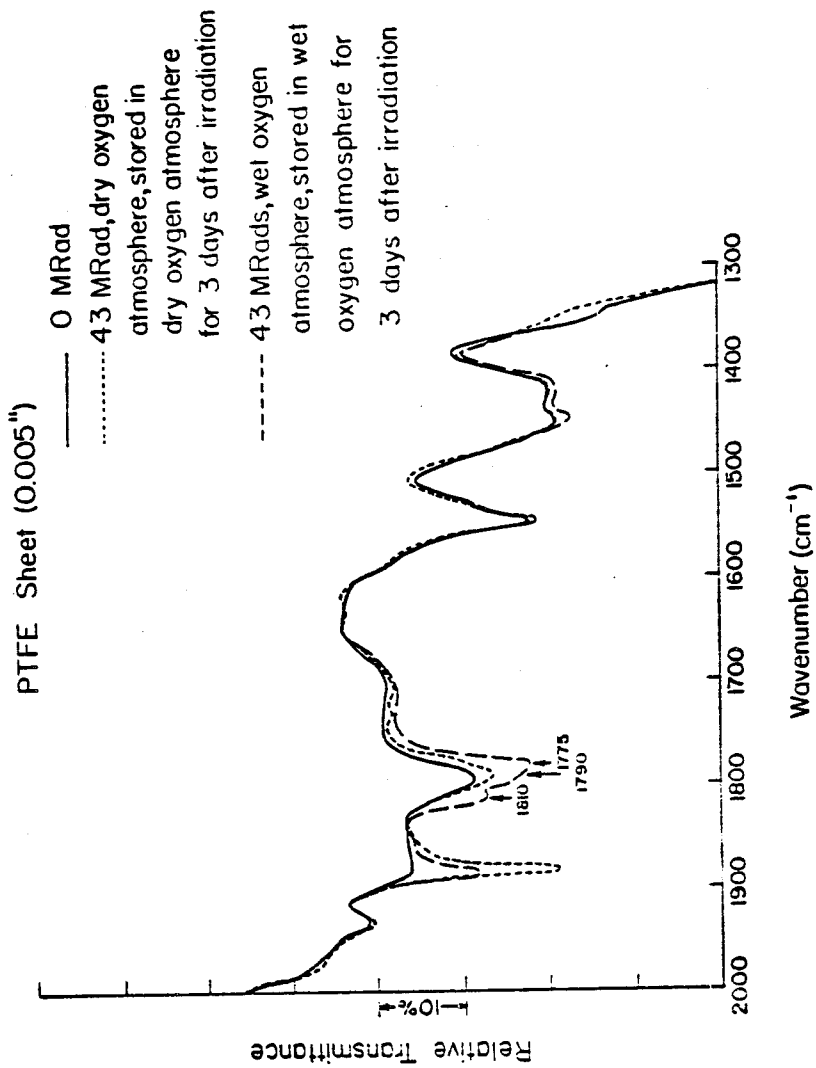


Figure 12: IR spectra between 2000 and 1300  $\text{cm}^{-1}$  of PTFE sheet irradiated to 43 MRads in wet and dry oxygen.

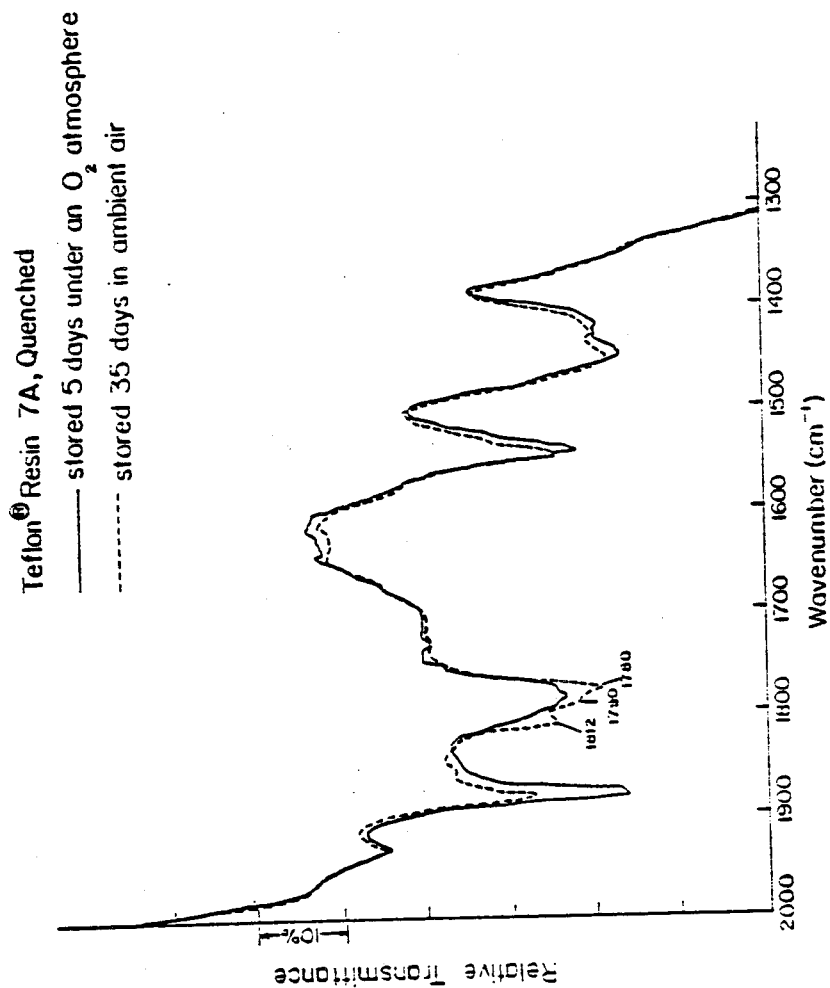


Figure 13: IR spectrum between 2000 and 1300 cm<sup>-1</sup> of quenched Teflon<sup>®</sup> resin 7A irradiated to 43 MRads in an oxygen atmosphere then stored 5 days in the oxygen atmosphere. Also shown is the IR spectrum of the same sample after storage for 35 days in ambient air.

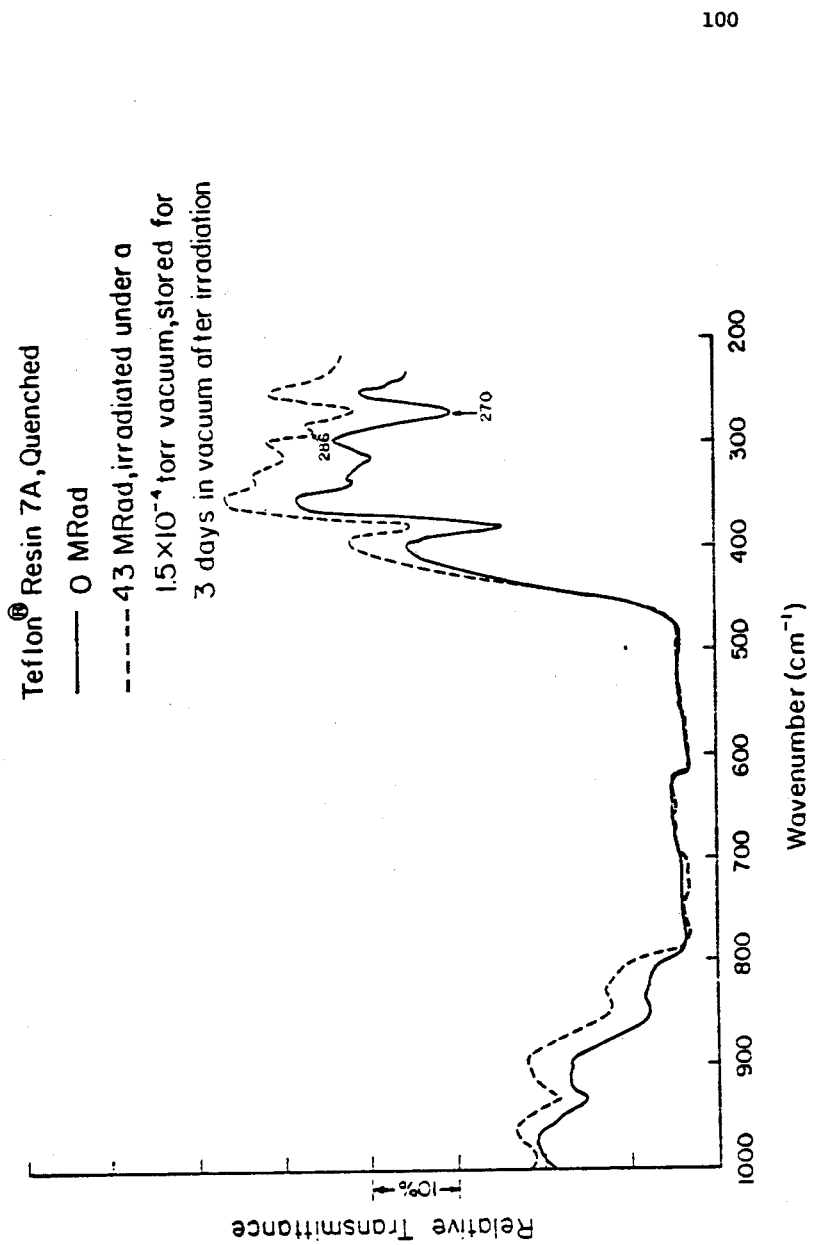


Figure 14: IR spectrum between  $1000$  and  $200 \text{ cm}^{-1}$  of quenched Teflon<sup>®</sup> resin 7A irradiated to 43 MRads in a partial vacuum ( $1.5 \times 10^{-4}$  torr).

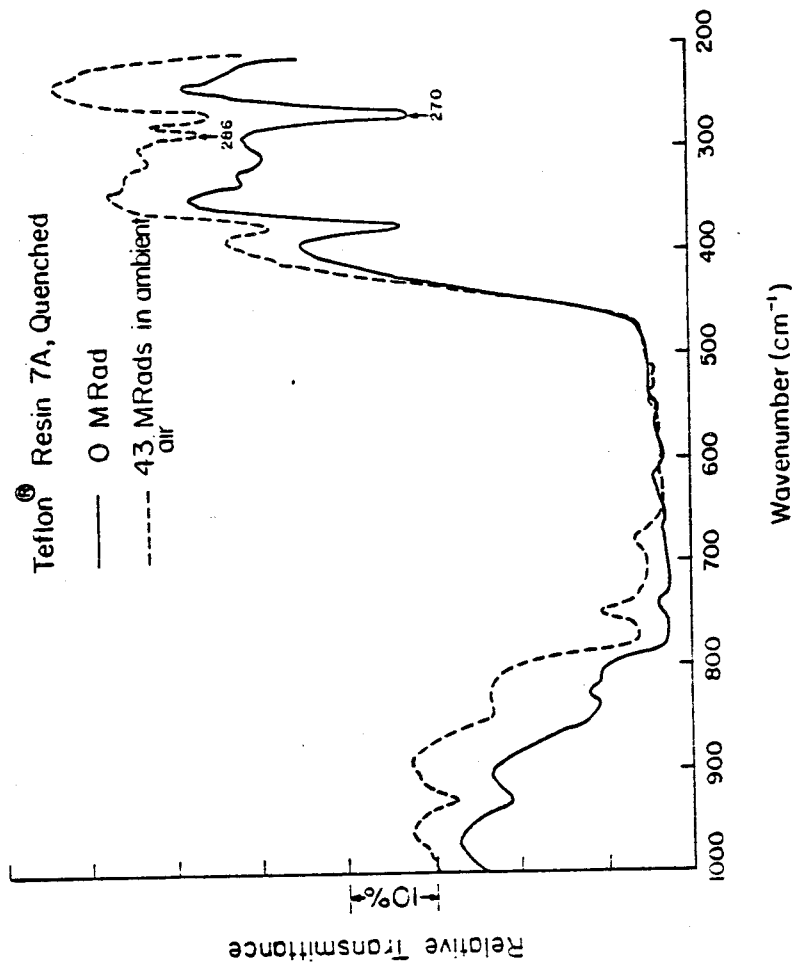


Figure 15: IR spectrum between 1000 and 200<sup>-1</sup> of quenched Teflon<sup>®</sup> resin 7A irradiated to 43 MRads in ambient air.

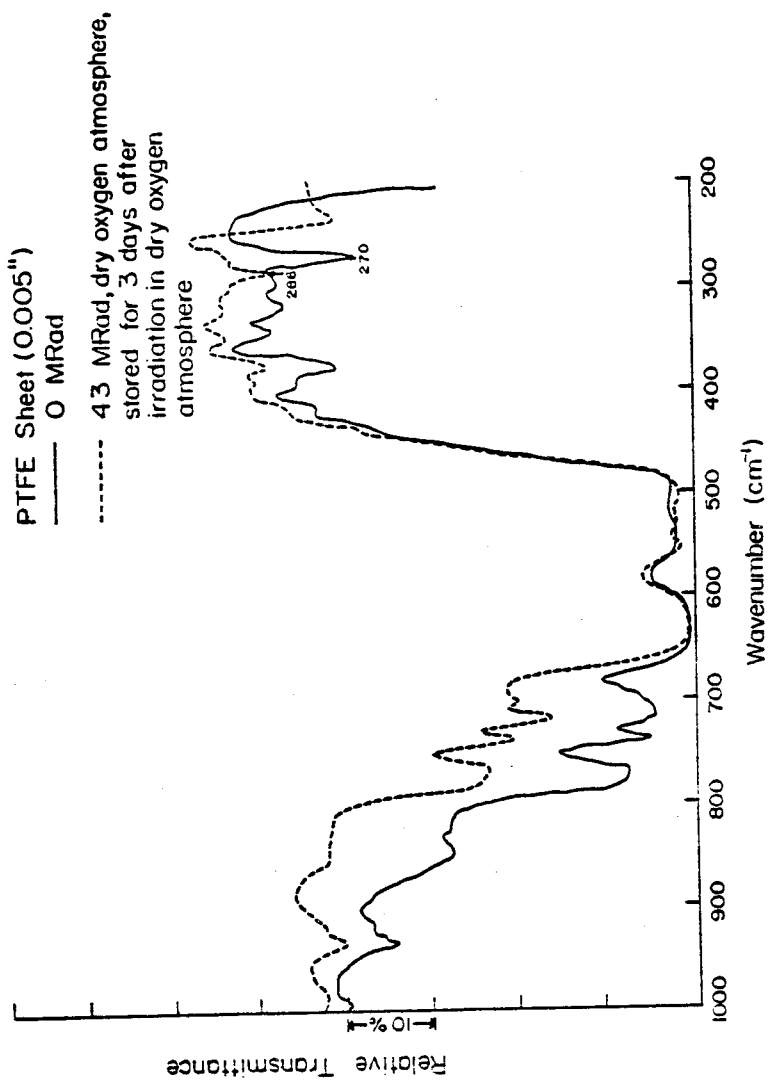


Figure 16: IR spectrum between  $1000$  and  $200 \text{ cm}^{-1}$  of PTFE sheet irradiated to 43 MRads in a dry oxygen atmosphere.

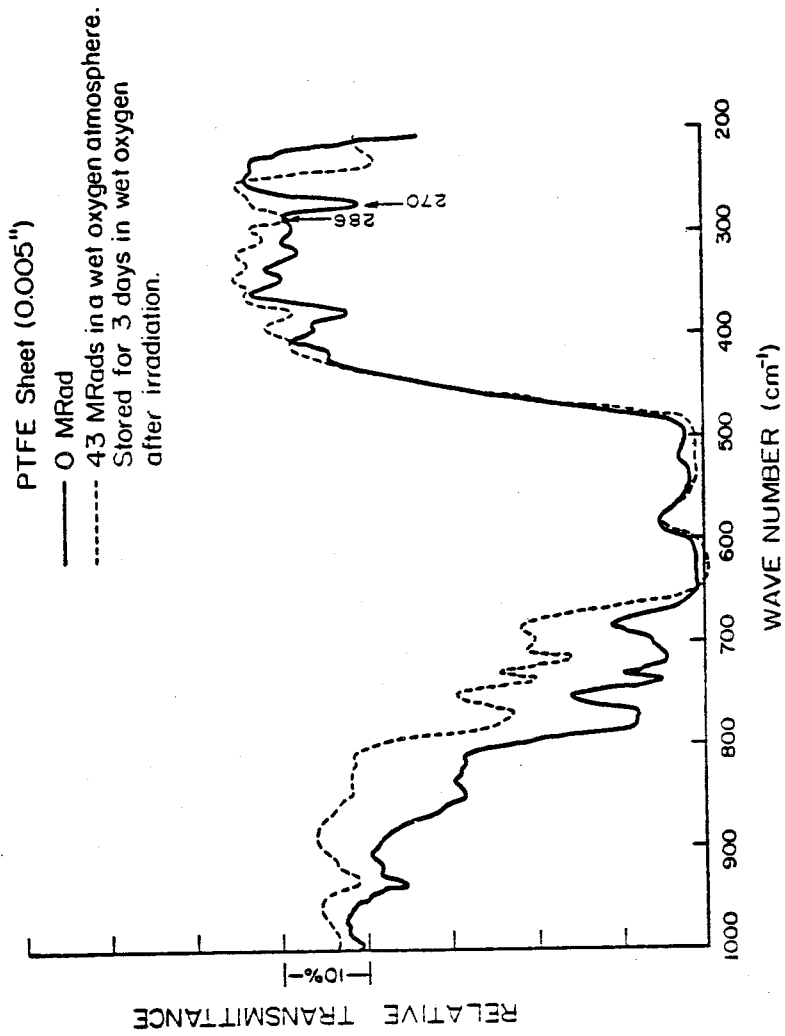


Figure 17: IR spectrum between 1000 and 200 cm<sup>-1</sup> of PTFE sheet irradiated to 43 MRads in a wet oxygen atmosphere.

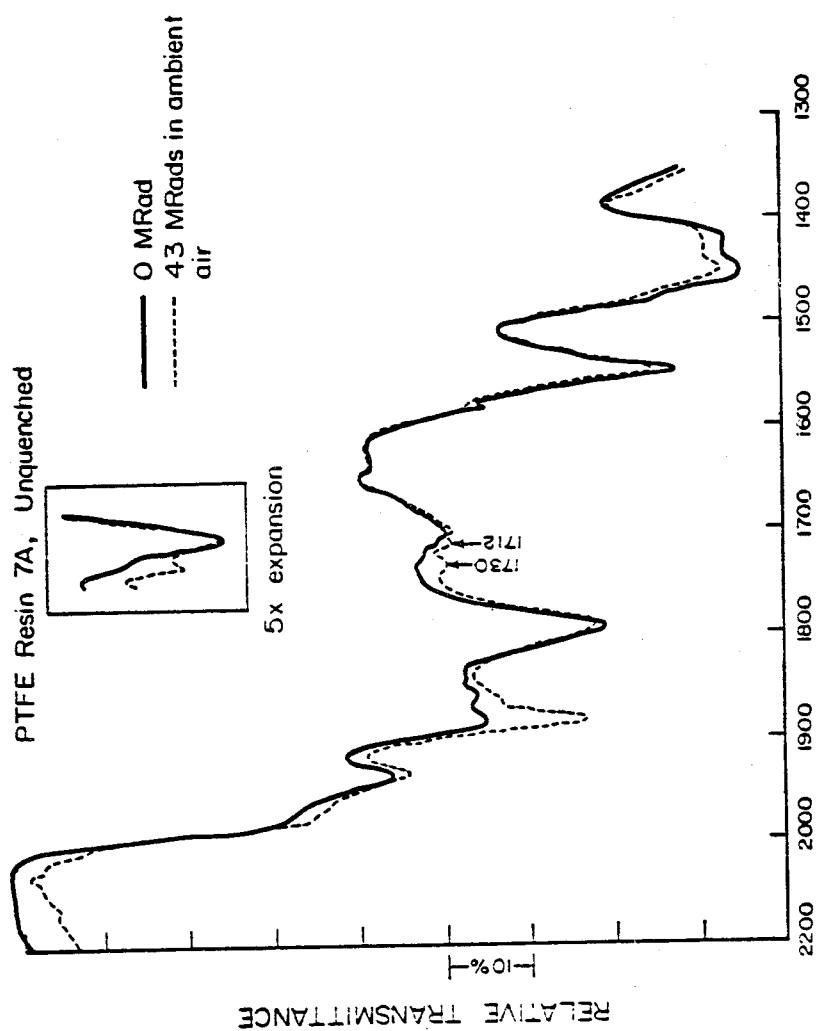


Figure 18: IR spectrum between 2200 and 1300  $\text{cm}^{-1}$  of unquenched Teflon<sup>®</sup> resin 7A irradiated to 43 MRads in ambient air.

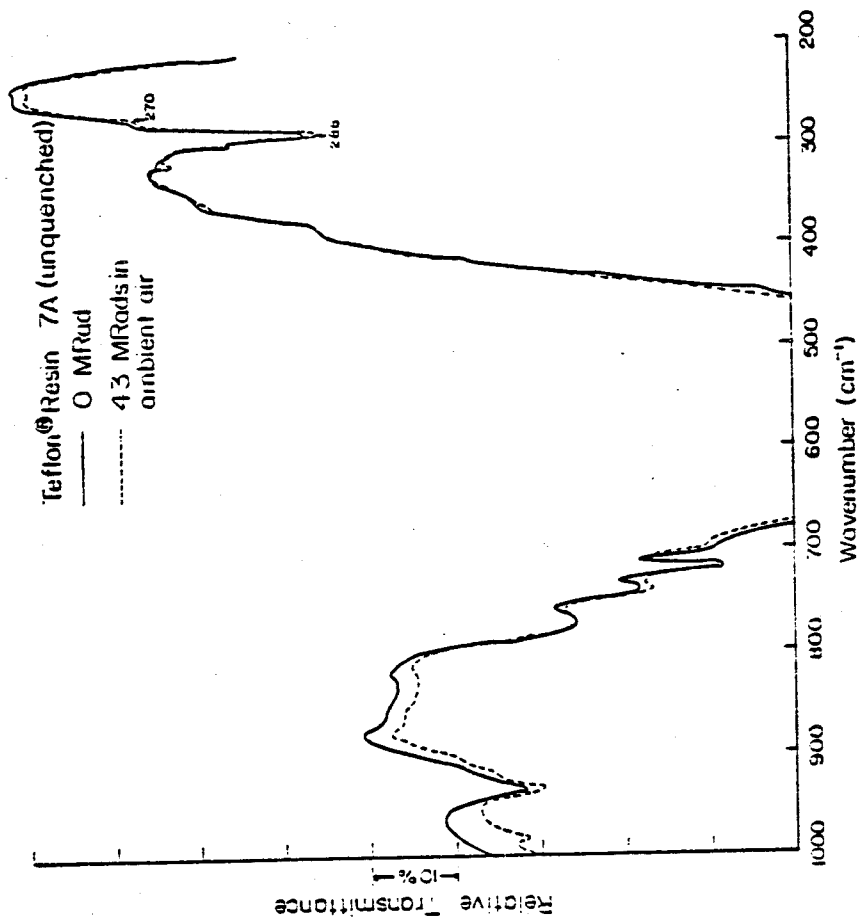


Figure 19: IR spectrum between 1000 and 200 cm<sup>-1</sup> of unquenched Teflon® resin 7A irradiated to 43 MRads in ambient air.

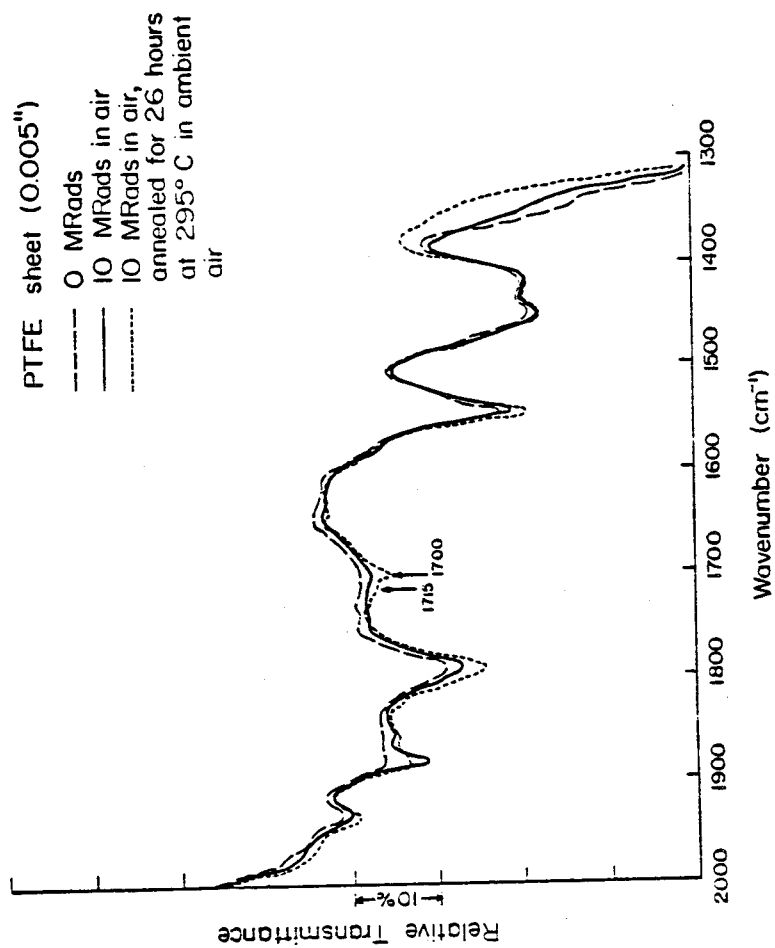


Figure 20: IR spectrum between 2000 and 1300  $\text{cm}^{-1}$  of PTFE sheet irradiated to 10MRads in ambient air and also the spectrum of the same sample after annealing for 26 hours at 295°C in ambient air.

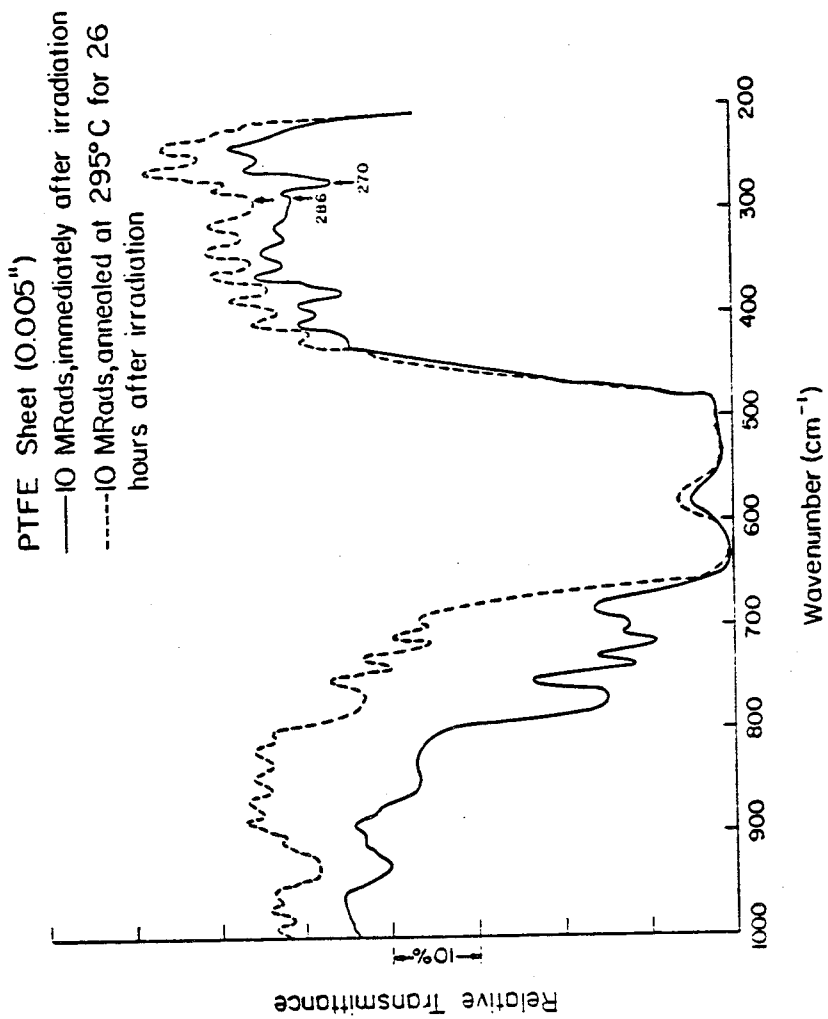


Figure 21: IT spectra of the same samples used for Figure 20 between 1000 and 200  $\text{cm}^{-1}$ .

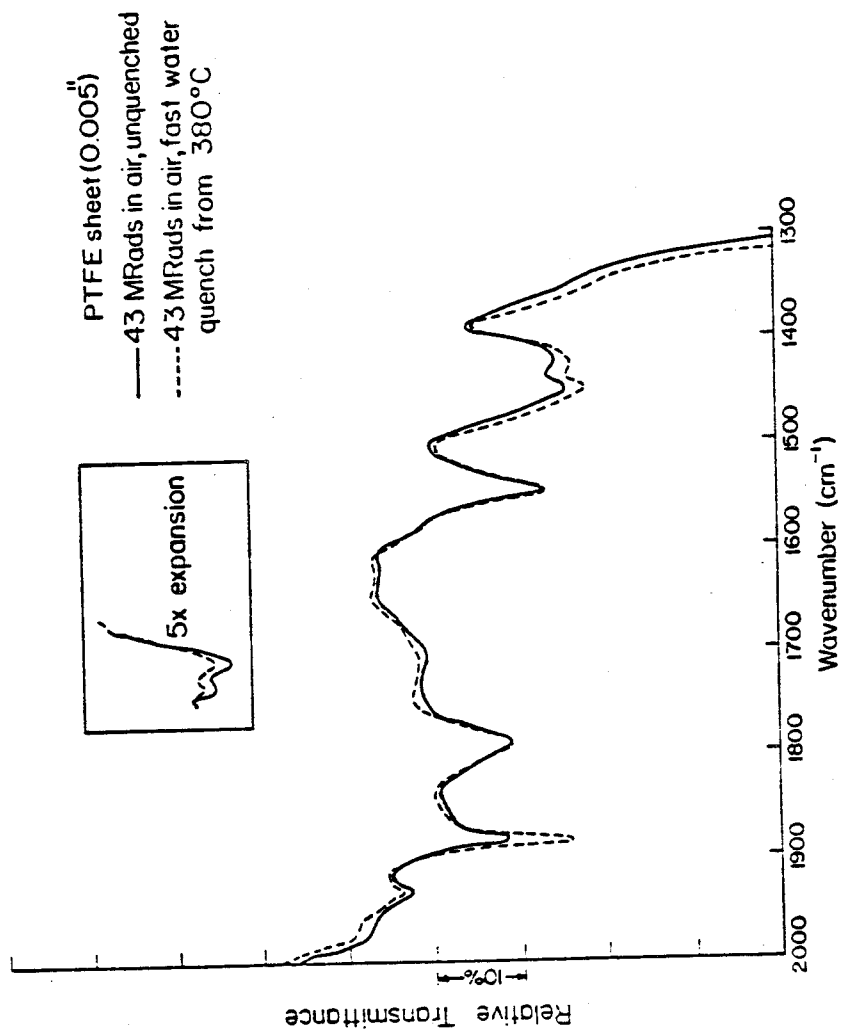


Figure 22: IR spectra between 2000 and 1300  $\text{cm}^{-1}$  of samples of PTFE sheet of differing pre-irradiation crystallinities irradiated to 43 MRads in ambient air.

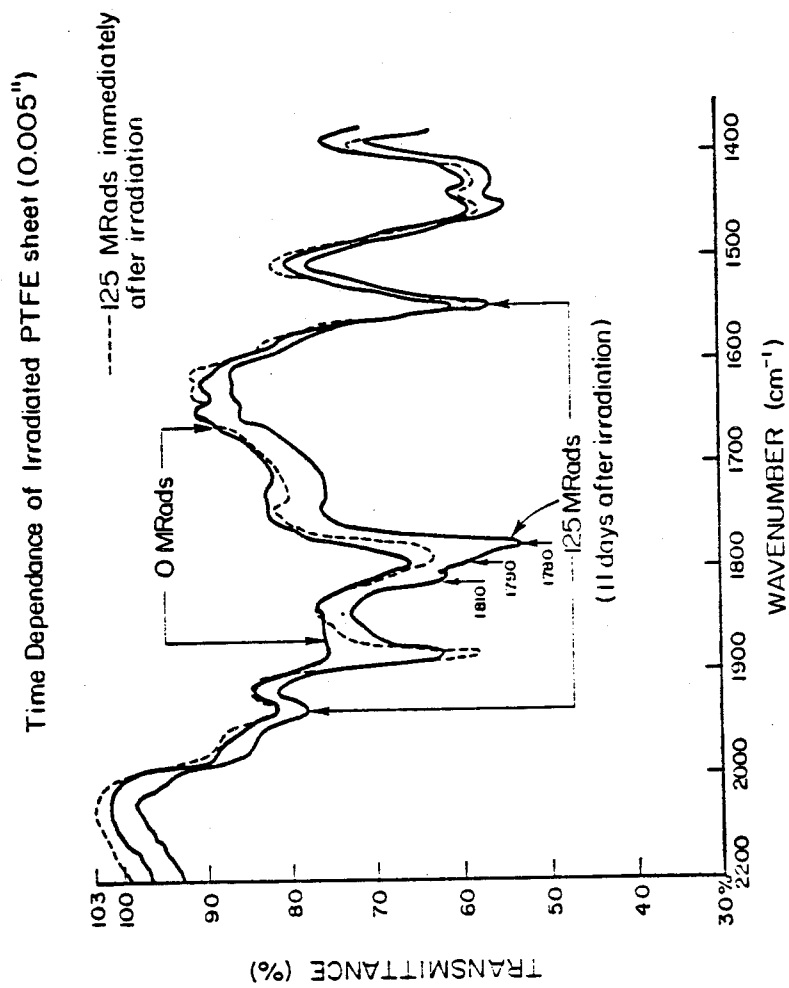


Figure 23: Time dependence of the IR spectrum between 2200 and 1400  $\text{cm}^{-1}$  of PTFE sheet irradiated to 125 MRads in ambient air and subsequently stored in ambient air.

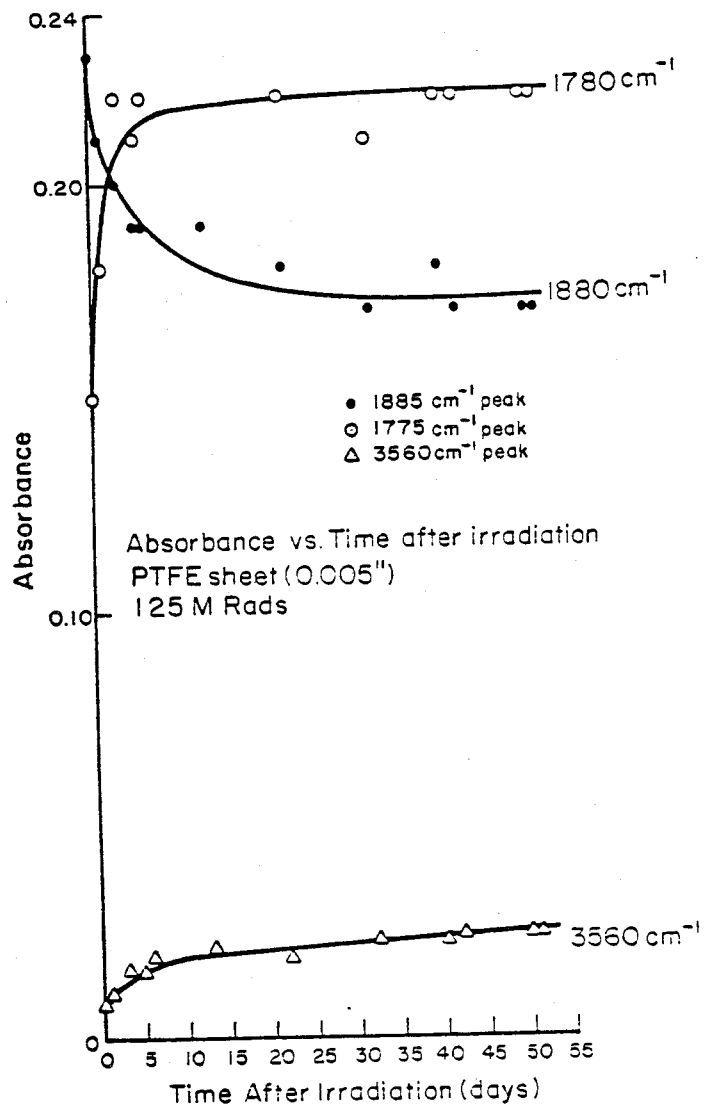


Figure 24: Absorbance vs. time after irradiation of the absorption bands at 3560, 1880 and 1780  $\text{cm}^{-1}$  for the same sample used in Figure 23.

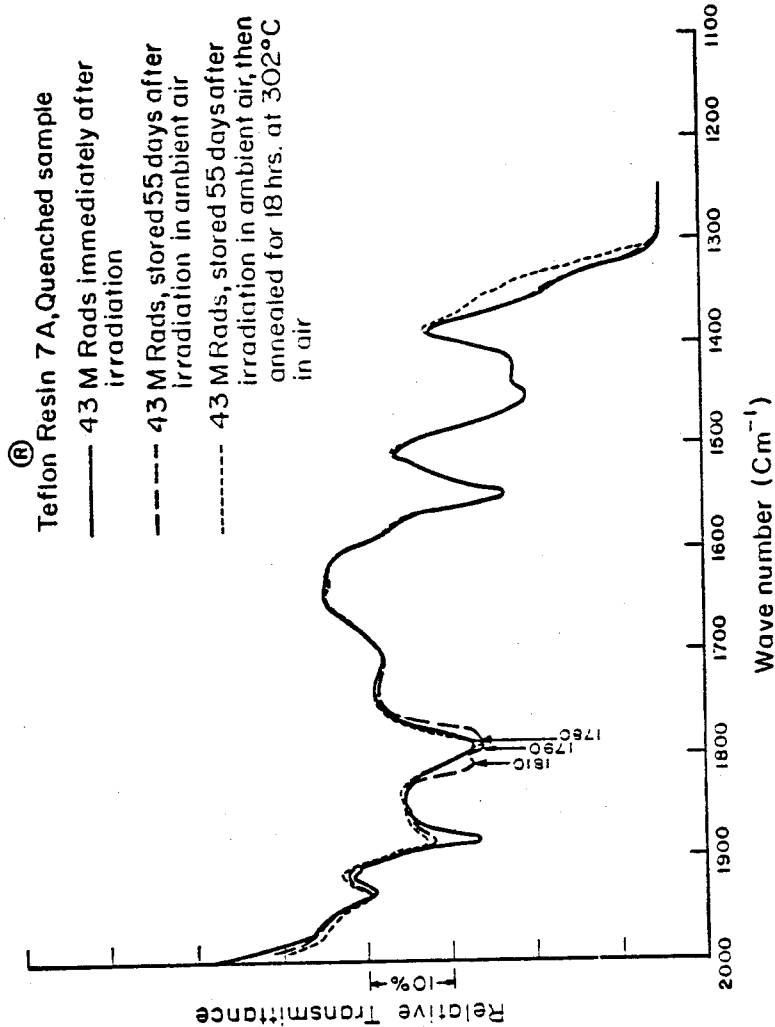


Figure 25: IR spectrum from 2000 to 1100 cm<sup>-1</sup> of quenched Teflon® resin 7A irradiated to 43 MRads in ambient air, stored for 55 days in ambient air, then annealed for 18 hours at 302°C in air.

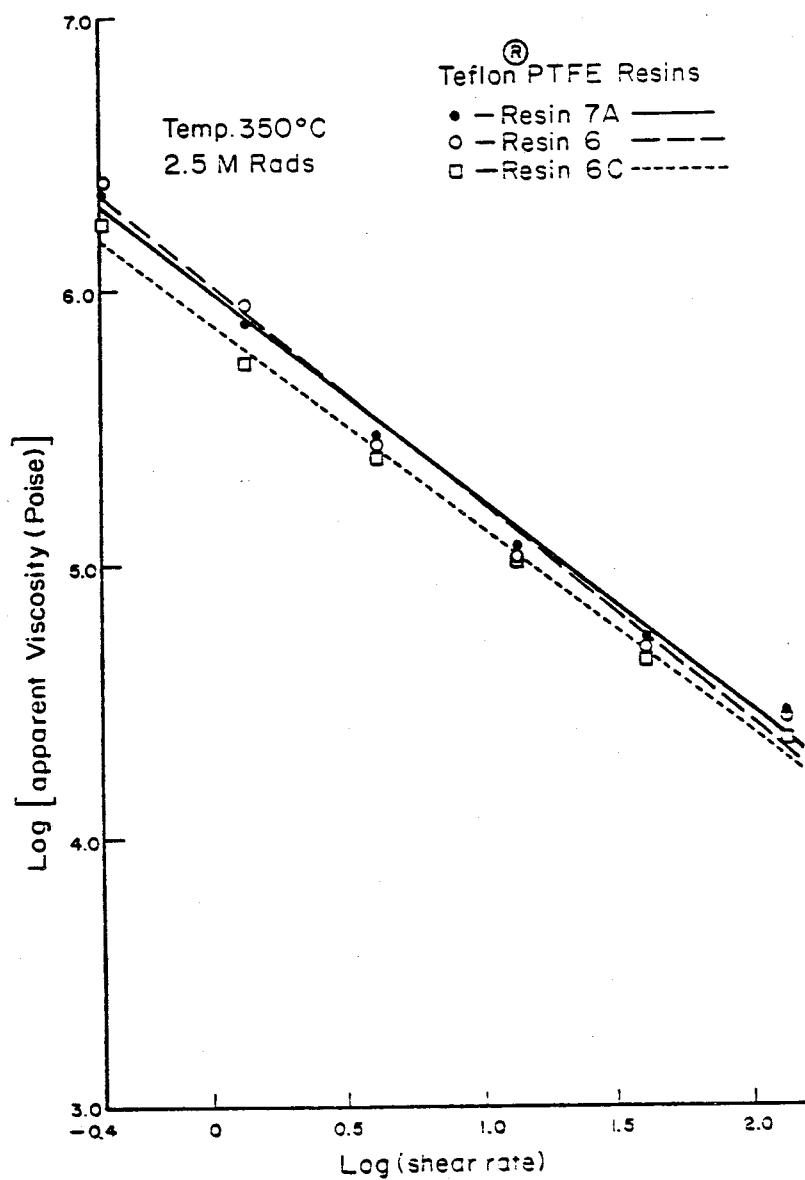


Figure 26: Plots of log apparent melt viscosity vs. log apparent shear rate measured at 350°C for samples of Teflon<sup>®</sup> resins 7A, 6 and 6C irradiated to 2.5 MRads in air.

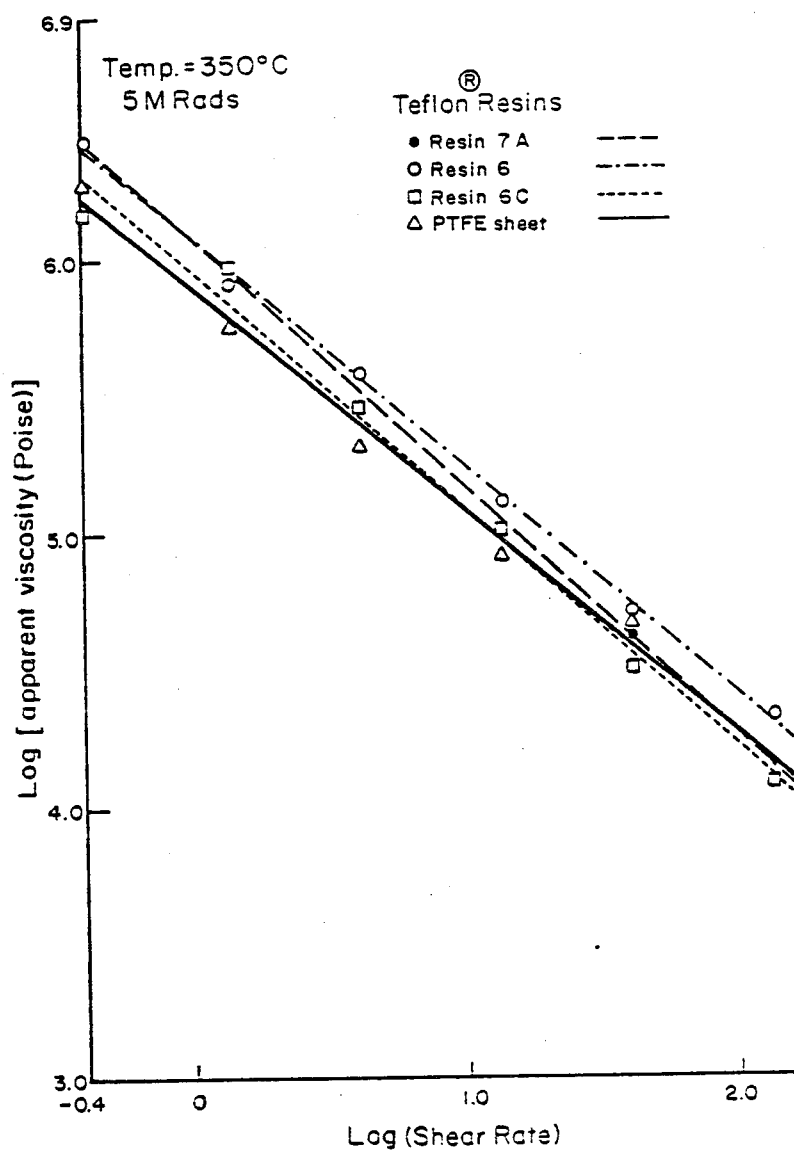


Figure 27: Plots of log apparent melt viscosity vs. log apparent shear rate measured at 350°C for samples of Teflon<sup>®</sup> resins 7A, 6 and 6C and PTFE sheet irradiated to 5 MRads in air.

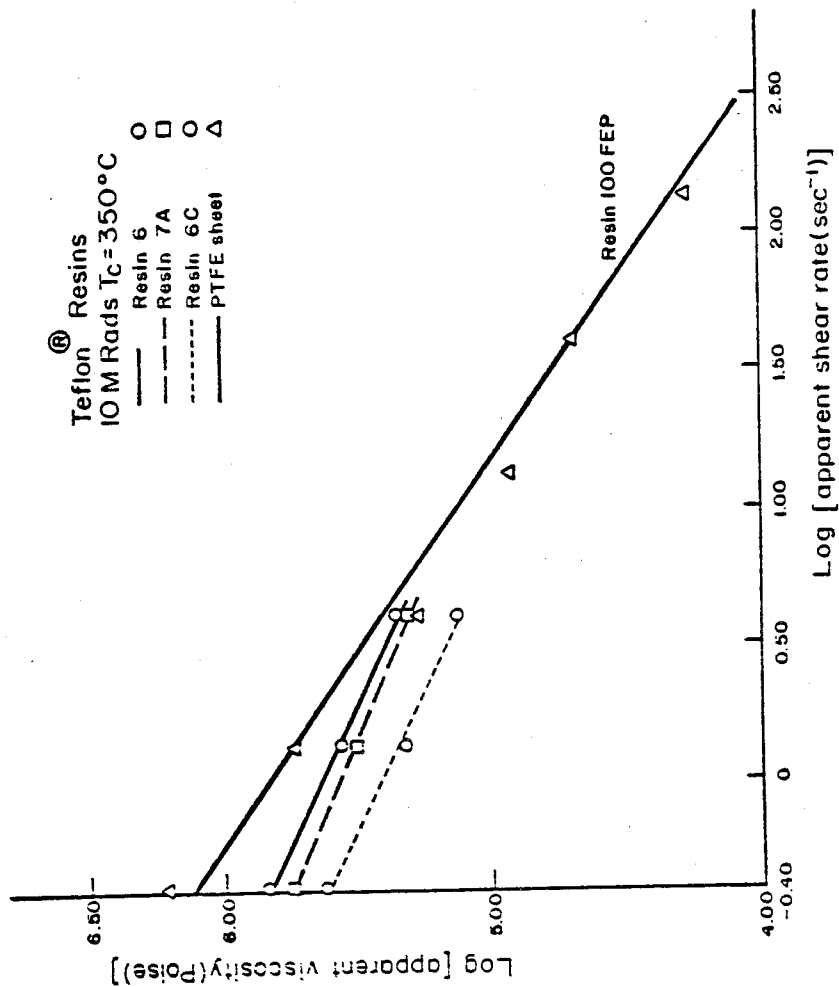


Figure 28: Plots of log apparent melt viscosity vs. log apparent shear rate measured at  $350^\circ\text{C}$  for samples of Teflon<sup>®</sup> resins 7A, 6 and 6C and PTFE sheet irradiated to 10 MRads in air.

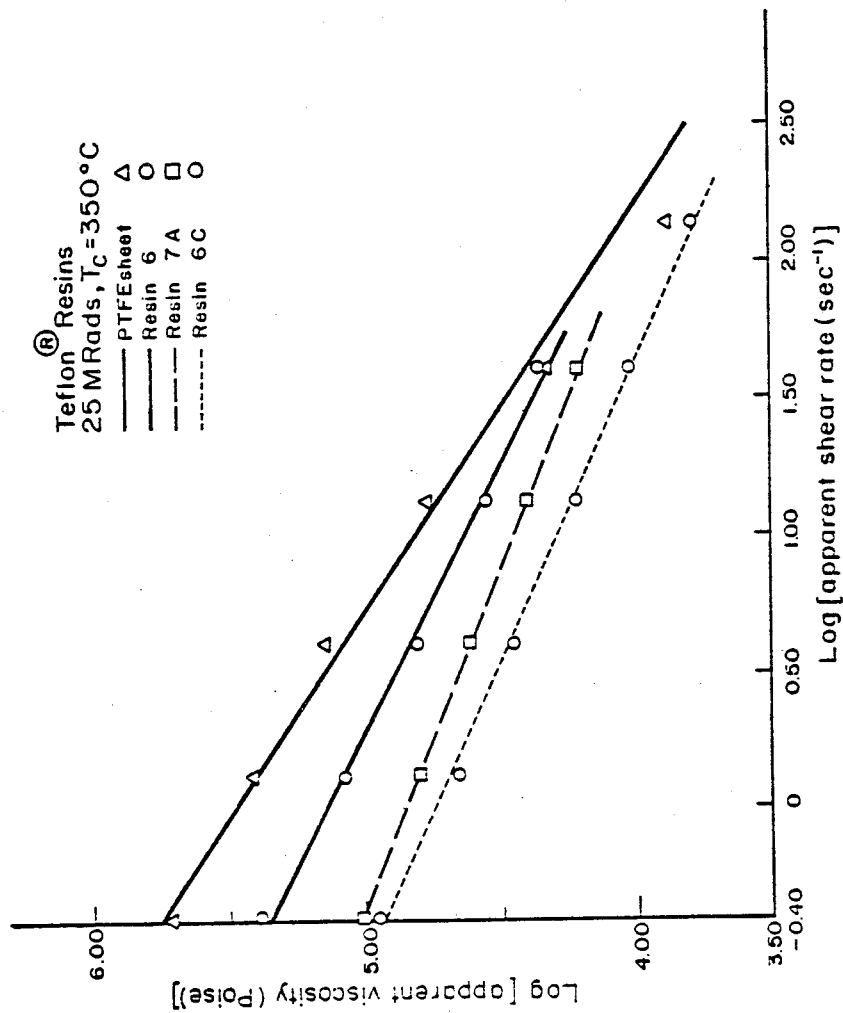


Figure 29: Plots of log apparent melt viscosity vs. log apparent shear rate measured at  $350^\circ\text{C}$  for samples of Teflon<sup>®</sup> resins 7A, 6 and 6C and PTFE sheet irradiated to 25 MRads in air.

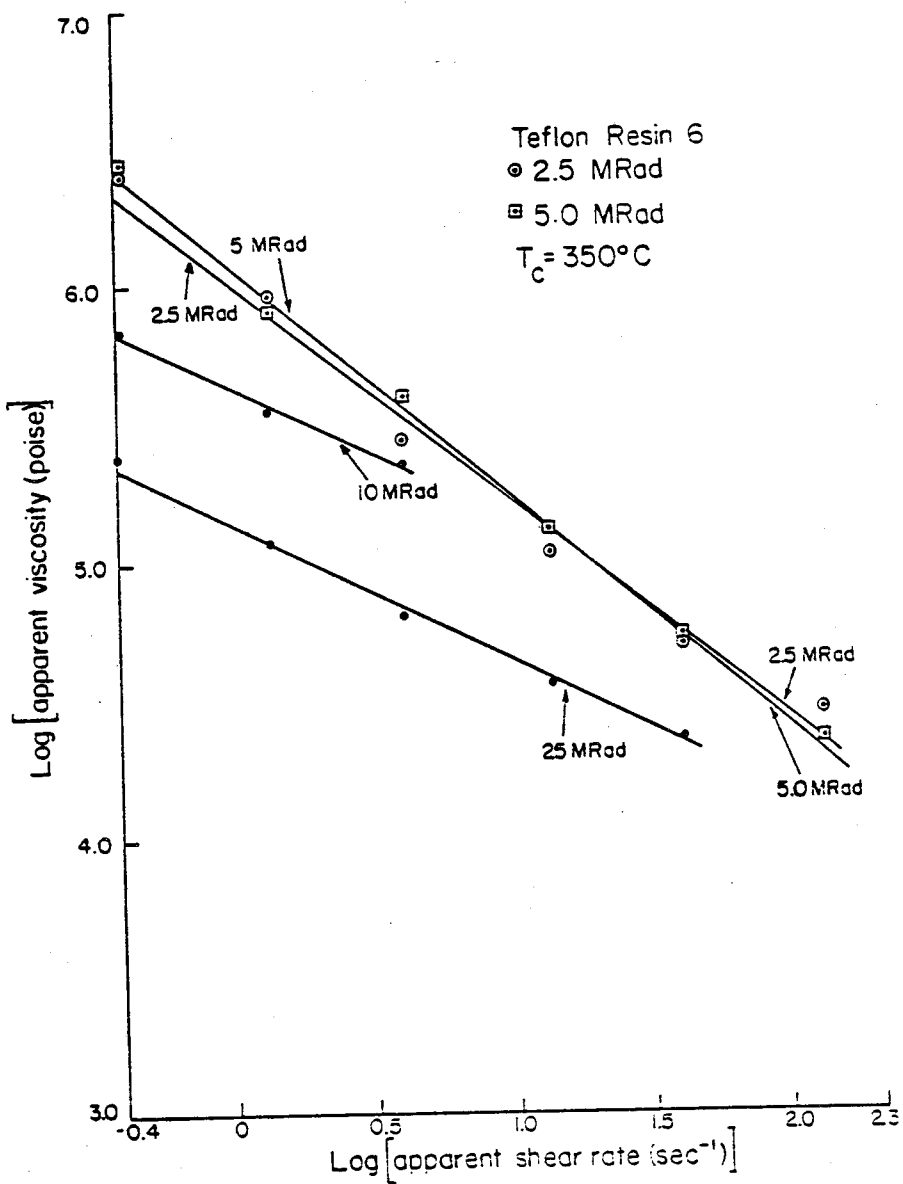


Figure 30: Plots of log apparent melt viscosity vs. log apparent shear rate measured at  $350^\circ\text{C}$  for Teflon<sup>®</sup> resin 6 irradiated to doses of 2.5, 5, 10 and 25 MRads in air.

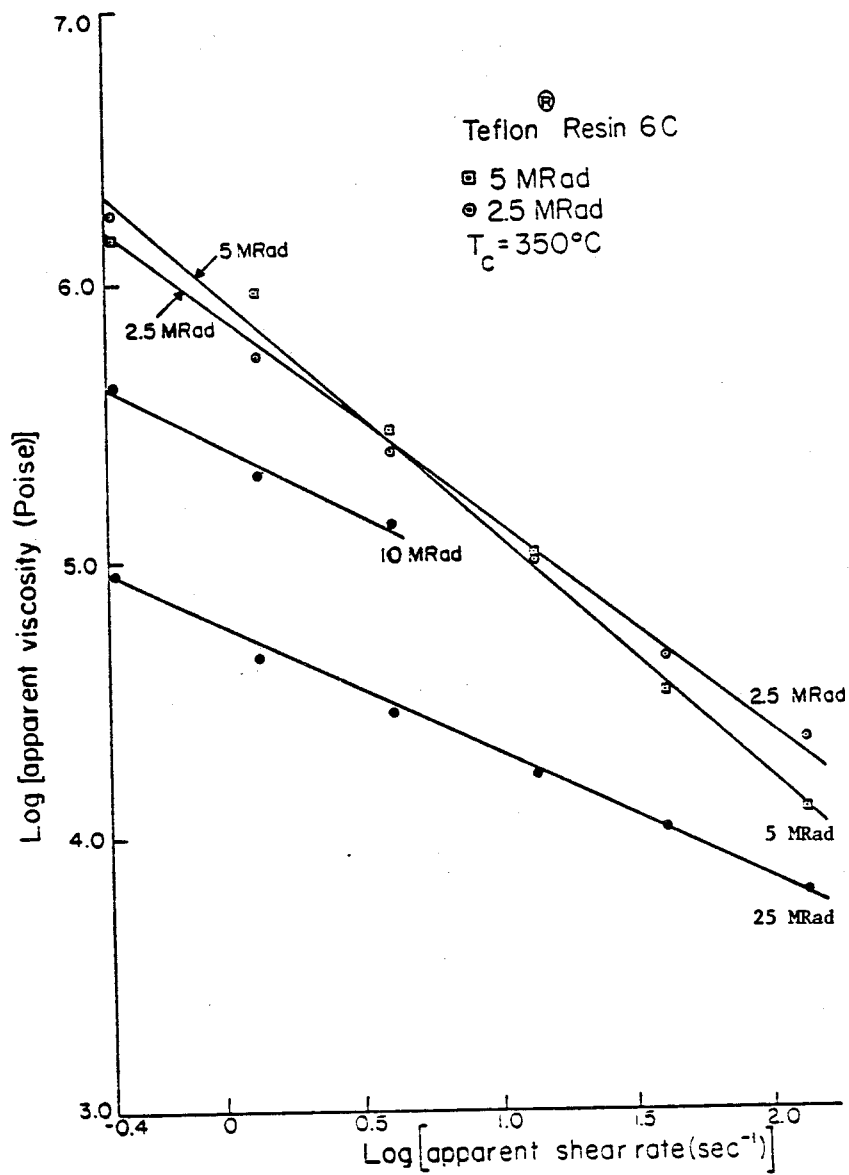


Figure 31: Plots of log apparent melt viscosity vs. log apparent shear rate for Teflon<sup>®</sup> resin 6C irradiated to doses of 2.5, 5, 10 and 25 MRads in air.

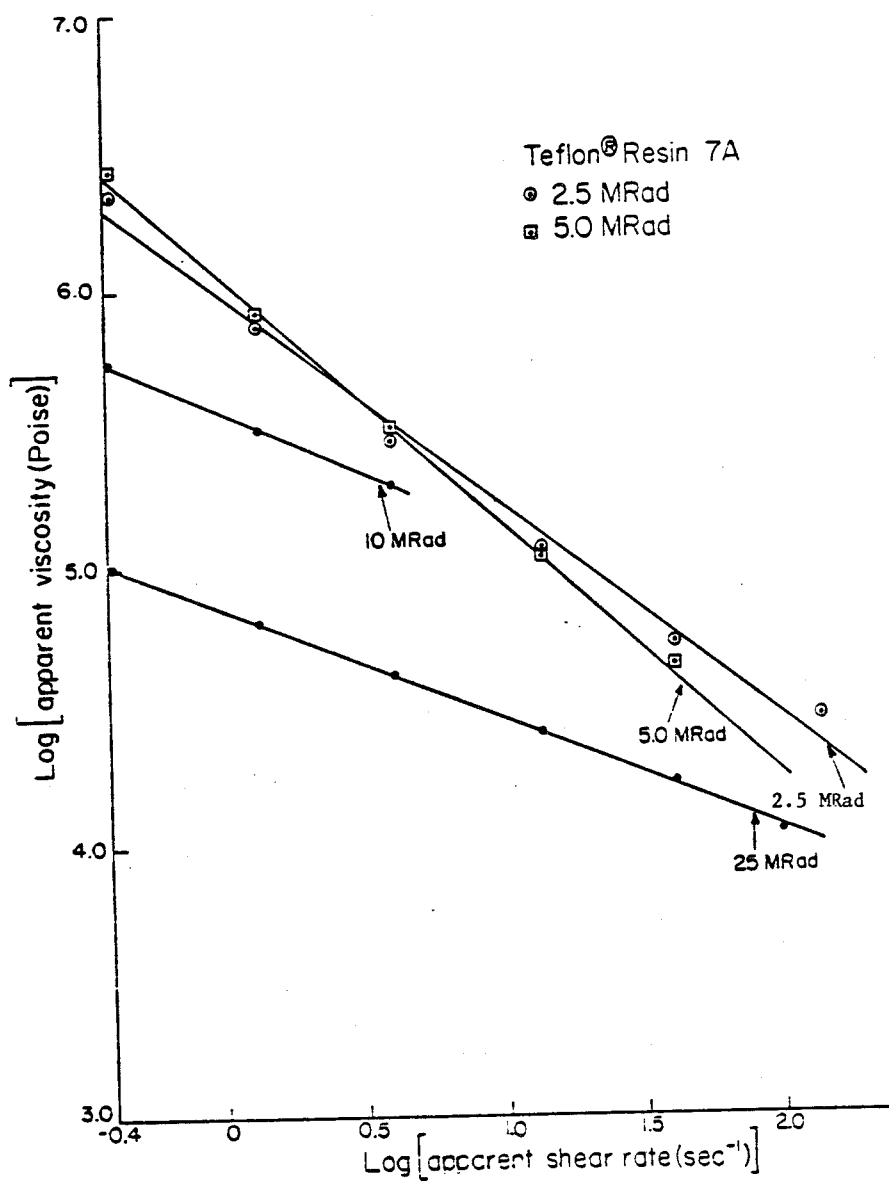


Figure 32: Plots of log apparent melt viscosity vs. log apparent shear rate measured at 350°C for Teflon<sup>®</sup> resin 7A irradiated to doses of 2.5, 5, 10 and 25 MRads in air.

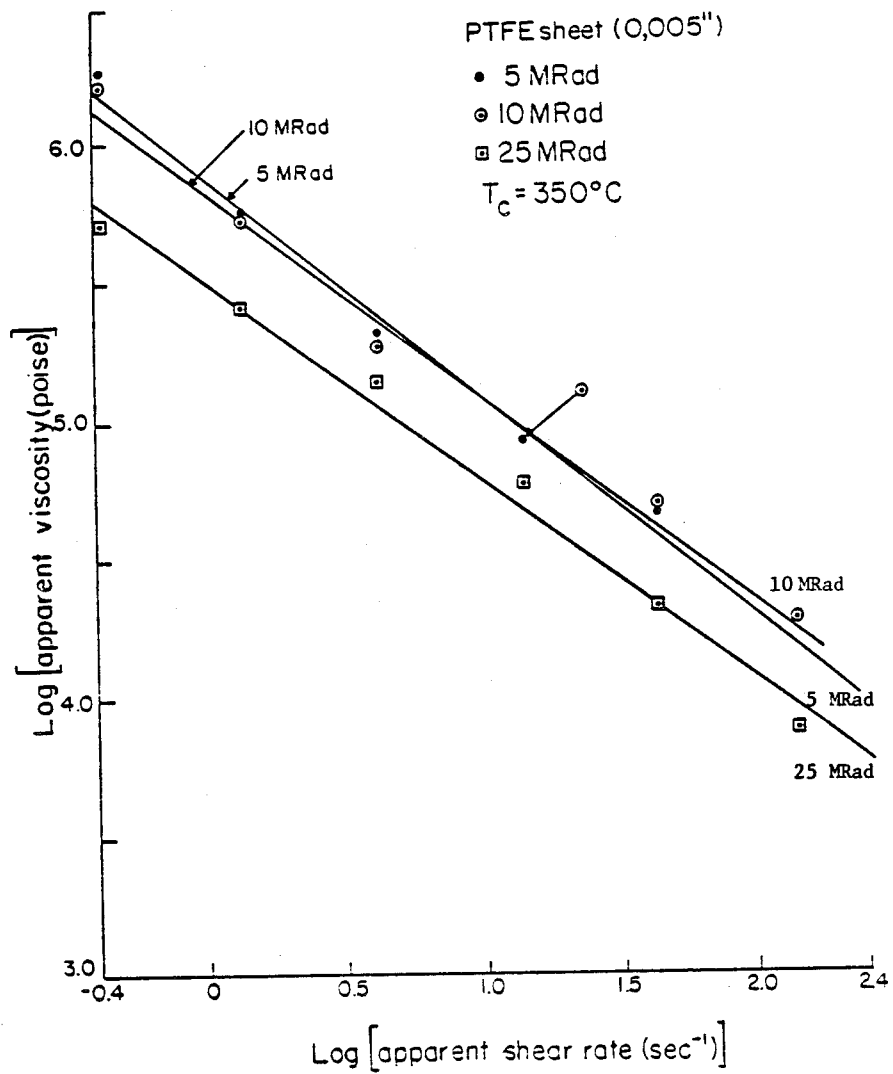


Figure 33: Plots of log apparent melt viscosity vs. log apparent shear rate measured at  $350^\circ\text{C}$  for PTFE sheet irradiated to doses of 5, 10 and 25 MRads in air.

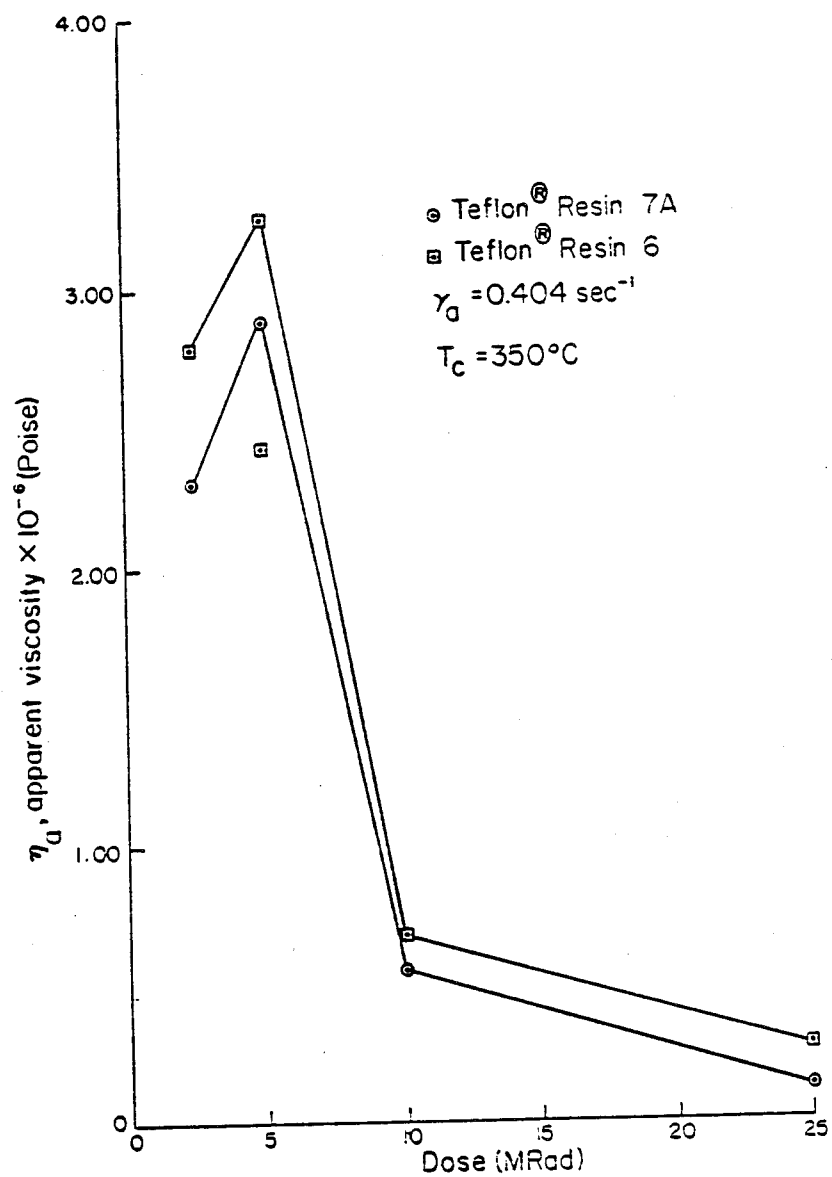


Figure 34: Plots of apparent melt viscosity vs. dose at an apparent shear rate of  $0.404 \text{ sec}^{-1}$  measured at  $350^\circ\text{C}$  for Teflon<sup>®</sup> resins 6 and 7A.

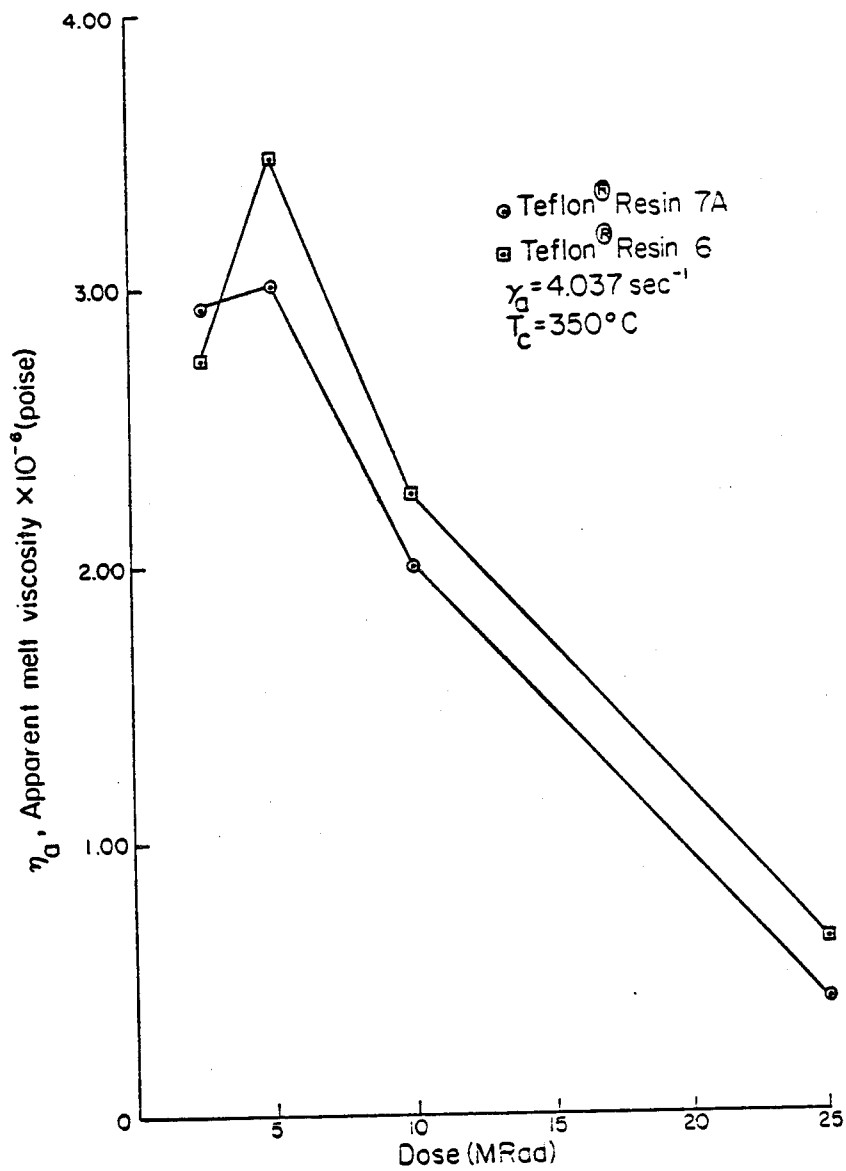


Figure 35: Plots of apparent melt viscosity vs. dose at an apparent shear rate of  $4.04 \text{ sec}^{-1}$  measured at  $350^\circ\text{C}$  for Teflon<sup>®</sup> resins 6 and 7A.

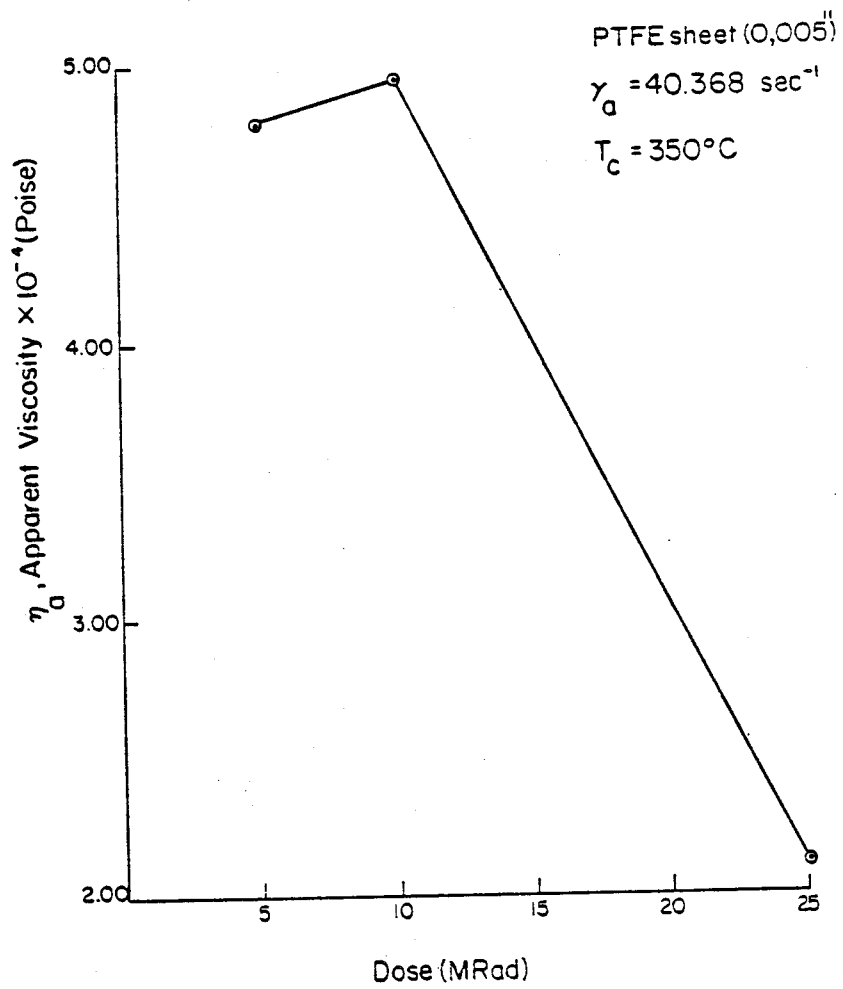


Figure 36: Plot of apparent melt viscosity vs. dose measured at 350°C for PTFE sheet at an apparent shear rate of 4.37 sec<sup>-1</sup>.

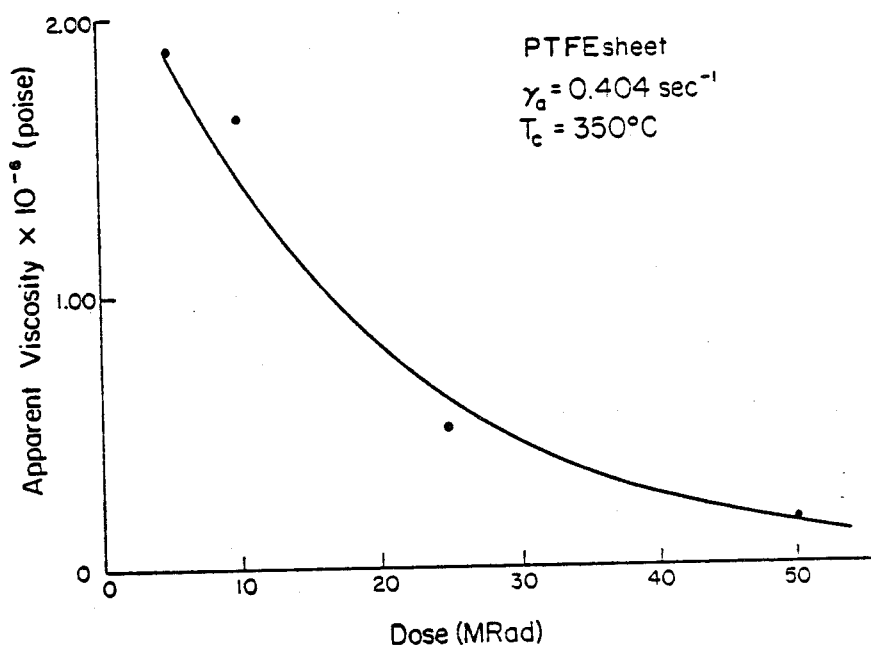
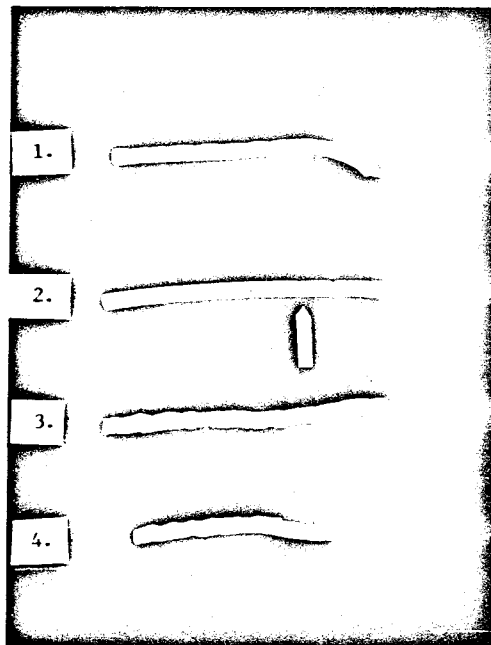


Figure 37: Plot of apparent melt viscosity vs. dose measured at  $350^\circ\text{C}$  for PTFE sheet at an apparent shear rate of  $40.37 \text{ sec}^{-1}$ .

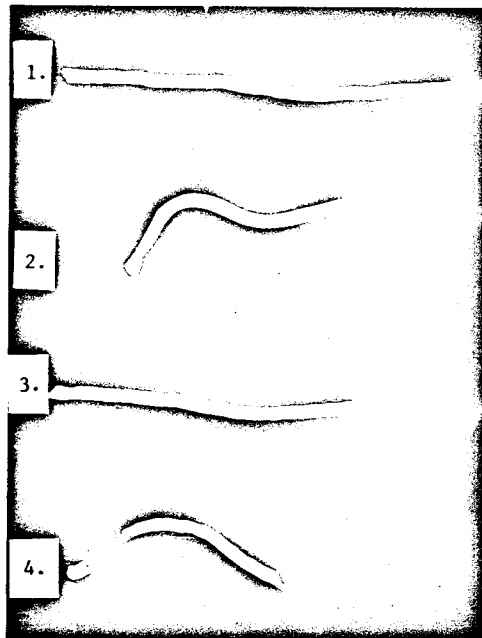
Teflon<sup>®</sup> Resin  
 Apparent Shear Rate =  $0.404 \text{ sec}^{-1}$   
 Capillary Temperature =  $350^{\circ}\text{C}$



	Dose (NRad)	Die Swell
1.	2.5	0.93
2.	5	0.98
Apparent Shear Rate = $13.46 \text{ sec}^{-1}$		
3.	2.5	0.98
4.	5	1.02

Figure 38: Extrudate samples of Teflon<sup>®</sup> resin 6.

Teflon<sup>®</sup> Resin 7A  
 Apparent Shear Rate =  $4,04 \text{ sec}^{-1}$   
 Capillary Temperature =  $350^{\circ}\text{C}$



	Dose (MRad)	Die Swell
1.	2.5	0.95
2.	5	1.01
Apparent Shear Rate = $13.46 \text{ sec}^{-1}$		
3.	2.5	0.96
4.	5	1.02

Figure 39: Extrudate samples of Teflon<sup>®</sup> resin 7A.

Teflon<sup>®</sup> Resin 6  
Apparent Shear Rate =  $1.35 \text{ sec}^{-1}$   
Dose = 5 MRads  
Die Swell = 0.95  
Capillary Temperature =  $350^{\circ}\text{C}$

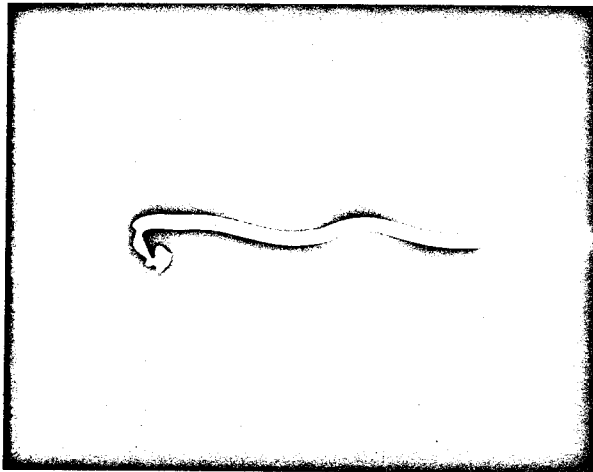


Figure 40: Example of a twisted extrudate

Teflon<sup>®</sup> Resin 7A  
Apparent Shear Rate =  $2.02 \text{ sec}^{-1}$   
Dose = 5 MRad  
Die Swell = 1.18  
Capillary Temperature =  $380^{\circ}\text{C}$

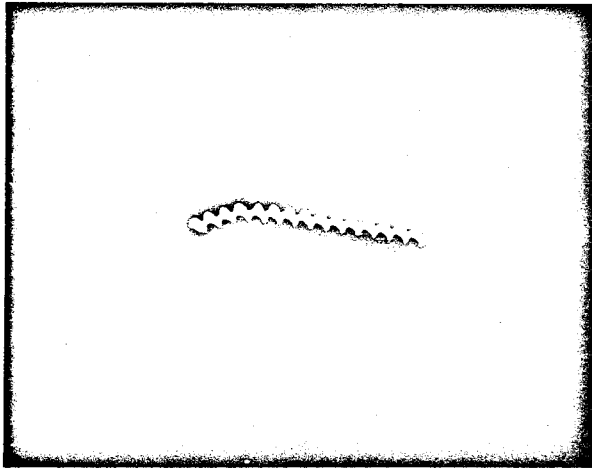


Figure 41: Example of an extrudate exhibiting screw dislocations.

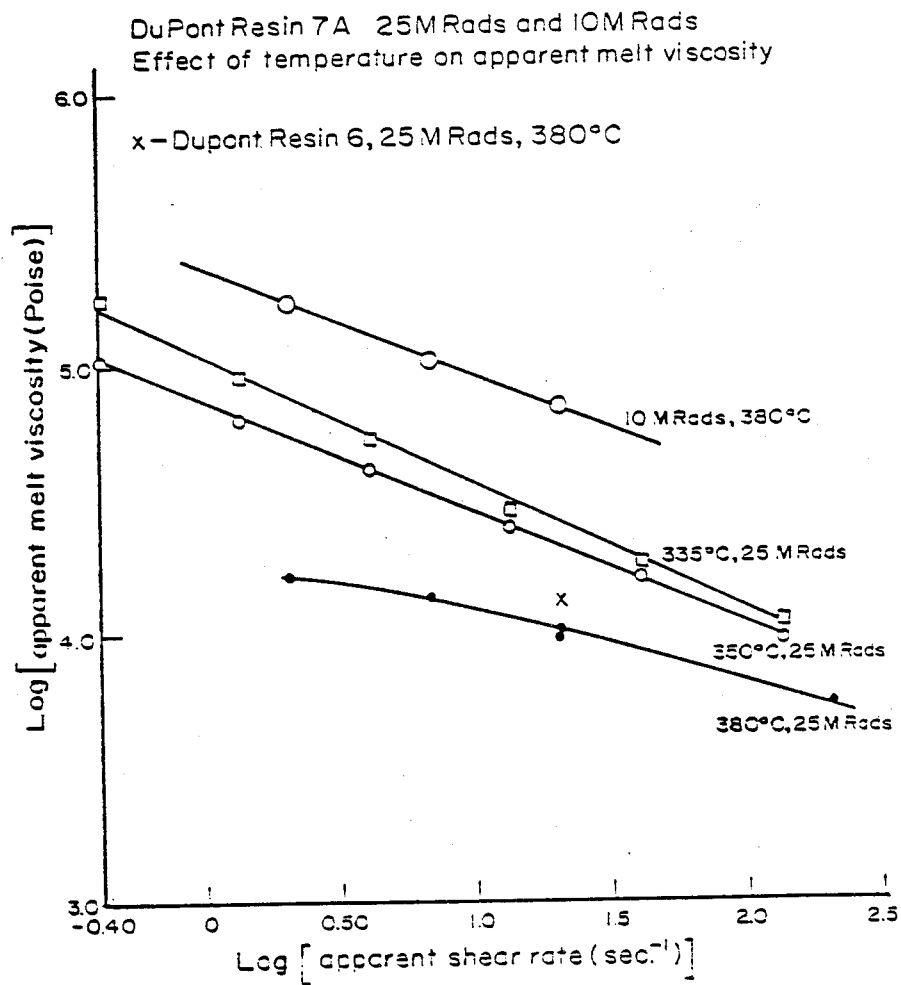


Figure 42: Plots of log apparent melt viscosity vs. log apparent shear rate for Teflon<sup>®</sup> resin 7A irradiated to 25 MRads in air taken at capillary temperatures of 335°C 350°C and 380°C. Also shown is a plot for resin 7A irradiated to 10 MRads in air determined at a capillary temperature of 380°C.

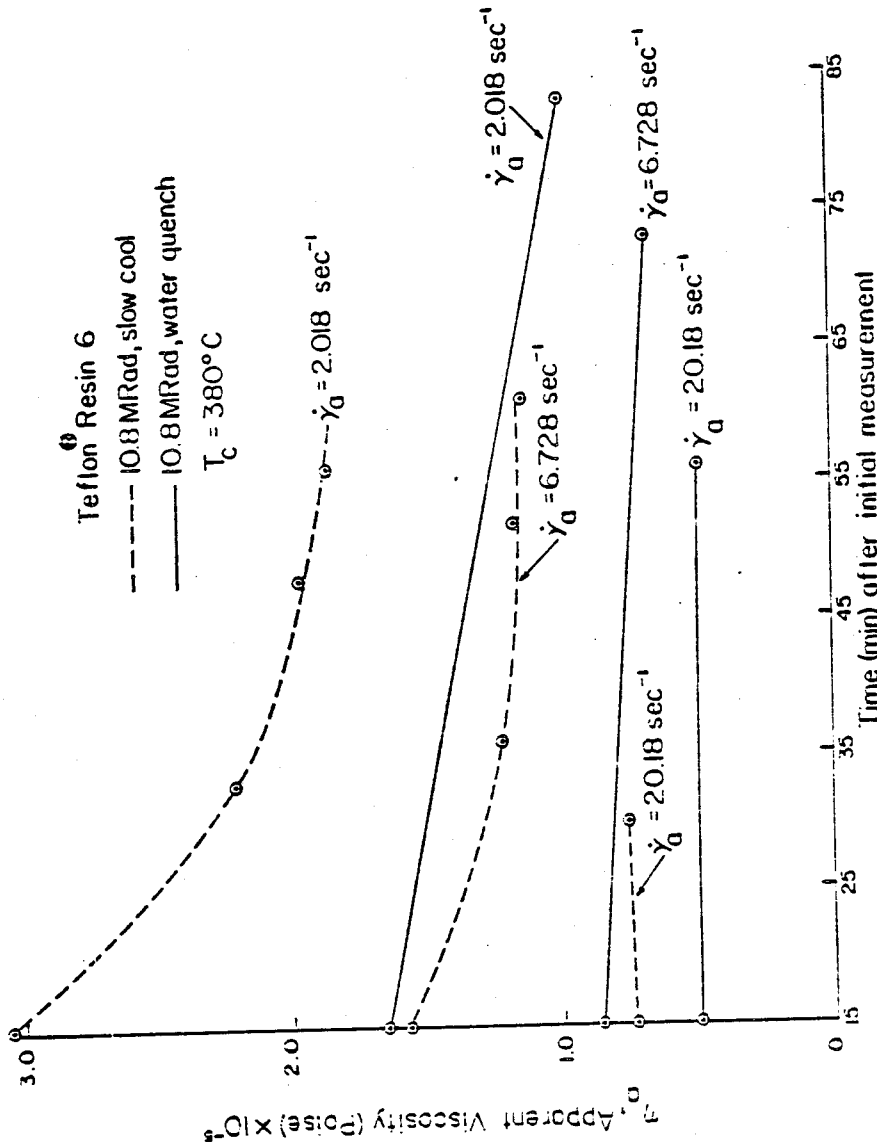


Figure 43: Effect of storage time in the rheometer barrel at  $380^\circ\text{C}$  and differences in pre-irradiation crystallinity in the post-irradiation melt: viscosity for Teflon resin 6.

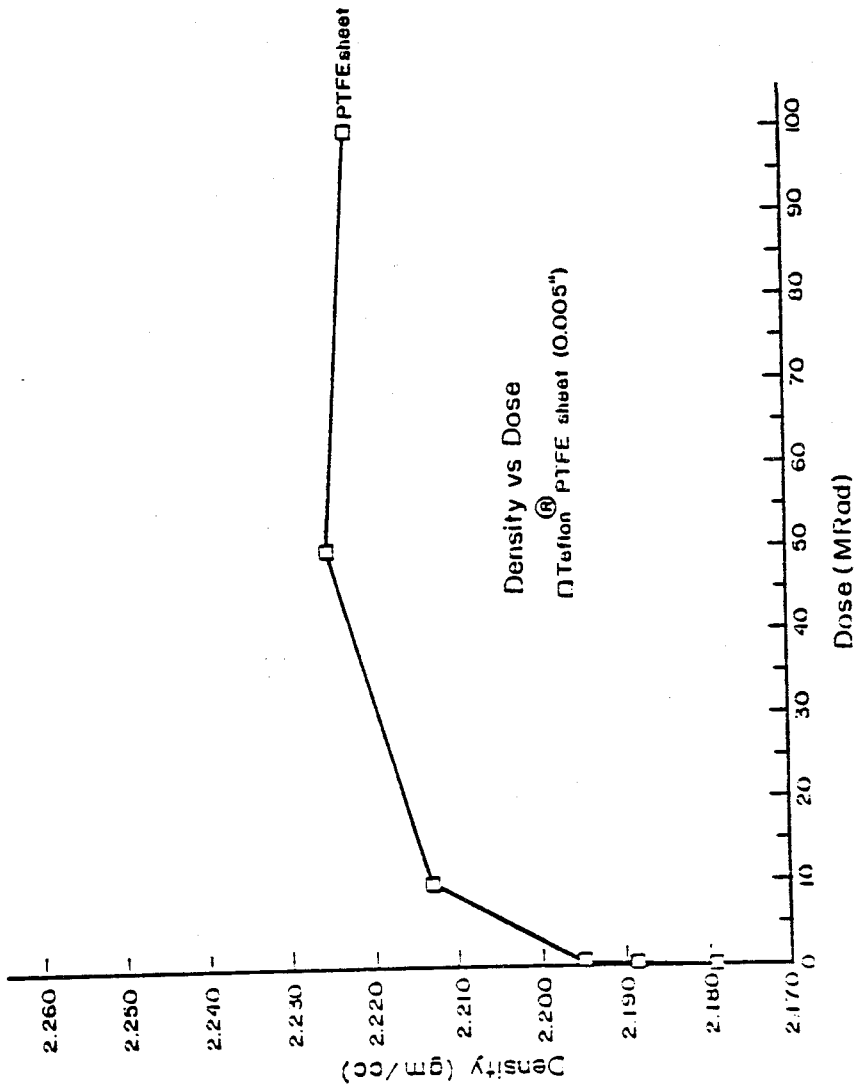


Figure 44: Density vs. dose for PTFE sheet irradiated in air.

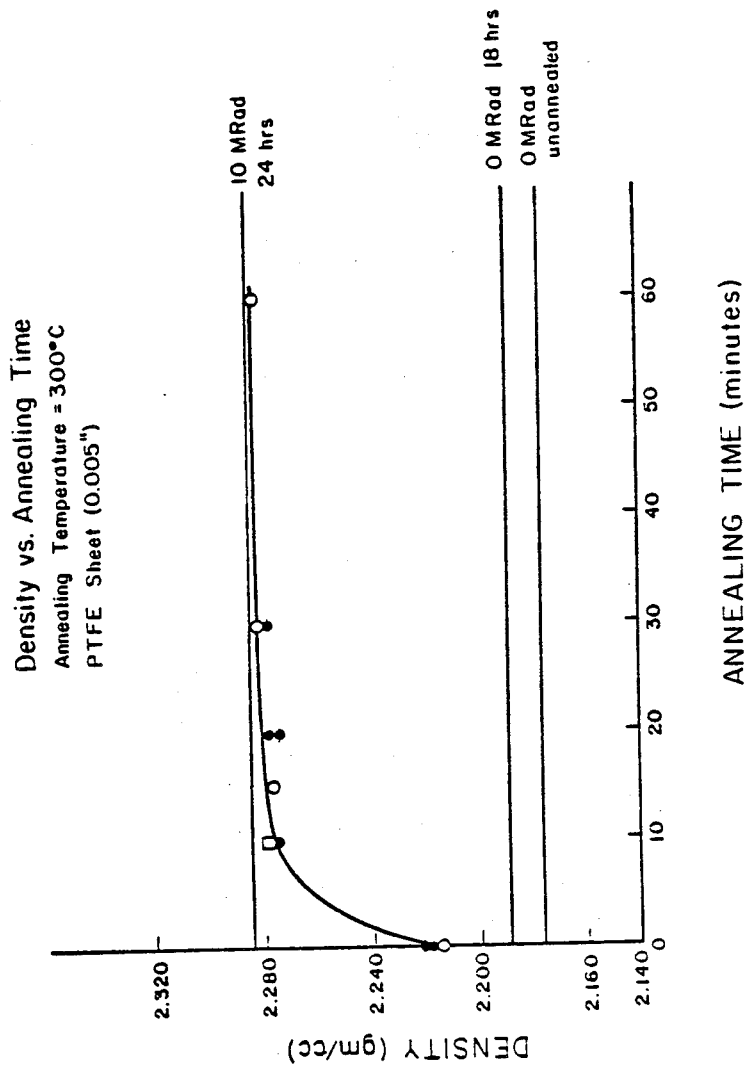


Figure 45: Density vs. post-irradiation annealing time at 300°C for PTFE sheet irradiated to 10 MRads in air.

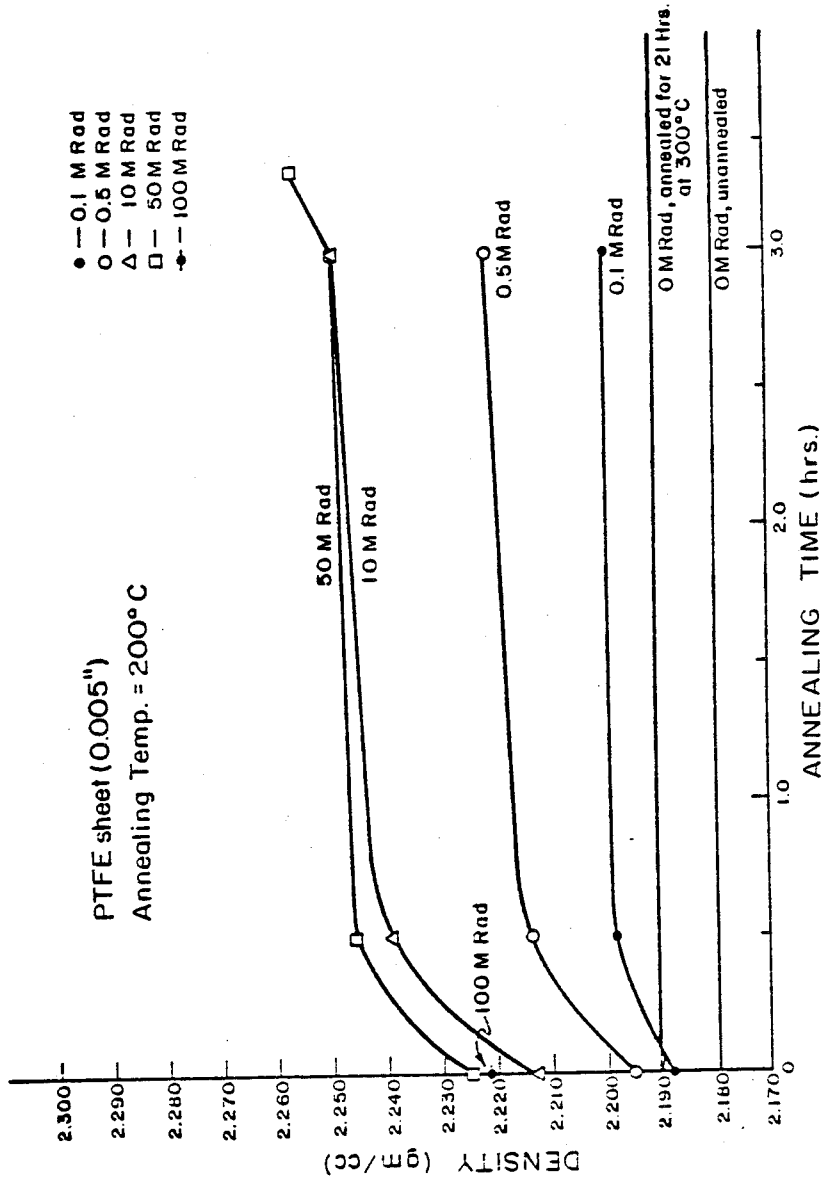


Figure 46: Density vs. post-irradiation annealing time at 200°C for samples of PTFE sheet irradiated to various doses in air.

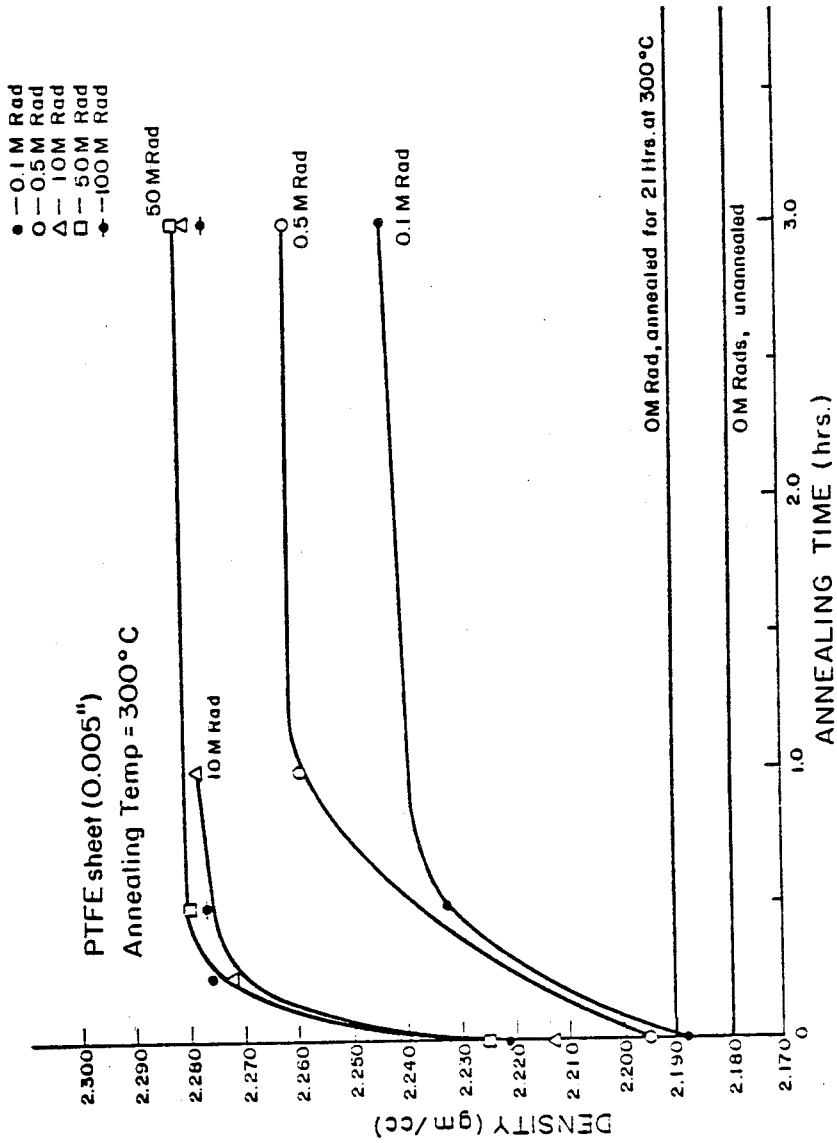


Figure 47: Density vs. post-irradiation annealing time at 300°C for samples of PTFE sheet irradiated to various doses in air.

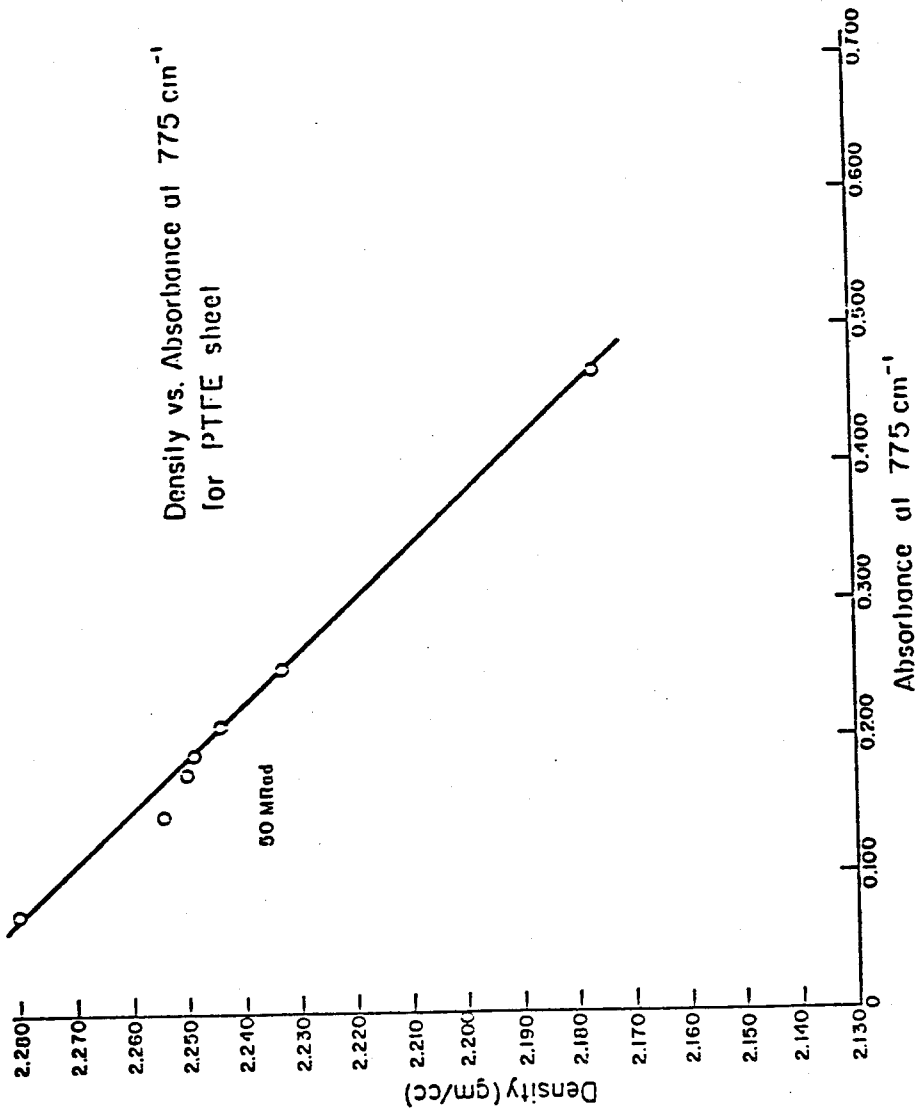


Figure 48: Density vs. IR absorbance at  $775\text{ cm}^{-1}$  for samples of PTFE sheet irradiated in air.

X-Ray Diffraction Scan of Unirradiated PTFE Sheet

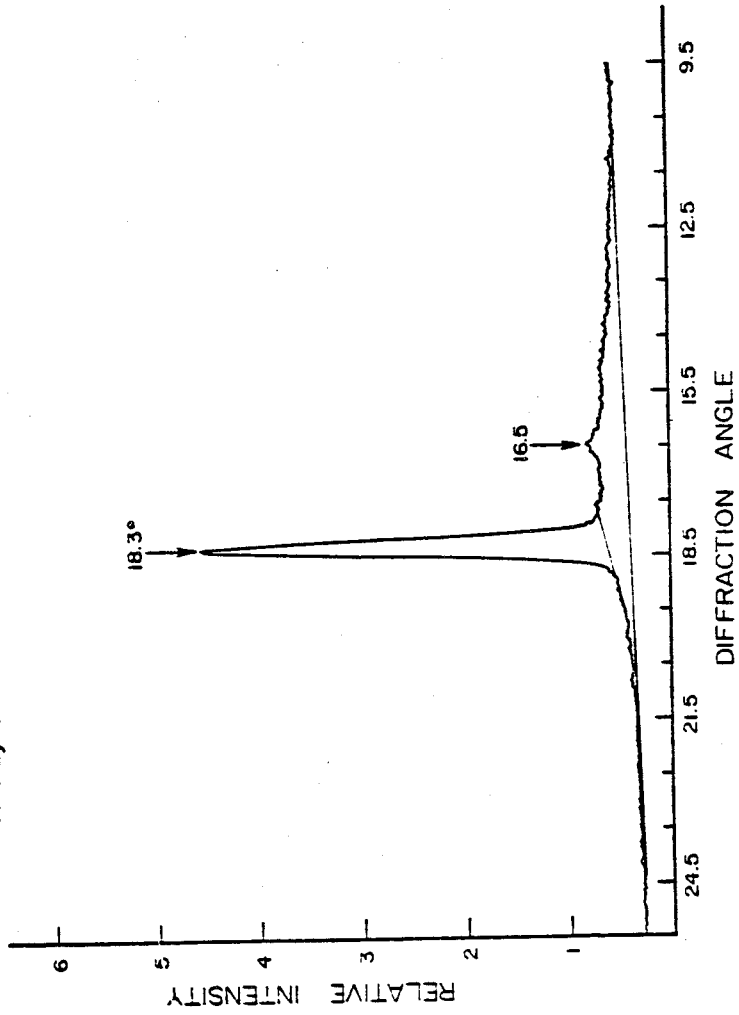


Figure 49: X-ray diffraction scan of unirradiated PTFE sheet.

X-Ray Diffraction Scan of PTFE Sheet Irradiated to 10 MRads

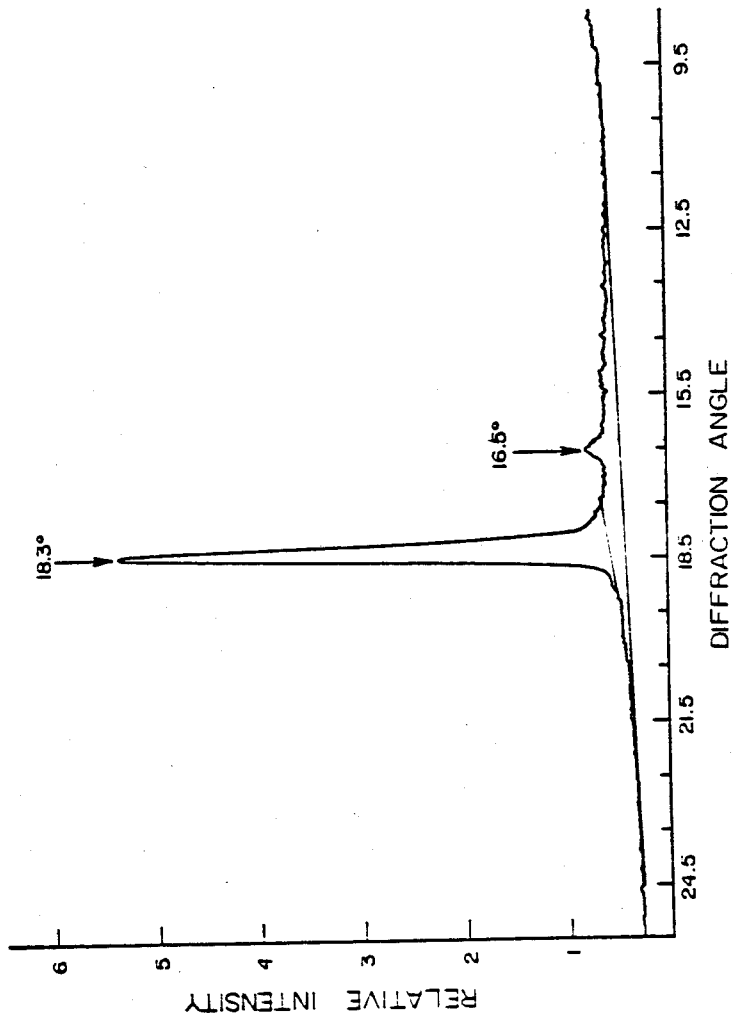


Figure 50: X-ray diffraction scan of PTFE sheet irradiated to 10 MRads in air.

X-Ray Diffraction Scan of PTFE Sheet Irradiated to 10 MRads  
Then Annealed For 1 Hour 10 Minutes at 298 °C

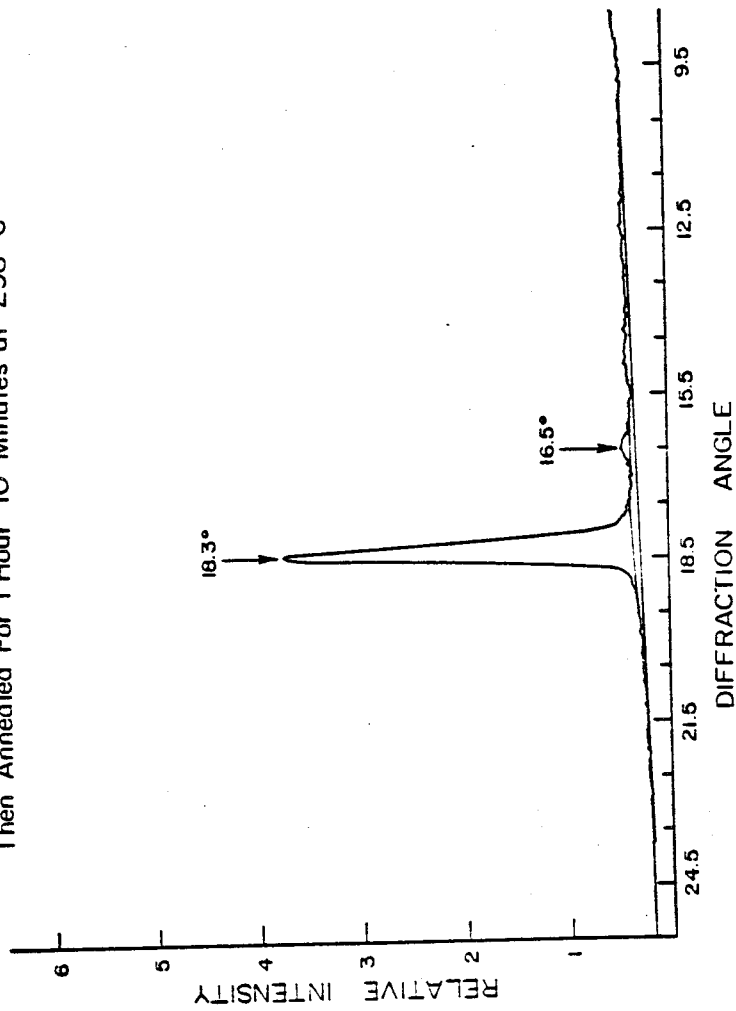


Figure 51: X-ray diffraction scan of PTFE sheet irradiated to 10 MRads in air then annealed for 1 hour 10 minutes at 298°C in air.

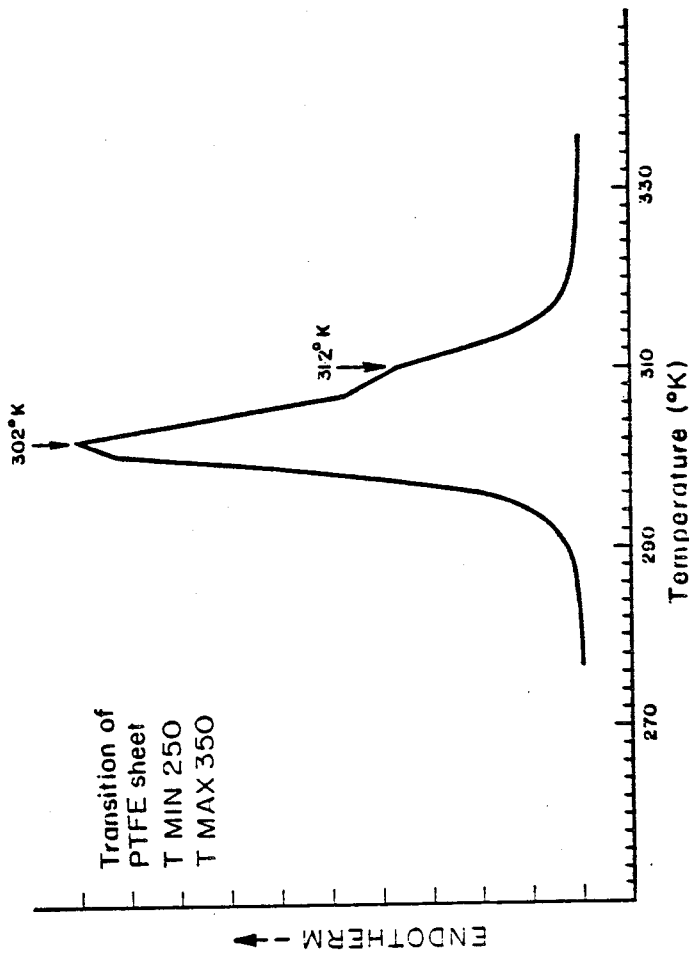


Figure 52: Composite heat of transition endotherm for the transitions at 302°K and 312°K for unirradiated PTFE sheet.

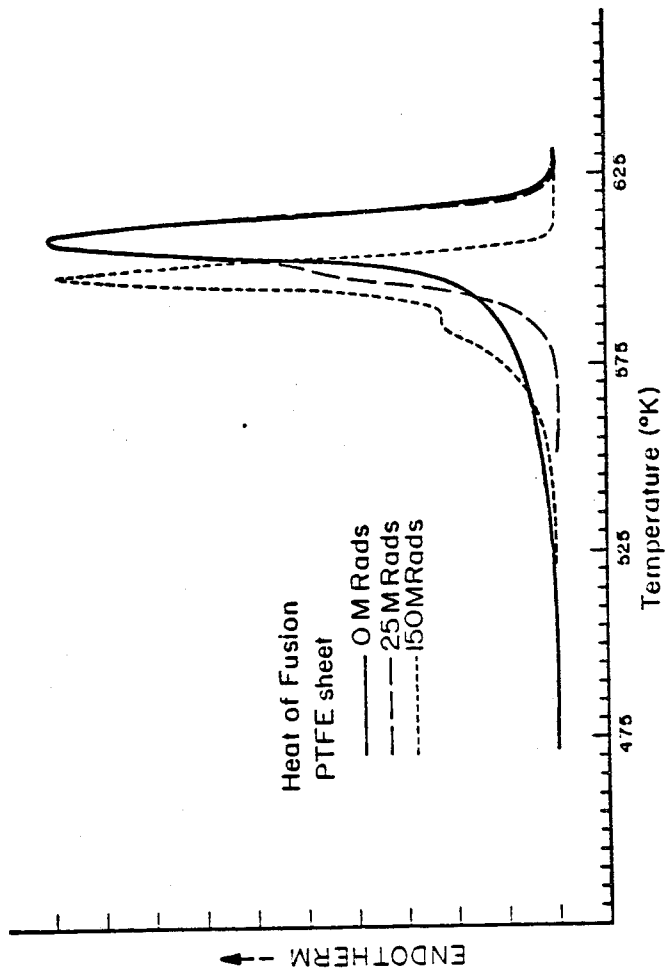


Figure 53: Heat of fusion endotherms for PTFE sheet irradiated to the indicated doses in ambient air.

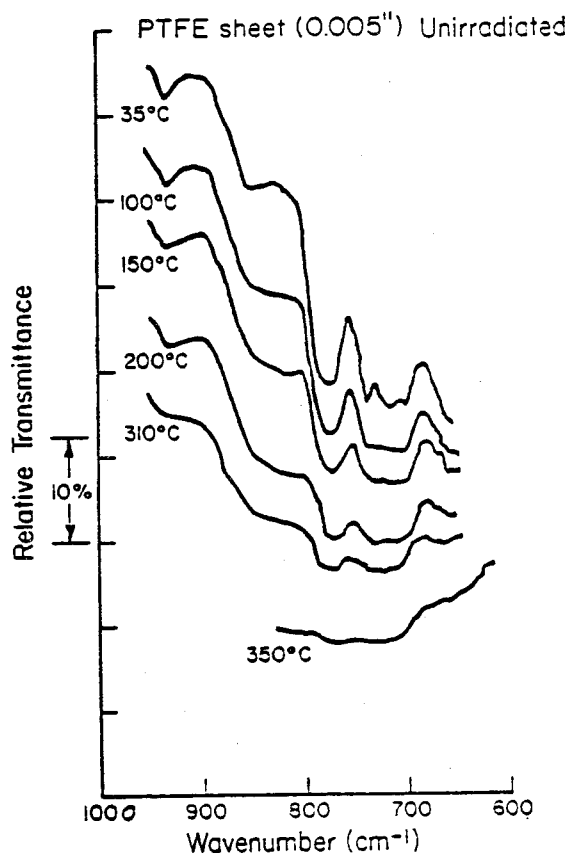


Figure 54: IR spectrum between 1000 and 600  $\text{cm}^{-1}$  of unirradiated PTFE sheet determined at the indicated temperatures.

Table 1  
Infrared Absorption Band Assignments

<u>Wavenumber (cm<sup>-1</sup>)</u>	<u>Assignment</u>	<u>Reference</u>
625	CF <sub>2</sub> wagging	6
982	-CF <sub>3</sub>	Sadtler Standard Spectra numbers 1870 and 16,954. Also comparison of IR spectrum of PTFE homopolymer and TFE hexafluoropropylene copolymer.
1757 } 3096 } 3472 }	Carboxyl groups	20
1780	-C = CF <sub>2</sub> F	20
1812	-O    C-OH Free carbonyl	23
1779	O    -C-OH Bonded carbonyl	23
	O    -C-H	4
3571	Free OH	23
3086	Bonded OH	23
1545	CF <sub>2</sub> Asymmetric stretch	14
1450	CF <sub>2</sub> Asymmetric stretch	14
282	CF <sub>2</sub> Wagging	14
384	Amorphous phase	14
700-800	Amorphous phase	14
1733	-C = C- F F	14
1870-1890	O    -C-F	4

Table 2  
Flow Index Values

Power law

$$\frac{\eta}{\eta_0} = \frac{\dot{\gamma}}{\dot{\gamma}_0}^{n-1}$$

$$\dot{\gamma}_0 = 1 \text{ sec}^{-1}$$

$$\log \eta = (n-1) \log \dot{\gamma} + \log \eta_0$$

<u>Sample</u>	<u>n-1</u>	<u>n</u>	<u>Correlation Coefficient</u>
Resin 100, 5 MRad	-0.808	0.192	0.993
Resin 100, 10 MRad	-0.748	0.252	0.995
Resin 100, 25 MRad	-0.681	0.319	0.994
Resin 100, 50 MRad	-0.541	0.459	0.991
Resin 7A, 2.5 MRad	-0.764	0.236	0.996
Resin 7A, 5 MRad	-0.905	0.095	0.999
Resin 7A, 10 MRad	-0.450	0.550	0.999
Resin 7A, 25 MRad	-0.400	0.600	1.000
Resin 6C, 2.5 MRad	-0.749	0.251	0.997
Resin 6C, 5 MRad	-0.866	0.134	0.994
Resin 6C, 10 MRad	-0.501	0.499	0.994
Resin 6C, 25 MRad	-0.456	0.544	0.998
Resin 6, 2.5 MRad	-0.796	0.204	0.993
Resin 6, 5 MRad	-0.832	0.168	0.999
Resin 6, 10 MRad	-0.481	0.519	0.998
Resin 6, 25 MRad	-0.519	0.481	0.997

Table 3

## DSC Results

Q  $\equiv$  liquid nitrogen quench from 380°C

Sample	$\Delta H_f$ (cal/g)	$T_f$ (°K)	$\Delta H_T$ (Cal/g)	$T_T$ (°K)	$\frac{\Delta H_f}{\Delta H_T}$
Teflon <sup>®</sup> 1st H PTFE Sheet 0 MRad	10.26	610.4	1.70	302.4	6.04
2nd H	8.84	608.4	1.40	304.0	6.31
Teflon <sup>®</sup> 1st H PTFE Sheet 0.1 MRad	11.14	610.8	1.66	302.4	6.71
Teflon <sup>®</sup> 1st H PTFE Sheet 1.0 MRad	14.90	610.8	1.73	300.8	8.61
2nd H	14.03	610.8	2.51	304.0	5.59
Teflon <sup>®</sup> 1st H PTFE Sheet 25 MRad	15.30	609.2	1.64	300.8	9.33
2nd H	13.82	607.6	2.37	302.4	5.08
Teflon <sup>®</sup> 150 MRad PTFE Sheet 1st H	15.50	600.0	1.18	292.8	13.14
PTFE 6, 1st H	16.75	618.8	2.43	299.2	6.89
PTFE 6Q, 1st H	6.11	602.8	1.24	299.2	4.93
PTFE 6Q, 1MRad 1st H	13.06	606.0	1.39	299.2	9.40
PTFE 6C, 1st H	15.88	617.2	2.02	296.0	7.86
PTFE 6CQ, 1st H	6.21	601.2	0.99	297.6	6.27
PTFE 7A, 1st H	-	-	2.04	299.2	-
PTFE 7A, 1.0 MRad, 1st H	16.52	615.6	1.96	299.2	8.43
PTFE 7AQ, 1st H	6.00	604.2	1.13	300.8	5.31
PTFE 7AQ, 1.0 MRad 1st H	13.09	607.6	1.21	299.2	10.82

## Appendix A

High Temperature Infrared Spectrum of PTFE Between 800 and 700  $\text{cm}^{-1}$ .

In an effort to obtain an absolute calibration between absorption at  $775 \text{ cm}^{-1}$  in the infrared spectrum and amorphous content of PTFE the infrared spectrum of PTFE sheet (0.005" thick) between 800 and  $700 \text{ cm}^{-1}$  was taken at various temperatures up to above the melting temperature. These spectra are shown in Figure 54. It can be seen by examining Figure 54 that the conformational structure of PTFE changes as the temperature is increased so that it is not possible to compare the high temperature spectra to the room temperature spectrum. The conformations responsible for the  $775 \text{ cm}^{-1}$  absorption completely disappear at  $350^{\circ}\text{C}$ . Thus one cannot calibrate the absorbance at  $775 \text{ cm}^{-1}$  so as to get absolute values of amorphous content using this method.